KTH Engineering Sciences

Master Thesis

Topological Defects in Dirty Two-Band Superconductors

Alberto Corticelli

Statistical Physics Group, Department of Physics,
School of Engineering Sciences
Royal Institute of Technology, SE-106 91 Stockholm, Sweden

Stockholm, Sweden 2018

Typeset in LaTeX

TRITA-FYS 2018:016
ISRN KTH/FYS/–18:016–SE

Printed in Sweden by Universitetsservice US AB, Stockholm February 2018

Abstract

Multicomponent superconductivity arises as a natural extension of the conventional theory, when materials have more than one superconducting band. The triviality of the extension does not reflect at all the multitude of new possible exotic phenomena. The topic of this thesis is to analyze some of them, in the context of a microscopically derived Ginzburg-Landau two-band model. In particular the model studied has repulsive interband coupling interaction and interband impurity scattering. The model hopes to describe some of the physics of iron-based superconductors, a new class of high temperature superconductors recently discovered. The impurity will have a central role in the model, allowing transitions between gap states, from $s_{\pm}$ to s_{++}. This transition can happen abruptly with a crossover, producing a new form of vortex matter, the so called "moat-core" vortices or can happen smoothly through an intermediate $s + is$ state. The latter is an example of broken time-reversal symmetry state (BTRS), impossible in conventional superconductivity, and presenting peculiar magnetic properties, like the appearance of spontaneous magnetic field inside the material, in contrast with the usual London electrodynamics. BTRS states also affects vortex interaction, opening the possibility of type-1.5 superconductivity, an intermediate new state involving vortex clusterization. Apart from vortex, other topological defects are possible in multicomponent systems, like Skyrmions and domain walls, that will be studied during the thesis. All the phenomena above mentioned have been extensively analyzed inside the model and numerically simulated, within a finite element framework.

Key words: superconductivity; multicomponent superconductivity; two-band model; BTRS; $s + is$ state; topological defects; type-1.5; vortex matter.

Preface

This thesis is the result of my Master's degree project at KTH's Department of Theoretical Physics under the supervision of Egor Babaev. The project embraced several months, from winter to autumn 2017, coinciding with my Erasmus exchange ending period in Stockholm. The works started with the general aim of using finite element simulations on Ginzburg-Landau models related to iron-based superconductors. After reproducing several different models from already published results, like $U(1) \times U(1)$ model with equal and different charges or two and three components models with Josephson coupling, I started to work on the dirty two-band model in this thesis. This model was already under study by Egor Babaev, Julien Garaud and Mihail Silaev and I focused on its magnetic properties in general.

Acknowledgments

I would like to thank my supervisor, Egor Babaev, for introducing me to the wonderful subject that is multicomponent superconductivity, constantly finding the time to reply to all my questions, and always pushing me in the right direction during the research. I am very thankful to Thomas Winyard for assisting me on my first months of works and opening the door to a more mathematical understanding of the theory. A special thanks goes also to Julien Garaud, for sharing his multiple expertise, in particular on finite element method and multicomponent superconductivity, he found always how to solve my problems in the most elegant way. I have really learned a lot from him. My office fellows deserve an heartfelt "tack", David Aceituno for spending really a lot of time helping me trough all kind of computer-based problems and together with Oskar Palm for all their advices during my time here. A lot of gratitude goes also to Mikael Twengström and Emil Blomquist who endlessly keep my spirit up. I am also grateful to Claudia Dallera, my italian coordinator, who was always available and kind with me. Finally, I'd like to thank my family for the encouragement during all my years of education and my girlfriend Susanna for her support and patience with me at all times.

Contents

Acronyms

AF Antiferromagnetic.

BCS Bardeen, Cooper, Schrieffer.

BdG Bogoliubov-deGennes.

BTRS Broken Time-Reversal Symmetry.

BZ Brillouin Zone.

DW Domain Wall.

FEM Finite Element Method.

FeSCs Iron-based superconductors.

FS Fermi Surface.

GL Ginzburg-Landau.

KZ Kibble-Zurek.

NLCG NonLinear Conjugate Gradient.

SC Superconducting.

Chapter 1

Introduction

In this chapter a small introduction about the field of superconductivity, along with an historical overview, is given. A comprehensive treatment can be found in references [1, 2] or any introductory book. After stating some basic concepts in the subject, the new field of multiband superconductivity is put in perspective. Finally the objective of the thesis is defined.

1.1 Conventional superconductivity

Superconductors (SC) have an history longer than a century, started in 1911, when Kamerlingh Onnes used the liquid helium-4 (produced for the first time few years before) to cool down mercury and reach a state with zero electrical resistivity, after a sudden drop at 4.2 K [3]. This is not the only remarkable property of superconductors, indeed years later in 1933 the so called Meissner-Ochsenfeld effect [4], the perfect diamagnetic response of these materials, was discovered.

Nonetheless the theoretical physics could not keep pace with the experimental one. The first phenomenological macroscopic theory, the London equations, was developed by the London brothers in 1935 [5]. This theory was able to explain the Meissner-Ochsenfeld effect,but only postulating a new fundamental law for the electromagnetic field valid only in superconductors, that physically describes the onset of a supercurrent (Meissner current) on the surface of the material in order to screen the external magnetic field. Later in 1948, F. London interpreted the supercurrent as coming from a sort of condensation in momentum space, similar to the Bose-Einstein condensation. A natural consequence was that the magnetic flux has to be quantized in a toroidal superconductor with a trapped magnetic flux inside, due to the coupling between phase of the wave function condensate and the vector magnetic potential [6].

A phenomenological description, with a more solid background and

capable of describing superconductors in a more complete way, was put forward by Ginzburg and Landau in 1950 [7]. This model is based on the theory of second-order phase transition, developed by Landau in 1937 [8], where the cornerstone of the theory was the notion of order parameter, an emergent entity characterizing the degree of spontaneous symmetry breaking. Differently from other phase transitions, the superconducting one was described through a *complex-field* order parameter ψ, in powers of which the free energy functional was assumed to be expanded near critical temperature. The Ginzburg-Landau (GL) free energy reads as

$$\mathcal{F} - \mathcal{F}_N = \frac{\hbar^2}{2m^*} \left| \left(\boldsymbol{\nabla} + i\frac{e^*}{\hbar c}\boldsymbol{A} \right) \psi \right|^2 + \alpha \left|\psi\right|^2 + \frac{\beta}{2} \left|\psi\right|^4 + \frac{\left(\boldsymbol{\nabla} \times \boldsymbol{A}\right)^2}{8\pi}, \quad (1.1)$$

where $\mathcal{F}_N$ is the free energy in normal state, $\boldsymbol{A}$ the vector potential, m^* and e^* are the effective mass and charge, that can vary depending on the normalization of the order parameter. In particular e^* it is linked with the electric charge of the elementary particle of the condensate.

The phenomenological GL theory still do not explain how fermions can form a condensate, maturing a long-range order. For this we had to wait until 1957, when Bardeen, Cooper and Schrieffer developed the homonym theory, that describe how fermions can bound in pairs when a small attractive coupling, mediated by phonon, is present [9]. After the publication of BCS theory, the relation between this microscopic theory and the Ginzburg-Landau approach was unclear. However in 1959 Gor'kov, formulating the BCS theory in the language of Green functions, managed to derive the GL equations, as an effective free energy functional emerging near the critical temperature, giving finally a physical meaning to the order parameter ψ [10]. We will sketch how this was done in Section 3.2. This finally closed the circle about superconductor understanding, at least until new unconventional superconductors were found...

Let us now return on the Ginzburg-Landau free energy Eq. (1.1), since we will deal with it during the entire thesis. As the theory of second-order phase transition states, the coefficient of the quadratic term behaves like $\alpha \propto (1 - T/T_c)$, therefore is the one driving the transition at temperature T_c, being negative for $T < T_c$ and making favorably having $\psi \neq 0$. Moreover the quartic term must have a positive coefficient $\beta > 0$, to ensure that the free energy is bounded from below.

If we interpret the order parameter as a wavefunction, we can see how Eq. (1.1) resemble a quantum mechanical non-linear Schrödinger equation, where $|\psi|^2$ can be identified as the density of superconducting particles. From this point of view we can attach a physical meaning to the GL free energy, where now the term containing the gradient is related to the kinetic energy of a particle in external magnetic field, the quadratic is

related to a potential that make favorable having superconducting state, and the quartic is a self-interaction between superconducting particles (a density-density potential) that limits the presence of the superconducting state.

This equation was a breakthrough in many respects. First of all the theory covers egregiously all the physics of London equations (and thus the Meissner-Ochsenfeld effect) and magnetic flux quantization. Secondly, the already highlighted complex parameter, that for the first time was associated to supertransport phenomena, therefore essentially associating a classic-field behaviour to quantum particles (later this equation has been used for superfluid, in the limit $e^* \to 0$). A complex order parameter means that the spontaneously broken symmetry is U(1), i.e. the circle group, coming from the rotational phase invariance of ψ in the free energy Eq. (1.1). Moreover being the matter field ψ electromagnetically coupled with $\boldsymbol{A}$ through the kinetic term, the U(1) symmetry is not global, but a local gauge symmetry, therefore the free energy is invariant under a shift of phase that can vary from point to point in the space. When this U(1) symmetry is spontaneously broken, the Anderson-Higgs mechanism [11] gives a gapped mode to the gauge field $\boldsymbol{A}$ (i.e. a mode with finite energies at zero wavevector, so in field theory nomenclature a non-zero mass mode), through a mutual "cancellation" of gapless modes, i.e. gapless photons and a gapless mode in the superconducting state (phonons).

The gapped mode in the vector field $\boldsymbol{A}$ is the one that effectively expels the magnetic field in SC material. In fact we can define the *magnetic penetration length* λ as inverse of the non-zero gauge mass, so physically describing the length scale at which the magnetic field is screened from the bulk. Therefore it is the gapped mode that produces the new electromagnetic fundamental law postulated by London brothers.

A second characteristic length in this theory is the so called *coherence length* ξ, that describes how the superconducting density $|\psi|^2$ recovers from a perturbation. A remarkable prediction of GL theory is the existence of two fundamental different types of superconductor. Indeed we can define the so called Ginzburg-Landau parameter as

$$k = \frac{\lambda}{\xi} \,. \tag{1.2}$$

Type I superconductors have $k < 1$ (traditionally would be $k < 1/\sqrt{2}$, but here we absorb the $\sqrt{2}$ in ξ in the modern way). This state is characterized by a positive surface energy between SC and normal domains, therefore it is convenient to form macroscopically large domains well separated, with the minimum interface between them. This is the Meissner-Ochsenfeld effect, where inside the bulk of the material there is no normal

state and the field cannot penetrate. The field cannot penetrate until it does not reach the *thermodynamic critical field* H_c, corresponding to the condensation energy (i.e. simply when Eq. (1.1) is equal to zero, meaning the energy consumed to screen the field is the same as the one gained with the condensation). In this case the material goes directly from the Meissner state to the normal state.

Type II superconductors have $k > 1$. This state is characterized by a negative surface energy instead, so it will try to maximize the surface between superconductor and normal state. However the system will be in the Meissner state up to the *first critical field* H_{c1}, that corresponds to the energy required to form a single "defect", an inclusion of normal state inside the SC bulk. This inclusion is more precisely a vortex, due to the coupling of the phase with the gauge field $\boldsymbol{A}$. Therefore for $H > H_{c1}$ the system enters in a new phase of matter, the vortex state, where a hexagonal lattice of vortices is present (Abrikosov lattice [12]). Each vortex can be seen as a depletion of the SC state in favor of the normal one, so the magnetic field can pierce the material with tubes of magnetic flux, those are then screened from the rest of the material by the supercurrent generated around the vortices (that is why the defect has to be a vortex). Additionally each vortex bears precisely a quantum of flux $\Phi = \frac{2\pi\hbar}{e}$, where e is the electrical charge. The vortex density increases with the external field, and eventually the SC state will be suppressed at H_{c2}, called the *second critical field*. The field H_{c2} is always higher than the thermodynamical field H_c in type I, in fact type II superconductor can resist more, letting the magnetic field penetrate.

It has to be noted however that, especially in clean type II material, the real limiting factor is often the *critical density current* J_c that the superconductor can bear before being suppressed. The critical current is due to vortex movement, indeed vortex interacts with each other and with the Meissner current, producing a sort of friction able to suppress the SC state. Mathematically this is described as the break down of the topological invariant that gives superconductivity and superfluidity in field theory. In fact the total flux inside a closed path is not constant anymore, having the vortices the possibility of going in and out from it. However vortices are often pinned by defects in the lattice, and therefore can resist to be teared away up to the critical current, that strongly depends on the amount and strength of the pinning centers.

1.2 Multiband superconductivity

Soon, after the publication of the BCS theory, generalizations of superconductivity to multiband case came out. In 1964 Tilley [14] generalizes Gor'kov's microscopic derivation of GL theory to multiband case, obtain-

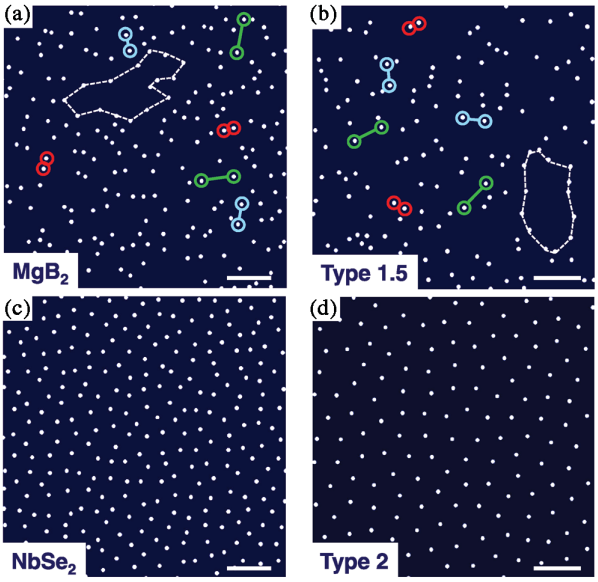

Figure 1.1: (a),(c) experimental vortex locations coming from a Bitter decoration in MgB_2 and $NbSe_2$ (known type II superconductor). (b),(d) corresponding numerical simulation. In MgB_2 is clear the presence of voids and clusters of different sizes, characteristic of type 1.5. Taken from reference [13].

ing a multicomponent classical field theory. These models can describes materials where electrons from different bands generate several superconducting components, where each component is not necessarily conserved. The non conservation is due to the possibility of Cooper pairs tunneling between bands, this phenomenon is called Josephson coupling and it is reminiscent of the Josephson effect, where a macroscopic supercurrent can tunnel from a superconductor to another separated by a weak link. Also more exotic situations can be described, for example a mixture of superconductors and superfluids, such as in neutron stars, where there is the possibility of condensates made of neutrons, protons and electrons.

A natural consequence of multiple components is the presence of multiple coherence lengths ξ_i, therefore the simple Ginzburg-Landau parameters in Eq. (1.2) cannot be defined anymore, and therefore the simple classification dichotomy type I/type II breaks down [15]. In fact a new intermediate regime can arise, when there is at least one coherence length larger and one smaller with respect to λ. In this case, as we will see, vortices do not form a lattice, but they regroup in clusters, having an attractive long-range and repulsive short-range interaction with each other. This regime was named *Type 1.5* superconductivity or *semi-Meissner* state, and was first recently observed in MgB_2 in Fig. (1.1).

MgB_2 is also the first clear two-band superconductor discovered (in 2001), and it has attractive coupling between bands. After that the set of discovered multiband materials kept growing, especially with the discovery of iron-based superconductors in 2008 [16]. These materials are the second class of high temperature superconductors observed, after the well known cuprates. Iron-based materials are thought to be described by several bands that can range generally from two to four. Additionally here, repulsive coupling interactions are present between bands, making these materials more interesting and complex than MgB_2, as we will see.

1.3 This thesis

1.3.1 Objective

The aim of this thesis is generically to apply numerical methods, principally the finite element method, in the study of Ginzburg-Landau models for unconventional multiband superconductors. In particular the thesis focuses on the microscopically derived two-band model with repulsive coupling interaction and with interband impurity scattering. This is a simple model that hopes to describe some physics of iron-based superconductors. The impurities in the material will have a central role in the thesis, not as pinning centers, but as scattering ones. This scattering centers help the two bands to be more coupled, producing transition from a physical state to another and especially allowing a new state of the matter, the broken time-reversal symmetry state (BTRS).

The objective of my thesis can be summarized as follow:

- Investigate the existence of BTRS states in ground states through phase diagrams.
- Investigate coherence lengths effects on vortex solutions, focusing on the experimental signatures.
- Investigate the possibility of skyrmionic solutions.
- Investigate general magnetic property of BTRS states.
- Investigate the presence of "moat" core solutions.

All these concepts will be unraveled during the chapters of the thesis.

1.3.2 Outline

This thesis is divided in six chapters which can be summarized as follow:

- **Chapter 1** (Introduction) This chapter sets the project into the context of superconductivity, introducing some basic knowledges.

- **Chapter 2** (Multicomponent Ginzburg-Landau) This chapter introduces the new field of multicomponent superconductivity and all the needed concepts through the studying of the U(1) × U(1) model, with special consideration for type 1.5 superconductivity and topological defects.

- **Chapter 3** (Dirty two-bands superconductors) The model studied in the thesis is presented here from the basis. The first part of the chapter will put the model in the context of iron-based superconductors, then the microscopical formalism of modern superconductivity will be sketched and used to derive our model. Finally its ground state and length-scale properties will be analyzed.

- **Chapter 4** (Numerical methods) The numerical methods used, like finite element and nonlinear conjugate gradient method will be shortly introduced here.

- **Chapter 5** (Results) This chapter presents all the numerical results obtained during the thesis work, and the necessary material to understand them.

- **Chapter 6** (Conclusions) Summary and short discussion of the results.

Chapter 2

Multicomponent Ginzburg-Landau model

Multicomponent superconductors are described by several complex fields, and their properties can be radically different from single component case. For example in this case the quantization of magnetic flux may be nonuniversal, and the magnetic field behaviour inside the material cannot be reduced to the usual London electrodynamics. Moreover we can have different type of topological defects, like domain walls and Skyrmions. The microscopic origin of the multiple complex fields can be the most different. They could arise from different bands in a superconducting material, and therefore being intrinsically intertwined with each other. However they could also be generated from a mixture of different particles, like Cooper pairs of electrons and protons in liquid metallic hydrogen, or in neutron stars where also neutron condensate is possible. The common denominator in this last case, is that the particles are physically different in each channel, and therefore independently conserved. This fact simplify a lot the model, and we will use it to introduce multicomponent superconductivity. An exhaustive treatment about multicomponent superconductivity can be found in Ref. [2].

2.1 U(1) x U(1) model

The mixture of two coexisting superconductor components can be described by the straightforward generalization of Eq. (1.1)

$$\mathcal{F} = \sum_{j=1}^{2} \left\{ \frac{1}{2} |\mathbf{\Pi}\psi_j|^2 + \alpha_j |\psi_j|^2 + \frac{\beta_j}{2} |\psi_j|^4 \right\} + \frac{(\boldsymbol{\nabla} \times \boldsymbol{A})^2}{2}\,, \tag{2.1}$$

where the constant normal state free energy $\mathcal{F}_N$ is neglected, $\mathbf{\Pi} = \boldsymbol{\nabla} + iq\boldsymbol{A}$ and the complex fields (also called matter fields) have the form

$\psi_j = |\psi_j| \mathrm{e}^{i\theta_j}$. The free energy has been rescaled in order to obtain dimensionless units, and q is the new defined parameter for gauge coupling between the matter fields and the vector potential, that is the same for both components (indicating the same elementary charge). As we can see from the potential, there are no terms with both the matter fields, that therefore are independent. This is only true regarding particle conservation, in fact through the kinetic term $\boldsymbol{\Pi}$ there is an unavoidable electromagnetic coupling, mediated by the vector field $\boldsymbol{A}$.

As we can note the model has a U(1) $\times$ U(1), being independent on both phases according the invariant transformation:

$$\psi_j' = \mathrm{e}^{i\phi_j}\psi_j \,, \tag{2.2}$$

where ϕ_j is any constant. Indeed in the free energy only gradients of the phases matter, related physically to the velocities of the condensates. In the invariance Eq. (2.2) is included also a discrete $\mathbb{Z}_2$ symmetry, so a symmetry having two equal states, not continuously connected (as spin up and down in Ising model). The $\mathbb{Z}_2$ here is called time-reversal symmetry, and mathematically is just the invariance in complex conjugation $\psi_j \to \psi_j^*$ that is equivalent to the transformation $t \to -t$. In this chapter this symmetry will play no role, being always conserved in independent mixture of superconductors.

The equilibrium configuration of the functional Eq. (2.1) is found by minimizing it with respect the three different physical functions ψ_1, ψ_2 and $\boldsymbol{A}$, obtaining the so call GL equations:

$$\boldsymbol{\Pi}^2\psi_j = 2\alpha_j\psi_j + 2\beta_j|\psi_a|^2\psi_j \tag{2.3a}$$

$$\boldsymbol{J} = \sum_j -q|\psi_j|^2(\boldsymbol{\nabla}\theta_j + q\boldsymbol{A}) = -q^2\rho^2\boldsymbol{A} + \sum_j(-q|\psi_j|^2\boldsymbol{\nabla}\theta_j)\,, \tag{2.3b}$$

where the supercurrent density $\boldsymbol{J}$ has been introduced through Ampere's law $\boldsymbol{J} = \boldsymbol{\nabla}\times\boldsymbol{\nabla}\times\boldsymbol{A}$. In Eq. (2.3b) the term $-q|\psi_j|^2$ is the electric charge density (q assumed positive), and we can see directly how the gradient $\boldsymbol{\nabla}\theta_j$, being related to velocity, is also linked with supercurrents. Also the gauge coupling is more clear, in fact are the gradients of the phases that couple with $\boldsymbol{A}$, in particular through the total density $\rho^2 = \sum_j |\psi_j|^2$.

Lastly it is useful sometime to use different formulations of current density, and also separate the two partial currents, so that the total current can be written as $\boldsymbol{J} = \sum_i \boldsymbol{J}^{(i)}$. Hence we have

$$\begin{aligned}\boldsymbol{J}^{(i)} &= -q|\psi_i|^2(\boldsymbol{\nabla}\theta_i + q\boldsymbol{A}) \\ &= \frac{iq}{2}(\psi_i^*\boldsymbol{\nabla}\psi_i - \psi_i\boldsymbol{\nabla}\psi_i^*) - q^2|\psi_i|^2\boldsymbol{A} \\ &= -q\,\mathrm{Im}(\psi_i^*\boldsymbol{\Pi}\psi_i)\,.\end{aligned} \tag{2.4}$$

2.2 Neutral and charged sectors

A stronger physical interpretation can be achieved by expanding the kinetic term in the free energy Eq. (2.1) as

$$\mathcal{F} = \sum_{j=1}^{2} \left\{ \frac{1}{2}(\boldsymbol{\nabla}|\psi_j|)^2 + \alpha_j|\psi_j|^2 + \frac{\beta_j}{2}|\psi_j|^4 \right\} + \frac{(\boldsymbol{\nabla}\times\boldsymbol{A})^2}{2} + \frac{\boldsymbol{J}^2}{2q^2\rho^2} + \frac{|\psi_1|^2|\psi_2|^2}{2\rho^2}(\boldsymbol{\nabla}\theta_{12})^2\,, \tag{2.5}$$

where we have introduced the phase difference $\theta_{12} = \theta_2 - \theta_1$. Doing that we have separated two contributions, in the last line of Eq. (2.5). The first dependent on $\boldsymbol{J}$ is called *charged* (or superconducting) sector, and it is associate with the coflow of both components. The coflow can be seen in the definition of $\boldsymbol{J}$ in Eq. (2.3b), where the phase gradient of both superconducting components are codirected. In this sector the transportation of charge is possible, and so it is the one related to superconductivity. The second term is dependent on the $\boldsymbol{\nabla}\theta_{12}$, i.e. counterdirected flows. This one is called *neutral* (or superfluid) sector because it cannot transport charge, but only matter, being the two flows compensating each other with opposite currents.

This transformation allows us also to be more precise about the symmetry. Now the characteristic local gauge symmetry U(1) of superconductivity is evident, enclosed in the charged sector. The free energy is in fact invariant under the transformation

$$\begin{aligned} \theta_1' &= \theta_1 + \phi(\boldsymbol{r}) \\ \theta_2' &= \theta_2 + \phi(\boldsymbol{r}) \\ \boldsymbol{A}' &= \boldsymbol{A} - q^{-1}\boldsymbol{\nabla}\phi(\boldsymbol{r})\,, \end{aligned} \tag{2.6}$$

where $\phi(\boldsymbol{r})$ is a single-value real function.

Separating the sectors in Eq. (2.5) we produced also a term that regards changing in the density ($\boldsymbol{\nabla}|\psi_j|$), and this together with the flows can have peculiar effects on the electrodynamics of the SC mixture. To see this clearly let us invert Eq. (2.3b) as

$$\boldsymbol{A} = \frac{1}{q^2\rho^2}\left[-\boldsymbol{J} + \frac{iq}{2}\sum_j(\psi_j^*\boldsymbol{\nabla}\psi_j - \psi_j\boldsymbol{\nabla}\psi_j^*)\right]. \tag{2.7}$$

Now applying the curl we can use it to compute the magnetic field as:

$$\boldsymbol{B} = \boldsymbol{\nabla}\times\boldsymbol{A} = -\boldsymbol{\nabla}\times\left(\frac{1}{q^2\rho^2}\boldsymbol{J}\right) \tag{2.8a}$$

$$+\boldsymbol{\nabla}\times\left(\frac{i}{2q\rho^2}\sum_j(\psi_j^*\boldsymbol{\nabla}\psi_j - \psi_j\boldsymbol{\nabla}\psi_j^*)\right). \tag{2.8b}$$

We see that $\boldsymbol{B}$ necessarily contains terms with products of density gradients and gradients of the phase:

$$\boldsymbol{\nabla}\left(\frac{|\psi_j|^2}{\rho^2}\right) \times \boldsymbol{\nabla}\theta_{12}\,. \tag{2.9}$$

If the two gradients are not collinear they can generate a spontaneous magnetic field in the material, even in absence of supercurrents. In general also these terms mix with the supercurrent effects and this makes the electrodynamics of the SC mixture dramatically different from the London electrodynamics in single component (where we have a theory of a massive vector field only, so the magnetic field has just the behaviour of being screened following the penetration length λ, coincident with the inverse of the mass).

A physical interpretation can be traced analyzing terms in Eq. (2.9). The phase difference gradient $\boldsymbol{\nabla}\theta_{12}$ is associated to the counterflow of the two components, but this is not enough, otherwise we would have had neutral flow that cannot produce a magnetic field. We also need a relative density gradient with a component perpendicular to the counterflow, in this way the two flows do not balance each other anymore, even if counterdirected, and a resulting current is possible (different from the supercurrent $\boldsymbol{J}$) . If a spontaneus field is produced in a sample, the Meissner current will be automatically "activated" screening this effect, that anyway can be still detectable.

2.3 Ground states and length scales

The ground state is the state at lowest energy, the one which should be recovered after a perturbation in the system is performed. Since in Eq. (2.1) the kinetic term is always positive, it will never be convenient to have gradients in the system, so the ground state will be homogeneous and we can neglect that term in the calculation ($\boldsymbol{\Pi}\psi_j = 0$). Also the magnetic energy is quadratic, so always positive therefore it will be favourable having $\boldsymbol{\nabla} \times \boldsymbol{A} = 0$. Hence the vector potential is a pure gauge ($\boldsymbol{A} = \boldsymbol{\nabla}\phi$ for arbitrary ϕ) that can consistently be chosen to be zero.

The ground state will be then the extremum of the remaining part, i.e. the potential part V. From U(1) $\times$ U(1) symmetry we know that each phase has an arbitrary ground state $\bar{\theta}_j$, which is constant due to homogeneity requirement. Finally the ground state density can be found minimizing the potential as

$$\frac{\partial V}{\partial|\psi_j|} = 2\alpha_j|\psi_j| + 2\beta_j|\psi_j|^3 = 0\,. \tag{2.10}$$

The solutions are two,

$$|\psi_{0j}| = \begin{cases} 0 \\ \sqrt{\frac{-\alpha_j}{\beta_j}} \equiv u_j \,. \end{cases} \tag{2.11}$$

Therefore the possible ground states can be written as

$$(|\psi_{01}|, |\psi_{01}|) = \begin{cases} (u_1, u_2) \\ (u_1, 0) \\ (0, u_2) \\ (0, 0) \,. \end{cases} \tag{2.12}$$

From the ground states we can see how there is the possibility to have the components superconducting independently. Now we are in position to study relevant informations about the system through an expansion in small parameter ε around the ground states found, as

$$\begin{aligned} |\psi_j| &= u_j + \varepsilon f_j \\ \theta_j &= \bar{\theta}_j + \varepsilon \frac{\phi_j}{u_j} \\ \boldsymbol{A} &= \varepsilon \boldsymbol{a} \,, \end{aligned} \tag{2.13}$$

where the terms proportional to ε are the fluctuations around the ground states and ϕ_j has been normalized for convenience. Inserting the expansion in the free energy Eq. (2.5) we order the term by power of ε. The constant part $\mathcal{F}^{(0)}$ is the ground state energy, $\mathcal{F}^{(1)}$ is zero by definition of ground state, and therefore the first relevant term is the $\mathcal{F}^{(2)}$ that reads as

$$\begin{aligned} \mathcal{F}^{(2)} =& \frac{1}{2} \Upsilon^T (\boldsymbol{\nabla}^2 + \mathcal{M}^2) \Upsilon + \frac{1}{2} (\boldsymbol{\nabla} \times \boldsymbol{a})^2 + \frac{1}{2} q^2 \bar{\rho}^2 \boldsymbol{a}^2 \\ =& E_{\text{Klein-Gordon}} + E_{\text{Proca}} \,, \end{aligned} \tag{2.14}$$

where we have defined the fluctuation basis as $\Upsilon = (f_1, f_2, \phi_1, \phi_2)$, the ground state total density $\bar{\rho}^2 = \sum_j u_j^2$ and the *mass* matrix $\mathcal{M}$. We can see how, at a linear level, the vector potential decouples from the matter fields. In particular the $\mathcal{F}^{(2)}$ splits in two energy functionals of well-known equations. In fact minimizing with respect to Υ and $\boldsymbol{a}$ we get the linearized GL equations (with respect the full Eq. (2.3)), reading as

$$\boldsymbol{\nabla}^2 \Upsilon = \mathcal{M}^2 \Upsilon \tag{2.15a}$$

$$\boldsymbol{\nabla} \times \boldsymbol{\nabla} \times \boldsymbol{a} = m_a^2 \boldsymbol{a} \,, \tag{2.15b}$$

where we have defined the (squared) gauge field mass $m_a^2 = q^2 \bar{\rho}^2$. The first equation is a system of Klein-Gordon equations, while the second a

Proca equation. The two are closely related being equations for massive fields, both with second order derivative in space (the difference is in the vectorial nature of $\boldsymbol{A}$ with respect to the scalar nature Υ elements).

The easier to solve is the Proca equation, being usually the mass matrix complicate (not in this case). Since we are eventually interested in vortex excitations in 2D we can assume axially symmetric perturbations in the form $\boldsymbol{a} = (\frac{a(r)}{r}\hat{\theta})$, in this way Proca equations simplify and we easily get a solution that in the limit of $r \to \infty$ is a decaying exponential, with characteristic length reading as

$$\lambda = \frac{1}{m_a} = \frac{1}{q\sqrt{\bar{\rho}^2}}\,, \tag{2.16}$$

where λ is exactly the penetration length. Here we can see indirectly the Anderson-Higgs mechanism. In fact if the superconductor was suppressed, $m_a = 0$ and therefore $\boldsymbol{a}$ would not be massive anymore. The equation Eq. (2.15b) would reduce to the Maxwell equations (without current), and therefore the gauge symmetry would be restored. While with $m_a \neq 0$ we can see how Eq. (2.15b) is gauged-fixed, and this process comes exactly from the "mutual cancellation" of massless modes between the vector field and the condensates.

Now shifting the attention to the Klein-Gordon equation, its mass matrix reads,

$$\mathcal{M}^2 = \begin{pmatrix} 2\alpha_1 + 6\beta_1 u_1^2 & 0 & 0 & 0 \\ 0 & 2\alpha_1 + 6\beta_1 u_2^2 & 0 & 0 \\ 0 & 0 & 0 & 0 \\ 0 & 0 & 0 & 0 \end{pmatrix}, \tag{2.17}$$

and its eigenvalues are the masses of each normal mode of Eq. (2.15a). The (squared) mass matrix corresponds exactly to the initial free energy Hessian matrix, evaluated at the ground state, with respect the matter fields variables. As done for the Proca equation, we can solve easily the Klein-Gordon equations for each normal mode. In total the normal modes are 4 but only 2 are massive as we can see from the eigenvalues. The two massless modes (Goldstone bosons) are related to the phases and reflect the symmetry U(1) × U(1). In particular a combination of these two will be the massless mode that, coupling with $\boldsymbol{A}$ in full theory, yields a massive vector field with mass m_a. This kind of mode (usually related to the total phase of the components) is always present and it is the hallmark of superconductivity. The other combination of phase will be related to the remaining U(1) symmetry, that usually is not present in electronic superconductors (due to coupling between components in the potential).

Finally the two remaining massive modes are related to the densities, and for different ground states yield

$$\begin{aligned} |\psi_{0j}|^2 = 0 \quad &\rightarrow \quad \xi_{0j} = \frac{1}{\sqrt{2\alpha_j}} \\ |\psi_{0j}|^2 = u_j \quad &\rightarrow \quad \xi_j = \frac{1}{2\sqrt{-\alpha_j}}\,, \end{aligned} \tag{2.18}$$

where both have to be well defined to be associated with stable solution (due to Hessian eigenvalues positiveness requirement). Indeed as we know from the theory of the second order phase transitions we have $\alpha_j \propto (T - T_{cj})$, so it is positive when $T > T_{cj}$ (no superconducting phase) and negative when it condensates (in multicomponent SC obviously we can have different critical temperatures).

The last thing to note is that in multiband superconductors the mass matrix is more complicate, and this can have several consequences. The first one is that usually normal modes are associated not to independent components, but to a linear combination of them (hybridization), so the coherence length are not linked to the single condensates. The second consequence is that we can have massive pure phase modes, called Leggett modes [17], and this is a drastic difference with respect to single component case, especially regarding vortex interactions. Additionally, in case like the presence of impurity and/or broken time-reversal symmetry, the phase modes can hybridize with density modes, and therefore exciting a phase will also perturb the densities, and this can produce new exotic feature.

2.4 Vortex solutions

As we said at the beginning, multiple components can bring with them a non universal flux quantization. Let us consider an infinite 2D superconductor, with a small hole in the center and an external magnetic field. Being the external field screened, it will penetrate mostly through the hole with a total magnetic flux

$$\Phi = \int_S \boldsymbol{B} \cdot d\boldsymbol{S} = \oint_\Gamma \boldsymbol{A} \cdot d\boldsymbol{l}\,, \tag{2.19}$$

where $\boldsymbol{S}$ is the surface normal vector and Γ a path inside the superconductor, such that all flux is included. Inverting now the relation Eq. (2.3b) we can substitute the value of $\boldsymbol{A}$ in the previous equation. Also being the path Γ well inside the SC, we can consider, for the Meissner effect, that the density current is $\boldsymbol{J} = 0$ on it and also the ground state recovers

in general. Therefore we get

$$\Phi = -\frac{1}{q}\left(\sum_j \frac{u_j^2}{\bar{\rho}^2}\oint_\Gamma \boldsymbol{\nabla}\theta_j \cdot d\boldsymbol{l}\right) = -\Phi_0 \sum_j \frac{u_j^2}{\bar{\rho}^2} N_j \,, \tag{2.20}$$

where we have identified the flux quantum $\Phi_0 = \frac{2\pi}{q}$ and the winding integer number N_j in each component. The winding number is a necessary condition, being the phase functions θ_j single-valued in the space. Therefore around a close path they have to return to the same value, and due to the periodicity $\theta_{start} = \theta_{end} + 2\pi N$, they can enclose N windings. Formally we can define the *vortex charge* as

$$N = \frac{1}{2\pi}\oint \boldsymbol{\nabla}\theta \cdot d\boldsymbol{l} \;\in \mathbb{Z} \,, \tag{2.21}$$

where it can assume any integer value, also depending on the phase winding orientation (positive and negative integer).

In one component the total flux Eq. (2.20) would reduce to $\Phi = -\Phi_0 N$, and so we would have a quantized flux, that can be multiple only of Φ_0. In two components we see that this is not true in general. In fact the ground states u_j can continuously vary, and so it is not possible to define an universal quantum, even if the single windings are still quantized. However in case the windings are the same $N_1 = N_2$, Eq. (2.20) reduces to the classic one. This usually happens in vortex solutions, let us try to understand why.

Physically vortices are points (lines in 3D) around which the phase winds and the superconducting density is suppressed. These are field defects related to the intrinsic U(1) symmetry in SC models. The phase winding around the center produces a gradient, that without the vector field $\boldsymbol{A}$, would be present also at infinite distance from the vortex center. Being the free energy dependent on these gradients (i.e. on condensates velocities) we would have to pay an infinite energy to produce a vortex, due to the infinite flow around it (like in superfluids). Nevertheless in superconductors we can see from the charge sector in Eq. (2.5), that the vector potential could wind itself to compensate the phase gradients of the condensates and limit the energy of a single vortex to a finite value. Physically what happens is that asymptotically from the center, the gauge coupling manages to suppress the current (according to the penetration length, with the Meissner effect).

When we have two components, the situation is a little bit different, since we can have windings in each one and only a single vector potential to compensate. Indeed here we can have a *composite* vortex with winding N_1 in the first component and winding N_2 in the second one, shortly indicated as (N_1, N_2). Obviously is also possible to have a winding in

one component only, these are called *fractional* vortices, indicated as $(N_1, 0)$ or $(0, N_2)$. Vortex ansatz solutions are in the form

$$\begin{aligned} \psi_j &= f_j(r) \mathrm{e}^{iN_j\theta_j} \\ \boldsymbol{A} &= a(r)\hat{\theta}\,. \end{aligned} \tag{2.22}$$

These ansatz can be inserted in the GL equations Eq. (2.3), to find the solutions (numerically). But important informations can be found just analyzing how these solutions affect the free energy Eq. (2.5). To ensure a stable solutions, the ground state has to be recovered, so $f_j(r \to \infty) = u_j$, additionally not to have infinite energy we need the density going to zero at the point of $\boldsymbol{\nabla}\theta_j$ singularity, i.e. the center of the vortex, so $f_j(0) = 0$. Also the charge sector requires that current circulation is zero far away from the vortex in order not to give an infinite energy contribution, hence

$$\oint_\Gamma \boldsymbol{J} \cdot d\boldsymbol{l} = -q^2\bar{\rho}^2 \oint_\Gamma \left(\boldsymbol{A} + \frac{1}{q\bar{\rho}^2} \sum_j (u_j^2 \boldsymbol{\nabla}\theta_j) \right) \cdot d\boldsymbol{l} = 0\,, \tag{2.23}$$

which is satisfied for

$$a(r \to \infty) = -\frac{N_1 u_1^2 + N_2 u_2^2}{q\bar{\rho}^2}\,. \tag{2.24}$$

Here we can see how the vector potential compensates the vortex windings in superconductors. But in multicomponent we have also another term in the free energy, the neutral sector that gives an energy contribution:

$$\begin{aligned} \int \frac{|\psi_1|^2|\psi_2|^2}{2\rho^2} (\boldsymbol{\nabla}\theta_{12})^2 &\approx \int \frac{u_1^2 u_2^2}{\bar{\rho}^2} \left(\frac{N_2 - N_1}{r} \right)^2 \pi r dr \\ &\propto (N_2 - N_1)^2 \ln \frac{R}{\xi}\,, \end{aligned} \tag{2.25}$$

where we have approximate the integral considering an infinite system with size $R \to \infty$, and we use as cutoff the smallest coherence length. The energy therefore diverges logarithmically if the windings are not the same, so the only stable vortices are composite with (N, N). That does not mean that fractional vortices are impossible to create, they can be created in bound states with equal number N in both components, such that they asymptotically reduce to a composite vortex (N, N). Physically the fact of having same winding numbers, means that we can have vortices in the charge sector (the superconducting one) but not in the neutral sector (the superfluid one), and this reflects perfectly what usually happens in superconducting and superfluid materials.

2.5 Vortex interactions

For well separated vortices one can linearize the GL equations Eq. (2.3) and calculate the interaction energy. In this way vortices have a particle-like behaviour, interacting logarithmically with different contributions. For now on we will talk about composite vortex (N,N). In linear theory we can generally separate two interaction contributions.

The first comes from the magnetic interaction of currents around vortices, this is repulsive if the currents are codirected, while attractive if they are counterdirected. This interaction prefers to split a vortex with winding number $N > 1$ into N vortices with single winding and with infinite separation, producing a type II behaviour. Coming from magnetic contributions, the characteristic length governing this interaction is the penetration length λ.

The second one is the core-core interaction, and it is always attractive coming from the density contributions. Indeed vortices are defects in the bulk density, so it is always convenient to merge them in a megavortex, to minimize the density suppressed. The megavortex represents a macroscopic normal state, well separated from the bulk, so a type I behaviour. The characteristic lengths governing this interaction are the coherence lengths. In the simple case of $\mathrm{U}(1) \times \mathrm{U}(1)$, we can separate clearly each contributes. So the coherence length ξ_1 affects the interaction of the first component vortices, and respectively does the ξ_2. However being the fractional vortices bound together, the composite vortex will feel both (in hybridize case we cannot even separate the contributions).

Finally the energy interaction between two codirected vortices reads

$$E_{int} = C_B^2 K_0(r/\lambda) - C_1^2 K_0(r/\xi_1) - C_2^2 K_0(r/\xi_2)\,, \tag{2.26}$$

where the prefactors are dependent on the GL free energy parameters as well, and $K_0(x)$ are the modified Bessel function, that asymptotically $K_0(x \to \infty) \to \mathrm{e}^{-x}/\sqrt{x}$. As we can note from the characteristic length dependence, the first term is the current-current repulsion, while the last ones are the attractive core-core interactions.

In the limiting case where one of the SC components is suppressed $u_2 \to 0$, then $C_2 \to 0$ and we end up in the usual single component limit. Here the interaction between vortices has only two possibilities and it is always monotonic. If $\lambda > \xi$ then $C_B > C_1$ and the total interaction will be repulsive for any distance, driving a type II behaviour. While if $\lambda < \xi$ we have $C_B < C_1$ and so a type I behaviour, and the vortex always attract themselves up to create a megavortex.

The things can be different if we rehabilitate the second component. Let us consider it still weak, so that $u_1 \gg u_2$ and therefore $\xi_1 \ll \xi_2$, indeed being u_1 strong, the free energy wants to recover its density rapidly. Also

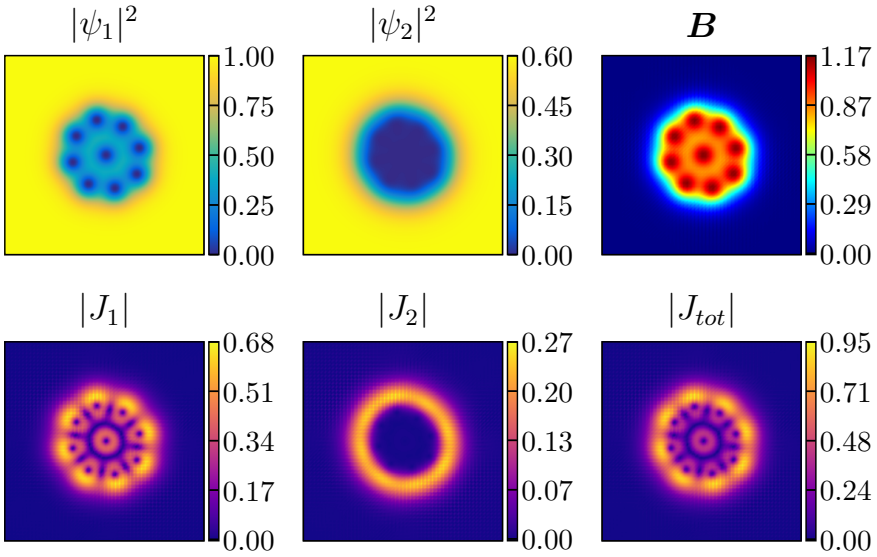

Figure 2.1: Numerical solutions for a cluster of N=9 flux quanta in type-1.5 U(1) × U(1) superconductor. The parameters of the potential are $(\alpha_1, \beta_1) = (-1, 1), (\alpha_2, \beta_2) = (-0.6, 1)$ and $q = 1.5$. The quantities displayed are: $|\psi_i|$ the density of first and second component, $\boldsymbol{B}$ magnetic field, $|J_i|$ the current densities in each component, and $|J_{tot}|$ the total one.

let us take an intermediate penetration length such that $\xi_1 < \lambda < \xi_2$. In this case being u_2 weak we do not expect a so different behaviour from the single component case, where if $\xi_1 < \lambda$ we get a repulsion. However even if weak, the second component has attractive forces that are longer than the ones related to λ. So eventually the system will have short-range repulsive and long-range attractive forces, and this non-monotonic behaviour creates clusters. This new SC state was predicted theoretically in [15] and then termed type-1.5 superconductivity when was the first time experimentally observed [13].

In Fig. (2.1) we can see a numerical simulation of U(1) × U(1) in type 1.5 regime, where the first component is the strongest one. From the densities plots, it can be clearly seen how the ψ_2 is completely depleted inside the cluster, forming a sort of megavortex, while the strong component ψ_1 has well defined vortices, that anyway are subjected to the long-range attractive forces of the weak component. Also the behaviour of the currents in the single components is quite explicative regarding the competition of type II and type I tendencies. Currents in ψ_1 are mostly around the vortices, while in ψ_2 around the cluster. Finally we note how the magnetic field resembles more the strong component. This is clear if we remember Eq. (2.20), in fact fractional vortices carries a fraction of the flux quantum weighted by their relative strength (i.e. relative density).

2.6 Skyrmion solutions

In multicomponent superconductors another kind of topological defect is possible, namely Skyrmions. Their physical interpretation is somehow more difficult with respect the well-know Skyrmionic defects in magnetic materials, so let us start by analyzing fractional vortices.

As we said fractional vortices are not stable alone, giving a contribution in the neutral sector that cannot be compensated by the gauge field. However balanced bound state of fractional vortices of different components can be stable, if the free energy allows it. In between their positions, there are gradients of phase difference, which give positive contributions in the neutral sector, making unfavourable the splitting for a free energy like Eq. (2.5). Therefore if we start with an initial guess of two fractional separated vortices $(1,0)$ and $(0,1)$, they will merge in $(1,1)$ to find the minimum solution.

However if we add to the free energy Eq. (2.5) quartic terms, like the repulsive density-density interaction $\gamma|\psi_1|^2|\psi_2|^2$ where $\gamma > 0$, we can stabilize the two fractional vortices. In fact, if $\gamma > 0$, it is convenient to have this term the smallest possible, and that can be achieved by separating the fractional vortices, in order to maximize the area with the product of the densities equal to zero. Obviously separating the vortices creates a positive energy contribution in the neutral sector, so γ has to be big enough to overcome it.

In between the two fractional vortices all possible values of relative densities are taken. The same is true for the phase differences, therefore their gradients cause the counterflow to wrap itself up in all direction. This is what physically causes the Skyrmionic defects, this self-generated counterflow term, coming from Eq. (2.8b). The 2D Skyrmion topological charge can be written as

$$Q[\Psi] = \int \frac{i\epsilon_{ji}}{2\pi|\Psi|^4}\left[|\Psi|^2\partial_i\Psi^\dagger\partial_j\Psi + \Psi^\dagger\partial_i\Psi\partial_j\Psi^\dagger\Psi\right]dxdy \ \in \mathbb{Z}\,, \qquad (2.27)$$

where $\Psi^\dagger = (\psi_1^*, \psi_2^*, ..., \psi_N^*)$ for a N component system, and ϵ_{ji} is the permutation symbol. For the case of 2 components, the charge density inside the integral reduces to the term in Eq. (2.8b) (up to a flux quanta). Again the charge is an integer number, reflecting how many time the counterflow wrap itself up in all direction, and also its orientation (positive and negative integer). In our case the bound state of $(1,0)-(0,1)$ will have a charge $Q = \pm 1$. In fact Q equals the number of enclosed flux quanta ($\Phi_0 Q = \int \boldsymbol{B} dS$).

To have an even more physical intuition, and in particular to trace a parallelism with Skyrmions in the magnetic case, in two components we can project the matter fields vector Ψ on a Riemann sphere, with the so

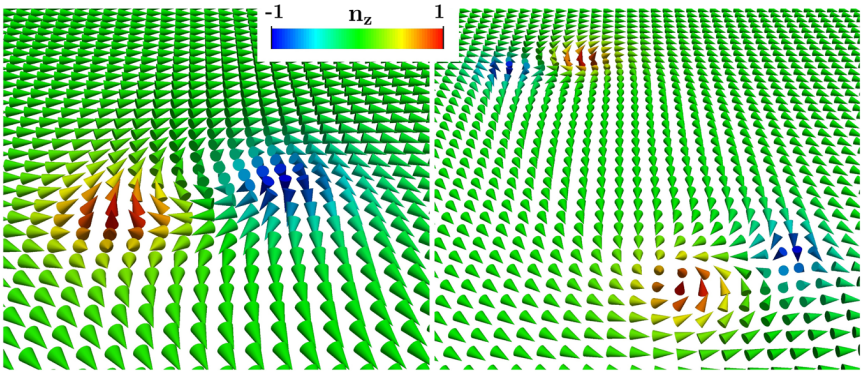

Figure 2.2: Texture of the pseudo-spin $\boldsymbol{n}$. The left panel shows a single-quanta solution with two fractional vortices, while the right panel corresponds to a bound state of 2 single quanta Skyrmion. The north (respectively, south) pole signals zero of ψ_2 (respectively, ψ_1) and thus the position of respective fractional vortices. It can be noted how the bound state has in the middle a uniform pseudo-spin, signaling the dipolar attractive force. Figure taken from reference [18].

called "pseudo-spin" map

$$\boldsymbol{n} = \frac{\Psi^\dagger \boldsymbol{\sigma} \Psi}{\Psi^\dagger \Psi}\,, \tag{2.28}$$

where $\boldsymbol{\sigma}$ are the spin-$\frac{1}{2}$ Pauli matrices. We will see in the next section why this mapping is not magic. For now let just look inside $\boldsymbol{n}$,

$$\boldsymbol{n} = \left[\frac{2|\psi_1||\psi_2|}{\rho^2}\cos\theta_{12}, \frac{2|\psi_1||\psi_2|}{\rho^2}\sin\theta_{12}, \frac{|\psi_1|^2 - |\psi_2|^2}{\rho^2}\right]. \tag{2.29}$$

The planar component xy are related to the counterflow of the two components (neutral sector), while the "zenith coordinate" to the relative density. Therefore we will be at zenith $n_z = 1$ when only the first component is present, so at the center of the ψ_2 fractional vortex ("spin up"), while we will be at nadir $n_z = -1$ when only the second is present, so the center of ψ_1 vortex ("spin down"). It can be easily checked that the module of the pseudo-spin is always one, being $\boldsymbol{n}$ living on the Riemann sphere.

Therefore the pseudo-spin behaves exactly like the unit vector of the local magnetization, and as in magnetic system its Skyrmion charge can be computed as

$$Q[\boldsymbol{n}] = \frac{1}{4\pi}\int \boldsymbol{n}\cdot(\partial_x \boldsymbol{n}\times\partial_y \boldsymbol{n})\,dxdy \;\in \mathbb{Z}\,, \tag{2.30}$$

where this equation is equivalent to the Eq. (2.27) in two components.

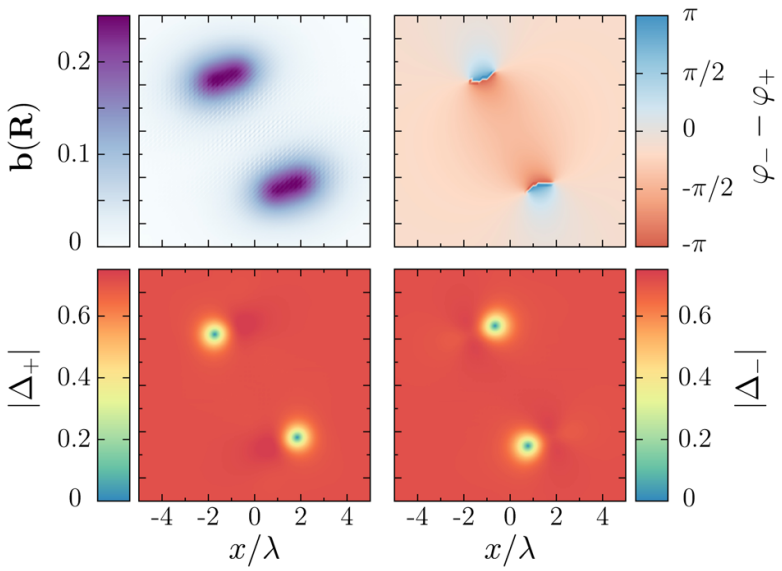

Figure 2.3: A close-up view of the bound state of two Skyrmions in right panel Fig. (2.2), carrying one flux quantum each. Each one is a well-localized bound state of two fractional vortices. The quantity displayed are: $\boldsymbol{b}(\boldsymbol{\mathcal{R}})$ magnetic field, $\varphi_- - \varphi_+$ phase difference, $|\Delta_\pm|$ first and second component densities. The dipole-like forces in the relative phase yields a long-range attraction, that binds the single-quanta vortices together. Note that the dipoles are antialigned in the bound state as dictated by relative phase interaction. Figure taken from reference [18].

An example of Skyrmion charge in two component system can be seen in Fig. (2.2). In the left picture, a single quanta solution with 2 fractional vortices, is clear how $\boldsymbol{n}$ wraps in all possible direction on the Riemann sphere. The right picture represents a bound state of two Skyrmion charges, coming from their dipole-like long-range interactions. It is exactly this property that make them interesting defects.

A pair of fractional vortices in a flux quanta have a dipole-like configuration of the relative phase, and this creates long-range forces, opening the possibility to multi-Skyrmion structure. Indeed the phase difference, that wants to minimize the area where it is different from its ground state, attracts the other Skyrmion, as can be seen in Fig. (2.3). Being a dipole force, the other Skyrmion must have an alternate north and south pole, otherwise they will repel. This property of Skyrmions can influence a lot the vortex lattice formation, for example the usual hexagonal symmetry could be unfavourable [19–21]. Moreover Skyrmions can have also long-range attractive interaction with boundaries, suggesting the possible abundance of these defects near them [18].

2.7 Topological solitons in GL model

A good reference for the underpinning mathematics of topological defects and topological solitons in general is [22]. In this section we will briefly focus on these mathematical details, always with an eye towards the physical meanings. This section is however not necessary to appreciate the results of the thesis, so the uninterested reader can safely skip this section.

The topological defects we are interested in, such as vortices and Skyrmions, fall into the broad category of topological *solitons*, where solitons are any solution of a set of partial differential equations that is stable against decay to the "vacuum solution" (the ground state). The most astonishing property of solitons, is that they behaves like particles, even if they come from continuous fields. This finite nature is due to the localized energy lump-like solutions that they exhibit. Solitons play an important role in effective field theory models of condensed matter systems, for example, as solutions to the Ginzburg-Landau equations.

The difference between *topological* solitons and other kinds of soliton, is that their stability is derived from the topological nature of the theory. Topological soliton solutions can be classified in homotopy classes, i.e. equivalence classes, with equivalence relation being the ability to linearly deform one map into another. Therefore each homotopy class cannot be transformed continuously into another class. So a solution with non-trivial class, exposed to a perturbation, can decay into other lower energy solutions in the same equivalence class, but it cannot alter continuously its class, reaching the vacuum solution for example. To do that a discontinuity need to be introduced, which requires infinite energy, due to the presence of gradients in the free energy.

For topological solitons to exist as stable solutions to a field theory, multiple requirements need to be satisfied, combining topological and energetic considerations. Obviously to apply topology the field needs to be continuous, but that is not sufficient. The first energetic consideration is that our theory, to be physical, has energy density decaying as $\rho \to \infty$, where ρ is the distance from the origin of our physical space. Having solitons finite energy density, we need boundary conditions imposing the field to be in its ground state on the boundary ($\rho \to \infty$). Therefore, in physical dimensions d, a field configuration $\phi : \mathbb{R}^d \to Y$, where Y is a general target manifold, defines the asymptotic map

$$\phi^\infty \ : \ S^{d-1}_\infty \mapsto \mathcal{V}\,, \tag{2.31}$$

where $\mathcal{V}$ is the space that contains all possible ground states, and the symbol S^n stands for n-sphere space, so for example S^1 is the circle, S^2 the surface of a 3D sphere, and so on. Hence S^{d-1}_∞ is the (d-1)-sphere

closed boundary at *infinity* in $\mathbb{R}^d$, that is homeomorphic to a sphere at $\rho \to \infty$.

In topology a *linear* theory is defined when a solution can be linearly transformed to any other solution with similar asymptotic map, for example GL equations Eq. (2.3). In this case if two different field solutions have homotopic asymptotic maps, then they are homotopic. Therefore the topological character of a field ϕ in a linear theory is determined uniquely by the homotopy class of its map ϕ^∞, which is an element of $\pi_{d-1}(\mathcal{V})$ homotopy group. The n-th homotopy group of M, $\pi_n(M)$, is defined as the group that collect all the maps from S^n into a given manifold M (space at least locally euclidean), where all the maps are subdivided in equivalent homotopy classes.

If we now consider the *nonlinear* case, we can exploit the finite energy condition in a different way. We can state that due to the presence of gradients in the free energy, at the infinite boundary we need ϕ^∞ to be a constant map, with a specific value picked out from $\mathcal{V}$ produced by the potential terms if present. In this way we are breaking any allowed symmetry in the ground state, and we can identify all points on the boundary as one. That allows us to do a topological compactification of the physical space $\mathbb{R}^d$ to S^d (in practice we are setting all the points on the boundary S^{d-1}_∞ as they were one single spatial point, the same as we take a paper, $\mathbb{R}^2$, and we merge together all its edges until we get a paper ball S^2). Our physical space is now a d-sphere, with homotopy group $\pi_d(Y)$ (where Y is again the target space of ϕ which is a closed compact manifold).

So reassuming, the non-trivial topological nature of the map from the physical space (boundary S^{d-1}_∞ or bulk compactified S^d for linear and nonlinear maps respectively) to the target space ($\mathcal{V}$ or Y respectively) leads to solitons. These topological solitons are classified then by the maps homotopy groups, and these homotopy groups will often coincide with the topological degree of the map (as we will see later in practical examples).

The requirements above are necessary for the existence of topological soliton solutions, but are not yet sufficient to demonstrate that such solutions are stable to spatial rescaling. This stability condition is addressed by Derrick *non-existence* theorem or scaling argument. This theorem applies to field theories defined in flat space, like $\mathbb{R}^d$, and it states that if the energy functional $\mathcal{F}(\lambda)$ has no fixed points with respect the spatial rescalings $\boldsymbol{x} \mapsto \lambda \boldsymbol{x}$, then there are no static solutions with finite energy other than the vacuum configuration, so no solitons are allowed. Heuristically it means that if we have a solution different from the vacuum, like a topological defect, we can spatially shrink it (λ decreasing) or stretch it (λ increasing) indefinitely while decreasing the energy. If there is a

minimum point with respect to λ with $\lambda \neq \infty$ then the soliton is energetically stable about this point and there is no way to shrink or stretch the defects indefinitely. The fact that there are not energetic reasons to not have a solitons does not imply immediately that we can have it always, but in general works (in fact it is just a non-existence theorem). The fixed point usually is produced by two terms in the free energy, one that decreases with λ and one that increases with it. The GL equations satisfy this condition due to the competition between the potential and derivative terms.

Now let us try to apply what we have learnt, in the case of ordinary vortices and Skyrmions, which on topological grounds are very different, as vortices belong to the "linear" category above, while Skyrmions belong to the "nonlinear" one.

Vortices, either fractional or composite, are complex field configurations characterized by the winding on the vacuum map (boundary map)

$$\psi^{\infty} \ : \ S^1_{\infty} \mapsto \mathcal{V} = S^1 \, . \tag{2.32}$$

As we said in Eq. (2.31) for general d dimensions, the first circle S^1 denotes the closed path faraway from the vortex core (that is homeomorphic to a circle) while the second one (the target circle) corresponds to the U(1) rotations of the ground state. So heuristically the map has the following meaning: it counts how many times the target circle is covered while going along the closed path faraway from the vortex core.

Therefore any map ψ^{∞} has a characteristic winding number N and therefore it belongs to the homotopy class of the maps ψ^{∞} with charge N. All together these classes can be collected in the homotopy group $\pi_1(S^1) = \mathbb{Z}$. The homotopy group $\pi_1(S^1)$ is an infinite cyclic group, and is isomorphic to the group $\mathbb{Z}$ of integers under addition: a homotopy class is identified with its winding number.

Skyrmion charges are derived instead by defining the vector of complex fields $\Psi^{\dagger} = (\psi_1^*, \psi_2^*)$ (in two components), which is a smooth holomorphic map $\mathbb{R}^2 \mapsto \mathbb{C}^2$, for 2D solutions. The crucial point is that Skyrmions only exist if the vortices in each component do not have coincident zeroes and hence the target space becomes $\mathbb{C}^2 \backslash \{0\}$. Now we can define the projection $\Sigma : \mathbb{C}^2 \backslash \{0\} \mapsto \mathbb{C}\mathrm{P}^1 \simeq S^2$, which is roughly speaking the stereographic projection of $\mathbb{C}^2$ on the Riemann sphere identified with the complex projective line $\mathbb{C}\mathrm{P}^1$, and so topologically equivalent to S^2. Finally, we note that Ψ recovers its ground state value as $\rho \to \infty$ and we can perform a one-point compactification of the plane, which is then homeomorphic to a sphere $\mathbb{R}^2 \cup \{\infty\} \simeq S^2$. Therefore now the composition $\phi = \Sigma \circ \Psi$ is

$$\phi \ : \ S^2 \mapsto Y = S^2 \, . \tag{2.33}$$

which has non-trivial topology due to winding, called Skyrmions (actually baby Skyrmions, as the real Skyrmions have one dimension more being $S^3 \mapsto S^3$).

Note that as we required the zero of Ψ to be removed from the target space for non-trivial topology to exist, the winding number here or Skyrmion charge can only be energetically conserved. This can be achieved by making it energetically favourable for the fractional vortices that form the composite multicomponent vortex not to coincide. This means their zeroes will not coincide and the zero has been effectively energetically removed from the target space of $\Psi \simeq \Psi/\{0\} : \mathbb{R}^2 \mapsto \mathbb{C}^2/\{0\}$.

The topological charge, rewritten for Ψ, is identical to Eq. (2.27). This equation can be safely used also for N-component case, where we can have $\mathbb{C}\mathrm{P}^{N-1}$ Skyrmion, where their charge Q can be viewed as QN spatially separated fractional vortices with combined flux adding up to Q flux quanta.

From the sketched derivation above, it is clear why the pseudo-spin $\boldsymbol{n}$ mapping works, indeed Eq. (2.28) has the role of stereographic projection Σ, so that $\boldsymbol{n} \ : \ S^2 \mapsto S^2$, with the charge Eq. (2.30) (Σ is just more easily extendable to multiple components). As with the vortex, we can define the homotopy class $\pi_2(S^2) = \mathbb{Z}$. It is also important to note that for the one-point compactification it is necessary to have $\boldsymbol{n}$ constant (i.e. Ψ recovers its ground state value) at the boundary of integration domain, so if there are Meissner currents, Q will be non-integer.

The critical difference between Skyrmions and vortices, is that the former required its map to be uniform at infinity (boundary) and its topological charge is set by the field distribution *inside* the infinite radius, while the latter has a non-uniform map at infinity and its charge is set by the *boundary* map. This difference is reflected by how we computethe charge, while both have an integral form, for vortices we must compute a closed line integral sufficiently faraway, while for Skyrmions we must perform a bulk integral.

As we have seen topological defects stem often from symmetries, indeed vortices and Skyrmions come from the U(1) (where Skyrmions need multiple fields). In the following chapter we will have a model breaking time-reversal symmetry, so $\mathbb{Z}_2$. This symmetry is discrete and the topological defects that stems from it are domain walls (DWs).

Domain wall treatment can be easily generalized from the defect called a kink in the 1D Sine-Gordon equation. In fact going to higher dimensions we have kink solutions that are independent of all but one spatial dimension (x), and these are what we call domain walls. Their homotopy group can be written as $\pi_0(\mathcal{V}) = \mathbb{Z}$ where $\mathcal{V}$ is the vacuum space of the variable having $\mathbb{Z}_2$. In our case this variable will be the phase difference θ_{12} with ground state $\theta_{12}^{\pm}$. The zero-sphere at infinity is just the set

$x = \pm\infty$, so the boundary in 1D. The charge can be trivially computed as

$$N = \frac{1}{\theta_{12}^{+} - \theta_{12}^{-}} \int \theta_{12}' \, dx \,, \tag{2.34}$$

where θ_{12}' is the derivative along x as θ_{12} is assumed to be independent of y. Physically what happens is that multiple ground states become disconnected, and θ_{12} for continuity has to interpolate between them, taking values outside the ground state.

The difference presented above between vortices, Skyrmions and domain walls characterizes the two main types of topological soliton; those in which the topology arises due to non-trivial vacuum values of a linear field at spatial infinity and the topological charge is an element of the homotopy group $\pi_{d-1}(\mathcal{V})$, and those in which there is a nonlinear field which is equivalent at infinity and the topological charge is associated with the mapping of the whole space into a target manifold Y, which gives an element of the homotopy group $\pi_d(Y)$ [22].

Chapter 3

Dirty two-band superconductors

The minimal model U(1) × U(1) serves as introduction of multicomponent superconductivity, but it implies independent matter conservation in each component, a condition rarely met. In particular in multiband superconductivity, i.e. when different components come from different electronic bands in the material, interband transitions of electrons lead to non-conservation of the particle number in each individual component. At the macroscopic (classical-field) level, this results in Josephson terms with structure $\psi_1\psi_2^* + \psi_1^*\psi_2$ (and higher orders), expressing the tunneling of a pair (or more) from a band to another one. These new terms bring along new physics inside the multicomponent GL equations, as for example the existence of phase modes (Leggett modes [17]) or the possibility of states with broken time-reversal symmetry (BTRS). BTRS states, like $s + is$, have been proposed for iron-based superconductors in particular range of parameters, and recently experimental evidences for $Ba_{0.27}K_{0.73}Fe_2As_2$ have been reported [23]. In this chapter, after the background about iron-based superconductors and the microscopic theory is laid down, the simplest possible model that supports $s+is$ state is discussed, a two-band superconductor with interband impurity scattering.

3.1 Iron-based superconductors

This section has the purpose to highlight some important concepts in iron-based superconductors and to put the following model in a physical prospective, a complete discussion on these materials can be found in [24–26].

Iron-based superconductors (FeSCs) were discovered in 2008 with the compound $LaFeAsO_{1-x}F_x$, having a critical temperature of 26 K [16].

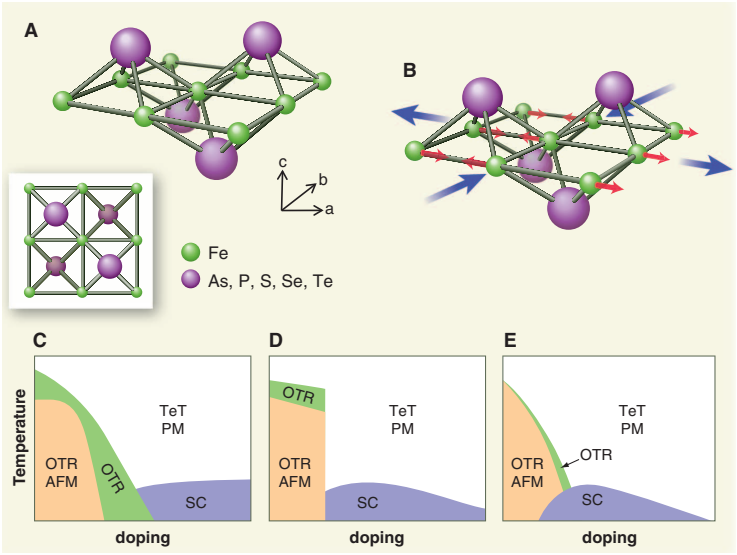

Figure 3.1: (A) Structural building block of FeSCs. (Inset) Top view of the FeX trilayer. The arrows a, b, and c are the crystallographic directions. (B) The AF order effect on the lattice. The red arrows represent the magnetic moments, and the blue ones indicate the directions of structural distortion. (C-E) Schematic phase diagrams for three families of Fe-based compounds (from left to right $CeFeAsO_{1-x}F_x$, $LaFeAsO_{1-x}F_x$, and $Ba(Fe_{1-x}Co_x)_2As_2$). OTR, orthorhombic; TeT, tetragonal crystal structure; AFM, antiferromagnetic; SC, superconducting; PM, paramagnetic phase. Taken from reference [25].

The following years entire families of materials were synthesized, reaching the critical temperature of 55 K, and capturing the attention of the superconductivity community. The existence of this new class of high temperature superconductors is important because parallelisms and differences with the well known cuprates could shed some light on the essential ingredients that drive these materials to have an high T_c.

The discovered FeSCs come in many chemical compositions, but the common building block is FeX, where X is typically a pnictide like As or P (when this is the case these materials are also called iron pnictides). The structure of FeX is a trilayer consisting of a square array of Fe sandwiched between two checkerboard layers of X (see Fig. (3.1)). These trilayers are separated by layers of alkali, alkaline earth, or rare earth atoms and oxygen/fluorine with a bridging function. The superconductivity is believed to originate from d orbitals of Fe in FeX trilayers [25].

Like cuprates superconductors, they are obtained from antiferromagnetic compounds (AFs) by doping or even by applying pressure, and phase diagrams like in Fig. (3.1) are very similar between the two classes. In

both cases the superconductivity region is a "dome", so there is always an optimal doping for reaching the highest critical temperature for that compound. But there are also many differences between cuprates and pnictides, for example while in cuprates the AF phase always vanishes before superconductivity appears, in FeSCs can happen that they coexist in a limited region (see Fig. (3.1E)). More importantly the undoped state is a semimetal in FeSCs, while in cuprates is a Mott insulator, so effects of correlations between electrons are smaller in FeSCs. Finally the symmetry of the gap in cuprates is universally d-wave, while in FeSCs can be different from material to material. Nevertheless, it seems possible that the ultimate source of the pairing interactions is fundamentally similar, therefore what causes different symmetries is the different geometry of Fermi surfaces (FSs), especially the fact that in FeSCs we can have multiple FSs in contrast to cuprates.

3.1.1 Gaps symmetry

In iron-based superconductors usually we can have 3-4 bands crossing the Fermi energy, producing hole and electron pockets. An example of a typical Brillouin Zone (BZ) can be found in Fig. (3.2). In pnictides the physical key aspects can be grasped by analyzing the 2D BZ of the Fe square lattice, instead of the full 3D, in fact the pockets are more or less cylindrical. In almost all pnictides we have two concentric hole pockets around Γ point and electrons and hole pockets, varying with doping, in tetragonal M or X points (in Fig. (3.2) we have only electron pockets in X points). Each pocket has, in principle, the possibility of having its own gap function that depends in general on intra- and inter-band pairing interactions.

It has been conjectured that the pairing interaction is repulsive and driven by AF spin fluctuations for both cuprates and FeSCs. This pairing interaction has a potential $U(\boldsymbol{k}, \boldsymbol{k}')$, where $\boldsymbol{k}$ and $\boldsymbol{k}'$ are the wave vectors of the interacting electrons. $U(\boldsymbol{k}, \boldsymbol{k}')$ is peaked for some value of $\boldsymbol{Q} = \boldsymbol{k}' - \boldsymbol{k}$, called nesting vector, and figuratively we can see it as a vector connecting Fermi surfaces in the BZ (for example in Fig. (3.2) the nesting vector is $\boldsymbol{Q} = (\pi, 0)$, where the lattice points distance is set to 1). The most favorable nesting vector is the one able to connect as more FS states as possible (and so being more effective than others), therefore typically coincides with the one linking parallel pieces of FSs.

For spin singlet pairs, so for even spatial symmetry of gap wave function like s- or d-wave cases, AF spin fluctuations are repulsive, and can lead to pairing if there is a sign change in the gap functions. Naively the sign change is crucial to extract an attractive component from the repulsive screened Coulomb interaction due to AF spin fluctuations. Such interaction could be written as $\int d\boldsymbol{k} d\boldsymbol{k}' \Delta_i(\boldsymbol{k}) U(\boldsymbol{k}, \boldsymbol{k}') \Delta_j(\boldsymbol{k}')$, where $\Delta_i(\boldsymbol{k}) =$

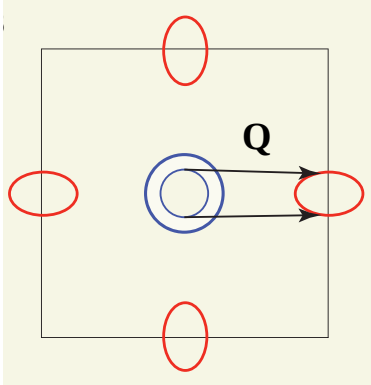

Figure 3.2: Schematic sketch of the Fermi surface sheets in the BZ of $Ba_{1-x}K_xFe_2As_2$ at moderate doping level of $x = 0.4$, with two small concentric hole pockets around $\Gamma = (0, 0)$ point and slightly elliptical electron pockets around $X = [(\pm\pi, 0), (0, \pm\pi)]$ points. For simplicity the "unfolded" BZ is sketched, i.e. the one containing 1 Fe atom, even if the physical one should have 2 Fe atoms per unit cell, having the As atoms an alternating pattern above and below the Fe layer as seen in Fig. (3.1A). The colors are related to the sign of the gaps, blue positive and red negative. The vectors represents the quasi-nesting vectors (quasi- due to different shapes of FSs) $\boldsymbol{Q} = (\pi, 0)$ responsible for inter-FS scattering. Taken from reference [25].

$|\Delta_i|e^{i\varphi_i}$ are the complex gap functions [26]. In cuprates there is only one gap function $\Delta(\boldsymbol{k})$, so if the $U(\boldsymbol{k}, \boldsymbol{k}')$ is positive (repulsive) and peaked at $\boldsymbol{Q} = (\pi, \pi)$ (as for cuprates), the only possibility to have a negative value for the previous interaction energy is to have a d-wave symmetry, which implies that the gap changes sign between $\boldsymbol{k}$ and $\boldsymbol{k}' = \boldsymbol{k} + \boldsymbol{Q}$ (therefore with a phase difference of π).

However in FeSCs, having multiple pockets, there is also the possibility to retain s-wave symmetry but changing sign between different Fermi surfaces [27]. This gaps structure is called $s_\pm$ and the majority of the superconductivity community believes it applies for weakly doped FeSCs (for higher doping we can have also the presence of d-wave characters). For example in Fig. (3.2) we can see how the vector $\boldsymbol{Q} = (\pi, 0)$ is enforcing a changing in sign between hole pockets in Γ and electron pockets in X.

The simplest model that can have $s_\pm$ structure is a two-band model, and has the ability to capture some of the physics, being the two concentric holes close in size, so in certain situations approximable as one band. In this way we can have a simple description of the pairing mechanism, where there is a sign change of $\Delta_i(\boldsymbol{k})$ between electron and hole pock-

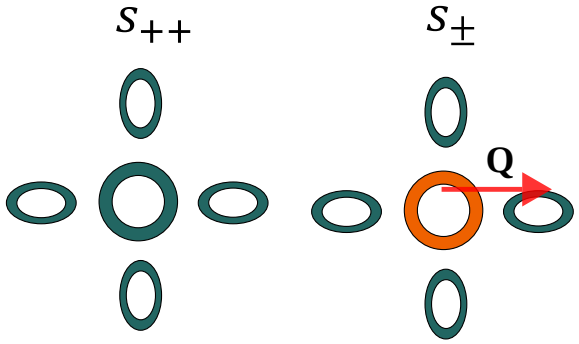

Figure 3.3: Cartoon of the order parameters in the 2D 1-Fe Brillouin Zone for a two-band FeSCs with s-wave symmetry. The thickness stands for the module of the order parameter while the different colors stands for the different signs of the gaps. $\boldsymbol{Q} = (\pi, 0)$ is the quasi-nesting vector that enforces the sign changing. Taken from reference [24].

ets. In case no sign change happens we call the state s_{++} as depicted in Fig. (3.3). It is worth noting that both $s_{\pm}$ and s_{++} belong to the same symmetry class (s-wave or more properly A_{1g}), the only difference is in the order parameter structure, defined as the k-dependence of $\Delta_i(\boldsymbol{k})$ within a given symmetry class. Different gap structures can anyway lead to many different properties.

3.1.2 Impurities effects on $s_{\pm}$ states

Impurities effects were studied in the context of conventional s-wave superconductors by Anderson [28]. His result was named Anderson theorem and states that the bulk T_c as well as the average bulk superconducting gap are unaffected by weak non-magnetic impurity scattering [29]. The reason is naively understandable in the following way: scattering mixes states inside the band, but for isotropic s-wave each state is equivalent to another one, contributing in the gap with the same phase. That is no longer true in cuprates for example, where a d-wave symmetry like $d_{x^2-y^2}$ makes the states $\boldsymbol{k_1} = (k_x, 0)$ and $\boldsymbol{k_2} = (0, k_y)$ contributing with different phase, so scattering between them brings the system toward a s-wave situation and effectively suppresses the order parameter being s-wave not favorable for superconductivity in these materials.

In two-band $s_{\pm}$ systems the effect depends on two factors: the type of impurity scattering and the pair interactions. The impurity scattering could be only intra-band, and therefore producing a mixing of states just inside the different pockets, making Anderson theorem still valid with the subsequent no effect of the impurities. But the defects can also scat-

ter carriers with large momentum change and therefore give comparable intra-band and inter-band scattering. In this case the $s_{\pm}$ state is not favorable, and the impurity scattering gradually averages out the two gaps and the closer they get to each other, the less effective the pair-breaking from impurities is [30, 31]. This averaging weakens the SC state and decreases the critical temperature. Now what happen depends on the pair interactions, if they can sustain a s_{++} symmetry the SC states can survive and T_c saturates, on the contrary if $s_{\pm}$ is necessary for the existence of superconductivity, the order parameter is completely suppressed. These two scenarios are decided by the interplay between spin fluctuations (repulsive) and electron-phonon coupling (attractive) [32]. This interplay can be effectively described by the coupling matrix $\hat{\Lambda}$, which has as elements the intra-band pairing interactions λ_{ii} and the inter-band ones λ_{ij}. In the context of pnictides usually λ_{ii} are positive (attractive) while λ_{ij} are negative (repulsive). So if the determinant of this matrix is positive (attractive intra-band interactions dominate) the system can sustain s_{++}, while if it is negative not.

The disorder induced transition $s_{\pm}$-s_{++} can happen in two qualitative different ways as shown in Fig. (3.4): the first one is a crossover where the weaker gap goes to zero and then reappears with opposite phase, in order to have same phase as the stronger one; the second way involves a continuous transformation through the intermediate complex $s+is$ state (can be thought as an $s_{\pm}+is_{++}$) where the phase difference between the two gaps is a value different from 0 or π and where the gaps modules never go to zero [30, 31, 33].

3.1.3 s + *i*s time-reversal symmetry breaking

The $s+is$ state is called in this way because it breaks the time-reversal symmetry (BTRS), in fact complex conjugation ($s \pm is$) leads to another ground state that cannot be rotated back to the initial ground state by a gauge transformation. Complex conjugation is related to the transformation $t \to -t$, i.e. time-reversal transformation, and here the name of the symmetry. Therefore $s+is$ states do not break any crystal symmetries and represents a new type of superconducting state beyond the lattice point group-based classification. Such states were discussed in a wide range of systems, and in particular in three-band superconductors with frustrated interband interactions [34–38].

The s +is states have been predicted to host a broad range of interesting new phenomena, among which can be mentioned different massless [39] and "phase-density mixed" [36, 37, 40, 41] collective modes, unconventional thermoelectric properties [42, 43], additional mechanisms of damping of the vortex motion [44], and unconventional magnetic signatures induced by defects [45, 46].

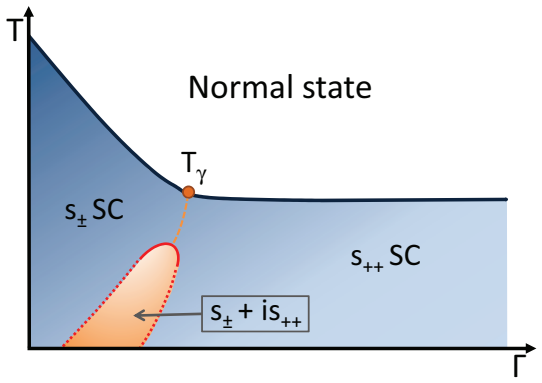

Figure 3.4: Phase diagram of two-band SC with weak repulsive inter-band pairing. The x-axis represents the inter-band impurity scattering rate Γ. The orange dashed line $T_\gamma(\Gamma)$ denotes the temperatures at which we have the direct $s_\pm$ to s_{++} transition (crossover), and the orange region represents the complex $s_\pm + is_{++}$ state. We can notice how in this case T_c saturates to a constant value. Taken from reference [31].

Multiple broken symmetries in $s+is$ superconductors give rise to several strongly disparate coherence lengths. This can lead to a state with attractive intervortex interaction, originating in the magnetic field penetration length being smaller than some, and larger than other coherence lengths, thus leading to type 1.5 superconductivity [36, 47].

Besides vortices, the $s + is$ state also allows other types of topological excitations that include domain walls and Skyrmions [48–50]. The s +is state also exhibits complex beyond-mean-field physics with new fluctuation-induced phases [51–53]. We will see some of these properties in the following sections.

3.2 Microscopic theory of superconductivity

An important characteristic of the Ginzburg-Landau model under study, is that it is derived directly from the microscopic theory of multiband superconductors, and therefore its phenomenology can be linked directly to microscopic parameters. In this section we review rapidly the modern microscopic apparatus used for superconductors, arriving at the so called Usadel equations, microscopic equations for superconductors in the dirty limit, stressing in particular all the approximations done along the way. The reader interested mainly in the physical phenomena rather than in the microscopic derivation of standard equations may skip this section, and go directly to Section 3.3.

3.2.1 Gor'kov equations and Matsubara Green functions

The complete microscopic formalism treatment can be found in [54, 55], here we limit ourselves to a simple review, highlighting the fundamental steps. The microscopical theory of superconductivity was developed by Bardeen, Cooper, Schrieffer (BCS) in 1957 [9, 56, 57], where it was noted that a normal state of a metal is unstable to the formation of bound states of electrons with opposite spins and momenta. The BCS theory is written in standard particle creation and annihilation operators for Bloch states, specified by a wave vector $\boldsymbol{k}$ and spin σ. However, the elementary excitations of a SC state are no longer single particle states, but instead broken Cooper pair states. This produce a very cumbersome treatment, especially for finite temperature. A new mathematical formulation of BCS was therefore developed by Bogoliubov [58], where he introduced the concept of coherent mixtures of particles and holes, where an excite state has always an electron-like and a hole-like part, and this led to the Bogoliubov-deGennes (BdG) equation. BdG equation is however still difficult to solve in general case and not ideal to work with in case of random impurity. The pursuit of a more manageable treatment brought to the introduction of Green function formalism, and their quasiclassical approximation, which is currently the modern framework for superconductivity.

The application of the quantum field theory to BCS model was performed by Gor'kov in 1958 [59]. To derive Gor'kov equations we start from the BCS Hamiltonian:

$$\begin{aligned}\hat{H} = &\int d\xi_1 \hat{\psi}^\dagger(\xi_1)\hat{\mathcal{H}}_k\hat{\psi}(\xi_1) \\ &+ \frac{1}{2}\int d\xi_1 \int d\xi_1' \mathcal{V}(|\boldsymbol{r}_1 - \boldsymbol{r}_1'|)\hat{\psi}^\dagger(\xi_1)\hat{\psi}^\dagger(\xi_1')\hat{\psi}(\xi_1')\hat{\psi}(\xi_1)\,, \end{aligned} \tag{3.1}$$

where $\xi_1 \equiv (\boldsymbol{r}_1, \alpha_1)$ is the particle state coordinate with $\boldsymbol{r}_1$ spatial coordinate and α_1 spin state. $\mathcal{V}(|\boldsymbol{r}_1 - \boldsymbol{r}_1'|)$ is a two-particles potential and $\hat{\mathcal{H}}_k$ the kinetic single particle Hamiltonian (containing also the vector potential $\boldsymbol{A}$ to include phenomena in magnetic field), while $\hat{\psi}^\dagger(\xi_1)$ and $\hat{\psi}(\xi_1)$ the creation and annihilation operator. For the following derivation it is better to use the notation

$$\hat{\psi}_1(\xi_1) \equiv \hat{\psi}(\xi_1)\,, \qquad \hat{\psi}_2(\xi_1) \equiv \hat{\psi}^\dagger(\xi_1)\,, \tag{3.2}$$

so that $\hat{\psi}_i^\dagger(\xi_1) = \hat{\psi}_{3-i}(\xi_1)$ holds $(i = 1, 2)$. Now we introduce the field operators, in the Heisenberg representation, and their equation of motion

$$\hat{\psi}_i(1) \equiv \hat{\psi}_i(\xi_1, \tau_1) \equiv \mathrm{e}^{\tau_1\hat{H}}\hat{\psi}_1(\xi_1)\mathrm{e}^{-\tau_1\hat{H}}\,, \tag{3.3}$$

$$\frac{\partial\hat{\psi}_i(1)}{\partial\tau_1} = \mathrm{e}^{\tau_1\hat{H}}[\hat{H}\hat{\psi}_i(\xi_1) - \hat{\psi}_i(\xi_1)\hat{H}]\mathrm{e}^{-\tau_1\hat{H}}\,, \tag{3.4}$$

where $\tau_1 \to it_1/\hbar$ is the imaginary time variable. Now inserting Eq. (3.1) in Eq. (3.4) we can obtain

$$\frac{\partial\hat{\psi}_i(1)}{\partial\tau_1} = (-1)^i \left[\hat{\mathcal{H}}_k^i\hat{\psi}_i(1) + \int d\xi_1' \mathcal{V}(|\boldsymbol{r}_1 - \boldsymbol{r}_1'|)\hat{N}\hat{\psi}_2(1')\hat{\psi}_1(1')\hat{\psi}_i(1)\right], \tag{3.5}$$

where $\hat{N}$ is the normal-ordering operator that places the creation operators to the left of the annihilation ones multiplying by $\sigma = -1$ for each exchange.

Now it is arrived the moment to introduce the Matsubara Green functions, defined as

$$\begin{aligned} G_{ij}(1,2) &\equiv -\theta(\tau_1 - \tau_2)\left\langle\hat{\psi}_i(1)\hat{\psi}_{3-j}(2)\right\rangle + \theta(\tau_2 - \tau_1)\left\langle\hat{\psi}_{3-j}(2)\hat{\psi}_i(1)\right\rangle \\ &= \left\langle\hat{T}_\tau\hat{\psi}_i(1)\hat{\psi}_{3-j}(2)\right\rangle \equiv G_{ij}(\xi_1,\xi_2;\tau_2-\tau_1)\,, \end{aligned} \tag{3.6}$$

where $\theta(x)$ is a step function and $\langle ...\rangle$ is the ensemble average that accounts for all possible paths from (ξ_1,τ_1) to (ξ_2,τ_2). $\hat{T}_\tau$ is the time-ordering operator that depends only on $\tau_2 - \tau_1$ for stationary problem, and which rearranges field operators to its right in descending order of τ, with the right sign. Diagonal elements $G_{ii}(1,2)$ are composed of a pair of creation and annihilation operators, which remain finite even for normal states. In contrast, the off-diagonal elements are characteristic of superconductivity, and are composed by two annihilation or two creation operators, and therefore are called "anomalous" Green functions. It is also sometimes convenient to explicitly separate them using the notation:

$$\begin{aligned} G_{11}(1,2) &\equiv G(1,2)\,, \quad G_{22}(1,2) \equiv -G^\dagger(1,2) \\ G_{12}(1,2) &\equiv F(1,2)\,, \quad G_{21}(1,2) \equiv -F^\dagger(1,2)\,. \end{aligned} \tag{3.7}$$

Regular Green functions hold information about the transport probabilities of single particles. More precisely $G(1,2)$ (resp. $G^\dagger(1,2)$) describes the probability amplitude for a particle(hole) to move coherently from the state ξ_1 to ξ_2 in time interval $\tau_2 - \tau_1$, affected by all kind of interactions (note that here the time is imaginary, in fact they are called "Matsubara" Green function, to be distinguished from the real-time ones). Therefore once they are known, all the system single-particle properties are known (like density of states and electrical current).

Differently the "anomalous" Green functions are related to Cooper pairs and their pairing coherence, in fact $F(1,2)$ (resp. $F^\dagger(1,2)$) can be seen as the probability to "find", or better to annihilate, in ξ_2 the remaining electron(hole) in a Cooper pair, after a time interval $\tau_2 - \tau_1$ from the first electron(hole) annihilation in ξ_1. Therefore it describes pair correlations and it is related to the superconducting order parameter,

which is a measure of the strength of the superconducting energy gap (indeed it uses the same symbol).

$$\Delta(\xi_1, \xi_2) \equiv \mathcal{V}(|\boldsymbol{r}_1 - \boldsymbol{r}_1'|) F(\xi_1, \xi_2; 0)\,. \tag{3.8}$$

More precisely we can see in Eq. (3.8) how the SC order parameter is proportional to the value of the anomalous Green function at coincident temporal arguments, and so corresponding to the wave function of a Cooper pair. This quantity is called "order parameter" because it will appear naturally as effective order parameter, when Ginzburg-Landau expansion close to T_c will be performed, linking finally the phenomenological theory of the SC phase transition with microscopic physics [10].

After this digression on Green functions we are now in position to derive Gor'kov equations. In order to do that we differentiate the Green functions obtaining

$$\begin{aligned}\frac{\partial G_{ij}(1,2)}{\partial \tau_1} =& -\delta(\tau_1 - \tau_2)\left[\left\langle \hat{\psi}_i(1)\hat{\psi}_{3-j}(2)\right\rangle + \left\langle \hat{\psi}_{3-j}(2)\hat{\psi}_i(1)\right\rangle\right] \\ & - \left\langle \hat{T}_\tau \frac{\partial \hat{\psi}_i(1)}{\partial \tau_1}\hat{\psi}_{3-j}(2)\right\rangle ,\end{aligned} \tag{3.9}$$

where $\delta(x)$ is the Dirac delta. Now substituting Eq. (3.5) in Eq. (3.9) and doing simplifications we get

$$\begin{aligned}\frac{\partial G_{ij}(1,2)}{\partial \tau_1} =& -\delta_{ij}\delta(1,2) - (-1)^i\Bigg[\hat{\mathcal{H}}_k^i \left\langle \hat{T}_\tau \hat{\psi}_i(1)\hat{\psi}_{3-j}(2)\right\rangle \\ & + \int d\xi_1' \mathcal{V}(|\boldsymbol{r}_1 - \boldsymbol{r}_1'|) \times \left\langle \hat{T}_\tau[\hat{N}\hat{\psi}_2(1')\hat{\psi}_1(1')\hat{\psi}_i(1)]\hat{\psi}_{3-j}(2)\right\rangle\Bigg] ,\end{aligned} \tag{3.10}$$

where the last term is a two-particle Green function. Now we apply the first serious approximation, using Wick's decomposition theorem and transforming the ensemble average of four field operators (the two-particle Green functions) in pair averages combinations. This is equivalent to adopt a mean-field approach, indeed basically we are replacing some operators (actually pair of operators) in the Hamiltonian by their mean values, assuming that deviations from those are small. And exactly in this process, the Cooper pairs condensation manifest itself analytically as the appearance of anomalous Green functions, described in the previous digression. Following the Wick's theorem we can approximate (for $i = 1$

and so without $\hat{N}$)

$$\begin{aligned}
&\int d\xi_1' \mathcal{V}(|\boldsymbol{r}_1 - \boldsymbol{r}_1'|) \left\langle \hat{T}_\tau \hat{\psi}_2(1') \hat{\psi}_1(1') \hat{\psi}_1(1) \hat{\psi}_{3-j}(2) \right\rangle \\
\approx &\int d\xi_1' \mathcal{V}(|\boldsymbol{r}_1 - \boldsymbol{r}_1'|) \Bigg[\left\langle \hat{\psi}_2(1') \hat{\psi}_1(1') \right\rangle \left\langle \hat{T}_\tau \hat{\psi}_1(1) \hat{\psi}_{3-j}(2) \right\rangle \\
&- \left\langle \hat{\psi}_2(1') \hat{\psi}_1(1) \right\rangle \left\langle \hat{T}_\tau \hat{\psi}_1(1') \hat{\psi}_{3-j}(2) \right\rangle + \left\langle \hat{\psi}_1(1') \hat{\psi}_1(1) \right\rangle \left\langle \hat{T}_\tau \hat{\psi}_2(1') \hat{\psi}_{3-j}(2) \right\rangle \Bigg] \\
= &- \int d\xi_1' \Big[\mathcal{U}_{HF}(\xi_1, \xi_1') G_{1j}(1', 2) + \Delta(\xi_1, \xi_1') G_{2j}(1', 2) \Big] . \qquad (3.11)
\end{aligned}$$

In the equation Eq. (3.11) we identify the Hartree-Fock potential (also called generally self-energy) $\mathcal{U}_{HF}(\xi_1, \xi_1')$, that includes all single particle interactions, and the pair potential $\Delta(\xi_1, \xi_1')$, that express the energy gained by forming pair bound states and it coincides with the order parameter in eq. Eq. (3.8). From this point we substitute equations like Eq. (3.11) in Eq. (3.10), and we write equations for the Fourier coefficients ($\tau \to \omega_n$) where ω_n are the Matsubara frequencies (and their cut-off frequency is Ω_d, the Debye frequency). We can express then concisely all the 4 equations ($i, j = 1, 2$) in 2×2 matrix notation (these matrices live in the particle-hole space, called Nambu space, that is a generalization of the phase space, involving multiple Hamiltonians). In addition we can explicit the spin degree of freedom as matrices, so for example $F(\xi_1, \xi_2, \omega_n) \equiv F_{\alpha_1 \alpha_2}(\boldsymbol{r}_1, \boldsymbol{r}_2, \omega_n) \to \underline{F}(\boldsymbol{r}_1, \boldsymbol{r}_2, \omega_n)$ where $\alpha = \uparrow, \downarrow$ and $\underline{F}(\boldsymbol{r}_1, \boldsymbol{r}_2, \omega_n)$ a 2×2 matrix . In this way the final Gor'kov equation will be in a 4×4 Nambu$\otimes$Spin space:

$$\begin{aligned}
&\begin{bmatrix} (i\hbar\omega_n - \hat{\mathcal{H}}_k)\underline{\sigma}_0 & \underline{0} \\ \underline{0} & (i\hbar\omega_n + \hat{\mathcal{H}}_k^*)\underline{\sigma}_0 \end{bmatrix} \hat{G}(\boldsymbol{r}_1, \boldsymbol{r}_2; \omega_n) - \int d^3 r_3 \hat{\mathcal{U}}_{BdG}(\boldsymbol{r}_1, \boldsymbol{r}_3) \hat{G}(\boldsymbol{r}_3, \boldsymbol{r}_2; \omega_n) \\
&\qquad = \hat{\delta}(\boldsymbol{r}_1, \boldsymbol{r}_2) , \qquad (3.12)
\end{aligned}$$

where $\underline{\sigma}_0$ is the identity matrix and we have identified:

$$\hat{G}(\boldsymbol{r}_1, \boldsymbol{r}_2; \omega_n) \equiv \begin{bmatrix} \underline{G}(\boldsymbol{r}_1, \boldsymbol{r}_2; \omega_n) & \underline{F}(\boldsymbol{r}_1, \boldsymbol{r}_2; \omega_n) \\ -\underline{F}^*(\boldsymbol{r}_1, \boldsymbol{r}_2; \omega_n) & -\underline{G}^*(\boldsymbol{r}_1, \boldsymbol{r}_2; \omega_n) \end{bmatrix} , \qquad (3.13)$$

$$\hat{\mathcal{U}}_{BdG}(\boldsymbol{r}_1, \boldsymbol{r}_2) \equiv \begin{bmatrix} \underline{\mathcal{U}}_{HF}(\boldsymbol{r}_1, \boldsymbol{r}_2) & \underline{\Delta}(\boldsymbol{r}_1, \boldsymbol{r}_2) \\ -\underline{\Delta}^*(\boldsymbol{r}_1, \boldsymbol{r}_2) & -\underline{\mathcal{U}}_{HF}^*(\boldsymbol{r}_1, \boldsymbol{r}_2) \end{bmatrix} , \qquad (3.14)$$

$$\hat{\delta}(\boldsymbol{r}_1, \boldsymbol{r}_2) \equiv \begin{bmatrix} \delta(\boldsymbol{r}_1, \boldsymbol{r}_2)\underline{\sigma}_0 & 0 \\ 0 & \delta(\boldsymbol{r}_1, \boldsymbol{r}_2)\underline{\sigma}_0 \end{bmatrix} . \qquad (3.15)$$

The matrix $\hat{\mathcal{U}}_{BdG}(\boldsymbol{r}_1, \boldsymbol{r}_2)$ is the same appearing in the Bogoliubov-deGennes eigenvalue equation, where eigenstates are expressed in quasiparticles while here in Green functions. Therefore the two equations are exactly the same, just two different formulation of a mean-field treatment of superconductivity.

3.2.2 Quasiclassical approximation and dirty limit

As they are, Gor'kov equations are not easier to solve with respect to BdG equations, but they are a convenient starting point for introducing simplifications. The first one to be introduced is the quasiclassical approximation, that reduce enormously the complexity of the equations. Cooper pairs are non-local objects with size of the order of the coherence length (for conventional SC) and therefore much larger than the Fermi wavelength λ_F. However the Green functions contains also fast oscillation on the scale of λ_F due to self-interference effects. These fast oscillations can be neglected when one is interested solely in superconductivity, which only feels the average of such oscillations. The main idea of the quasiclassical approximation is that the relative coordinate $\boldsymbol{r}_{12} = \boldsymbol{r}_1 - \boldsymbol{r}_2$ is responsible for the fast oscillations in the Green functions, while the center of mass $\boldsymbol{R} = (\boldsymbol{r}_1 + \boldsymbol{r}_2)/2$ for the slow ones. Therefore to neglect the irrelevant information coming from fast part, one could just average out the relative coordinate. Quantitatively this approximation holds when the energy gap is much smaller than the Fermi energy ($|\Delta| \ll E_F$).

A way to do this procedure is through the Wigner transform applied to the Green functions, i.e. the Fourier transform with respect their relative coordinates. In this way we can separate the fast and slow part of the spectrum, obtaining a relative momentum $\boldsymbol{k}$ that eventually will be integrated over all the possible energies (through the variable $\xi_k = \hbar^2 k^2/2m - \mu$). In this way we can define the 4 quasiclassical Green functions as

$$\hat{g}(\boldsymbol{R}, \boldsymbol{k}_F; \omega_n) \equiv \frac{i}{\pi} \int d\xi_k \int d^3 r \, \mathrm{e}^{-i\boldsymbol{k}\cdot\boldsymbol{r}_{12}} \hat{G}(\boldsymbol{r}_1, \boldsymbol{r}_2; \omega_n) \,, \tag{3.16}$$

where only the dependence on the shape of the Fermi surface (FS) it is left ($\boldsymbol{k}_F$ variable) and the matrix $\hat{g}$ has elements like $\underline{g}, \underline{f}$ and their complex conjugations. Applying the quasiclassical approximation to all Gor'kov equation Eq. (3.12) we get the so called "Eilenberger" equation [60]. In addition we do for now another strong approximation, placing $\underline{\mathcal{U}}_{HF} \to \underline{0}$, so consider electrons independent (apart from the attractive pair potential). In this case we don't have spin dependence so we use spin-independent green function ($\underline{f} \to f$). Now exploiting symmetries between quasiclassical Green functions and the normalization condition $|g|^2 + f f^\dagger = 1$ we actually just need to solve the (1,2) element of the Eilenberger equation, that can be written as:

$$\hbar \boldsymbol{v}_F \boldsymbol{\Pi} f + 2\omega_n f - 2\Delta g = 0 \,, \tag{3.17}$$

where $\boldsymbol{v}_F$ is the Fermi velocity and the kinetic operator is defined as $\boldsymbol{\Pi} = \boldsymbol{\nabla} + iq\boldsymbol{A}$ where $q = 2e/\hbar$ is the gauge coupling, related to Cooper pair charge. Here we can see where the name quasiclassical came from, in

fact the Eilenberger equation Eq. (3.17) describe a mixture of classical and quantum mechanics. It makes use of quantum mechanical field operators to find the probability amplitudes (the Green functions) of the motion of classical particles with velocity $\boldsymbol{v}_F$ (it is a transport-like equation). This equation can be already used to describe very clean superconductors like in [61, 62].

In presence of *impurity* the independent electron approximation cannot be used, and we are forced to introduce an additional impurity self-energy due to impurity scattering. To do that we assume a large amount of random non-magnetic impurities in the Born approximation, which implies that the scattering potential is small compared to the characteristic atomic potential (therefore integration will be just on the FS). Therefore we have to add to Eq. (3.17) a new term

$$n_{imp} \int \frac{dA_{\boldsymbol{q}}}{v_{\boldsymbol{q}}} |u_{\boldsymbol{kq}}|^2 [g(\boldsymbol{k}) f(\boldsymbol{q}) - f(\boldsymbol{k}) g(\boldsymbol{q})] \,, \tag{3.18}$$

where $\frac{dA_{\boldsymbol{k}}}{v_{\boldsymbol{k}}}$ means integration over the FS with the local density of states $\frac{1}{v_{\boldsymbol{k}}}$, $u_{\boldsymbol{kq}}$ is the scattering amplitude, n_{imp} the density of impurities, $v_{\boldsymbol{k}}$ the normal group velocity on the FS, the wave vectors $\boldsymbol{k}$ and $\boldsymbol{q}$ lie on the FS, and the other dependencies of $g(\boldsymbol{k}, \boldsymbol{r}, \omega_n)$ (resp. f) are not expressed (here we change notation $\boldsymbol{R} \to \boldsymbol{r}$).

As we said the dependence on $\boldsymbol{k}$ of quasiclassical Green functions makes them sensitive to the shape of the FS, and this greatly complicate solving the non-linear Eilenberger equations, especially in case of complicated FS or disconnected FS sheets, like in multiband SC material. However the situation can be simplified in the dirty limit, for which the impurity scattering within each FS sheet averages out the angular dependences of green functions, making them independent of $\boldsymbol{k}$. The dirty limit can be applied when the elastic electron mean free path satisfies the condition $\ell_e \ll \xi$, where ξ is the smallest coherence length. That means that a particle scatters a lot before loosing its phase coherence and this results in the loss of the initial momentum direction, so the Green function associated will be essentially isotropic, with a first order linear correction:

$$f(\boldsymbol{k}, \boldsymbol{r}, \omega_n) \approx f(\boldsymbol{r}, \omega_n) + (\boldsymbol{v}_F \delta \boldsymbol{f}(\boldsymbol{r}, \omega_n)) \,, \tag{3.19}$$

Inserting this expansion in the Eilenberger equations and averaging over the momentum directions results in the much simpler Usadel equations [63], in which all microscopic details are hidden in the electronic diffusivity D_i for each FS sheet and the interband scattering rates γ_{ij}. Usadel equations are diffusive equations where we can express the electron diffusivity as $D = \frac{1}{3} v_F \ell_e$, with $\ell_e = v_F \tau_{imp}$ and τ_{imp} impurity scattering relaxation time.

3.3 Dirty two-band model

Now we shift our attention to the model under discussion in this thesis: the dirty two-band model. As we said this model can describe part of the physics of iron-based superconductors, and it is the simplest presenting broken time-reversal symmetry. In this section we firstly introduce the microscopic set of equations that stands as starting point for the model, in continuation with the previous section. After that we derive and discuss the Ginzburg-Landau free energy from them, as an expansion close to critical temperature.

3.3.1 Usadel equations

For the case of a two-band superconductors, the Usadel equations where computed in [64] and gives:

$$\omega_n f_i = \frac{D_i}{2}\left(g_i \mathbf{\Pi}^2 f_i - f_i \nabla^2 g_i\right) + \Delta_i g_i + \gamma_{ij}(g_i f_j - g_j f_i)\,, \tag{3.20}$$

where $i = 1, 2$ is the band index. Here the quasi-classical propagators f_i and g_i obey the normalization condition $|f_i|^2 + g_i^2 = 1$ in each band. It should also be noted that the only impurity scattering terms γ_{ij} that survive after averaging over the momentum direction are the one related to interband scattering (while intraband scattering is ineffective, in accordance to Anderson's theorem, seen in Section 3.1.2). The components of the order parameter $\Delta_j = |\Delta_j| e^{i\theta_j}$ are determined by the self-consistency equations

$$\Delta_i(\boldsymbol{r}) = 2\pi T \sum_{n=0}^{N_d} \sum_j \lambda_{ij} f_j(\boldsymbol{r}, \omega_n), \tag{3.21}$$

that come exactly from the definition in Eq. (3.8). Here, T is temperature, $N_d = \Omega_d/(2\pi T)$ is the summation cut-off at Debye frequency Ω_d and the Matsubara frequencies are $\omega_n = (2n+1)\pi T$, with $n \in \mathbb{Z}$.

The coupling matrix $\hat{\Lambda}$ effectively describes the potential that brings the formation of bound pairs so the interplay between spin fluctuations (repulsive, negative term) and electron-phonon coupling (attractive, positive term). The diagonal elements λ_{ii} describe the intraband pairing, while the interband interaction is determined by the off-diagonal terms λ_{ij} $(j \neq i)$. The interband coupling parameters and impurity scattering rates satisfy the symmetry relation

$$N_1 \lambda_{12} = N_2 \lambda_{21} \quad \text{and} \quad \gamma_{ij} = \Gamma N_j\,, \tag{3.22}$$

where $N_{1,2}$ are the partial densities of states of the two bands and Γ the impurity scattering strength defined as $\Gamma = n_{imp}\pi u^2$, with n_{imp} and u impurities' concentration and potential respectively.

Finally the electric current can be computed as

$$\boldsymbol{J}(\boldsymbol{r}) = 2\pi \mathrm{e} T \sum_{n=0}^{N_d} \sum_j N_j \boldsymbol{v}_F^{(j)} \operatorname{Im} g_j(\boldsymbol{r}, \omega_n) \,. \tag{3.23}$$

3.3.2 Ginzburg-Landau expansion

We focus now on the two-band dirty model near T_c, in this way we can simplify the above Usadel equations in the Ginzburg-Landau ones. It should be stressed that the multiband expansion relies on the existence of multiple small parameters, and that is in contrast with the usual single-band GL expansion that is justified by a single small parameter $(1-T/T_c)$. In multiband using a single parameter would be in general incorrect, in fact we can have multiple broken symmetries or anyway even if the symmetry is one (like in this model when we are outside BTRS state) the expansion with a single parameter has vanishingly small applicability range [61]. In addition we should note the difference between the terms multiband and multicomponent, the first adjective is related to the microscopics while the second one to the phenomenology. A multiband SC is a material that can sustain superconductivity in different bands, and so can have different gaps Δ_i. While a multicomponent SC is a material that has to be described by different "order parameters" in the GL equations, usually identified with ψ_i ("order parameter" are called like that just for historical reason, since in case of multicomponent SC not every ψ_i is always related to a broken symmetry). There are cases where the order parameters can be a linear combinations of the gap functions and furthermore we can have for example a 3 bands SC described effectively by a 2 component GL free energy [62]. However in our case gap functions and components will coincide, and to stress this point (as well the microscopic origin) we will call also the order parameter Δ_i.

To obtain the GL equations we solve equation Eq. (3.20) perturbatively with respect to the gap functions $\Delta_i(\boldsymbol{r})$ by expanding the quasiclassical Green functions as

$$f_i = \sum_{\nu=0}^{\infty} f_i^{(\nu)} \,, \qquad g_i = \sum_{\nu=0}^{\infty} g_i^{(\nu)} \,, \tag{3.24}$$

where the νth order is with respect the power of $\Delta(\boldsymbol{r})$. Now substituting these expansions into Eq. (3.20), regarding differential operators as

$\mathbf{\Pi}, \boldsymbol{\nabla} \sim O(\Delta)$, and collecting same orders we get:

$$f_i^{(\nu)} = \frac{D_i}{2\omega_n} \sum_{k=0}^{\nu-3} \left(g_i^{(k)} \mathbf{\Pi}^2 f_i^{(\nu-k-2)} - f_i^{(\nu-k-2)} \nabla^2 g_i^{(k)} \right) + \frac{\Delta_i g_i^{(\nu-1)}}{\omega_n} + \sum_{k=0}^{\nu-1} \frac{\gamma_{ij}}{\omega_n} (g_i^{(k)} f_j^{(\nu-k)} - g_j^{(k)} f_i^{(\nu-k)}) \,. \tag{3.25}$$

From the self consistency Eq. (3.21) as well from the above equation we can see that $f_i^{(0)} = 0$. From the Green function normalization condition

$$\begin{aligned} g &= sign(\omega_n)\sqrt{1-|f|^2} \\ g^{(\nu)} &= sign(\omega_n) \left(\delta_{\nu 0} - \frac{1}{2} \sum_{k=0}^{\nu-1} f_i^{(k)\dagger} f_i^{(\nu-k)} \right) , \end{aligned} \tag{3.26}$$

where we can see how $g^{(0)} = sign(\omega_n)$ and $g^{(1)} = 0$.

The interesting physics of the model can be studied including all the terms up to the quartic ones in the final free energy, so in the expansion we just need to collect terms up to $\nu = 3$ order. Therefore inverting the self-consistency equation Eq. (3.21)

$$2\pi T \sum_{n=0}^{N_d} \sum_{\nu=1}^{3} f_i^{(\nu)}(\omega_n, \Delta_1, \Delta_2) = \hat{\Lambda}^{-1} \begin{pmatrix} \Delta_1 \\ \Delta_2 \end{pmatrix} . \tag{3.27}$$

These two equations coincide with the GL matter field equations $\frac{\delta \mathcal{F}}{\delta \Delta_i^*} = 0$. To complete the GL equations we need the gauge field equation $\frac{\delta \mathcal{F}}{\delta \boldsymbol{A}} = 0$, which can be found inserting in the Maxwell equation $\boldsymbol{\nabla} \times \boldsymbol{B} = \boldsymbol{J}$ the electric current equation Eq. (3.23) with the appropriate expansion.

Finally the Ginzburg-Landau functional free energy linked with those GL equations is:

$$\mathcal{F} = \sum_{j=1}^{2} \left\{ \frac{k_{jj}}{2} |\mathbf{\Pi}\Delta_j|^2 + a_{jj}|\Delta_j|^2 + \frac{b_{jj}}{2}|\Delta_j|^4 \right\} + \frac{\boldsymbol{B}^2}{2} \tag{3.28a}$$

$$+ \frac{k_{12}}{2} \Big((\mathbf{\Pi}\Delta_1)^* \mathbf{\Pi}\Delta_2 + (\mathbf{\Pi}\Delta_2)^* \mathbf{\Pi}\Delta_1 \Big) \tag{3.28b}$$

$$+ 2 \left(a_{12} + c_{11}|\Delta_1|^2 + c_{22}|\Delta_2|^2 \right) |\Delta_1||\Delta_2| \cos\theta_{12} \tag{3.28c}$$

$$+ \left(b_{12} + c_{12} \cos 2\theta_{12} \right) |\Delta_1|^2 |\Delta_2|^2 \,, \tag{3.28d}$$

where $\theta_{12} = \theta_2 - \theta_1$ is the relative phase. The coefficients of the Ginzburg-Landau functional a_{ij}, b_{ij}, c_{ij} and k_{ij} can be calculated from a given set of input microscopic parameters λ_{ij}, D_i, T and Γ (appendix A).

The coefficients of the gradient terms depend on both electronic diffusivity coefficient D_1 and D_2. Therefore the parameter space can be

reduced by absorbing one in the gradient term. Without any loss of generality, we choose D_1 to be the largest diffusivity coefficient ($D_1 > D_2$). Thus, in the dimensionless units, the coefficients of the gradient term depend only on the ratio of the diffusivities, or *diffusivity imbalance* $r_d = D_2/D_1 < 1$. In practice, the dimensionless variables are defined by normalizing the gaps by T_c and the lengths by $\xi_0 = \sqrt{D_1/T_c}$. The magnetic field is scaled by $B_0 = T_c\sqrt{4\pi N_1}$, where N_1 is the density of states in the first band, and the free energy by $\mathcal{F}_0 = B_0^2/4\pi$. The electromagnetic coupling constant is $q = 2\pi B_0 \xi_0^2/\Phi_0$, where Φ_0 is the flux quantum. In these units, the London penetration length λ_L is given by $\lambda_L^{-2} = q^2(\sum_i k_{ii}\Delta_{i0}^2 + 2k_{12}\Delta_{10}\Delta_{20})$, where Δ_{i0} is the bulk value of the dimensionless gap. From the new value of the gauge coupling constant q we can see now how we can play with this parameter, to change the type of our superconductor. For example a high q means a strong effective coupling with the magnetic field, so the SC will be pushed toward type I. This stronger coupling comes from the fact that inside q we find for example the density of states at Fermi energy, and increasing it the SC state is stronger, so it goes more toward type I.

3.3.3 Ginzburg-Landau free energy

Let us comment on the GL free energy, especially focusing on the intercomponents terms, indeed the part regarding the *independent* terms Eq. (3.28a) is exactly the same as in the $\mathrm{U}(1)\times\mathrm{U}(1)$ model already seen in Chapter 2. The two components can be seen as coupled in three different ways: electromagnetically coupled by the vector potential $\boldsymbol{A}$ through the gauge derivative $\boldsymbol{\Pi}$; via the mixed gradient term Eq. (3.28b); and finally via the potential intercomponent terms Eq. (3.28c) and Eq. (3.28c). In particular the last one is the one that break $\mathrm{U}(1) \times \mathrm{U}(1)$ symmetry in the ground state, by enforcing a particular value for the phase difference θ_{12}, and therefore makes the components intertwine with a leftover $\mathrm{U}(1)$ gauge symmetry related to the total phase.

Fundamentally important is the so called biquadratic Josephson terms related to the coefficient c_{12}, in fact being proportional to $\cos 2\theta_{12}$ allows to have non-trivial phase difference. In fact if we had only this term in the GL free energy, when $c_{12} > 0$, to minimize the energy would be convenient to have $\theta_{12} = \pm\pi/2$. As we said in Section 3.1.3, this is equivalent to break time-reversal symmetry, i.e. a discrete symmetry with 2 possible physical ground states, therefore being a $\mathbb{Z}_2$ symmetry. This is obvious, because θ_{12} can be $\pi/2$ or $-\pi/2$, and these are two physically distinct states but with same energy, and we can pass from one to another just complex conjugating (while $\theta_{12} = \pm\pi$ or ± 0 have just one ground state). If now we introduce again the other intercomponents terms, we can see how the bilinear Josephson term (proportional to $\cos\theta_{12}$) prefers having

$\theta_{12} = 0$ or π but never something else. So for $c_{12} > 0$ there will be a competition between the biquadratic Josephson and the bilinear one, resulting anyway in a complex states with $\theta_{12} \neq 0, \pi$.

It is also worthy to compare the free energy Eq. (3.28) with the one computed from the clean case with the Eilenberger equations [61]. In that case the free energy was much simpler and apart from Eq. (3.28a), we just had the bilinear Josephson term a_{12}. This term is sufficient to get a U(1) symmetry but not for producing BTRS states. The less intricate free energy is due to the fact that different components are coupled microscopically only through the interband coupling term in $\hat{\Lambda}$, i.e. through the pairing potential. However in the dirty case we have also impurity scattering contributions from the new term Eq. (3.18), that produces the last term in Eq. (3.20), proportional to γ_{ij}. The impurity scattering has an enhancing entangling effect for the components, that manifests in the GL free energy as new intercomponent terms.

We investigate now the physical meaning of the various GL interband terms, with the help of GL free energy microscopic origin. First of all we rewrite the intercomponent potential part with complex conjugate fields:

$$V_{12} = \left(a_{12} + c_{11}|\Delta_1|^2 + c_{22}|\Delta_2|^2\right)\left(\Delta_1^*\Delta_2 + \text{c.c.}\right) \tag{3.29a}$$

$$+ b_{12}|\Delta_1|^2|\Delta_2|^2 + \frac{c_{12}}{2}\left(\Delta_1^{*2}\Delta_2^2 + \text{c.c.}\right). \tag{3.29b}$$

As we said the term proportional to a_{12} is called Josephson coupling (more specifically bilinear Josephson coupling) and the reason is that it is the microscopical equivalent of the Josephson current that tunnels from a superconductor to another through an interface. In fact if we interpret $\Delta_1^*\Delta_2$ as creation and annihilation gap operators, the term indicates a tunneling of a Cooper pair from a band to another one. The biquadratic Josephson c_{12} is similar, but it is the contributions of two simultaneously tunneling Cooper pairs. The b_{12} term is the density-density interaction, associated with the interaction between the two gap densities and as we have seen in Chapter 2, if $b_{12} > 0$ could lead to fractionalization in vortex cores due to repulsion between the two components. Contributions like c_{11} and c_{22} are still related to tunneling of single Cooper pairs but modulated by densities in each band. Finally the mixed gradient term in Eq. (3.28b), is still a tunneling but in momentum space, so a "quantum of current" tunnels from a band to another one.

All this physical interpretations are very appealing, but we still have to remember that the Ginzuburg-Landau equations regard *classical* complex fields, that describe *effectively* and macroscopically the physics inside the superconductor. Only indirectly, after seeing from where the GL can be derived, we can attach some physical interpretation to the different coupling terms.

3.4 Phase diagrams

Eventually, for a given set of input microscopic parameters, λ_{ij}, Γ, r_d, and T close to T_c, we can reconstruct the coefficients (while q just controls the coupling with $\boldsymbol{A}$) and investigate the ground-state properties of the GL theory by minimizing the free energy Eq. (3.28) with respect to $|\Delta_j|$ and θ_{12} [65]. Being the parameter space very big to explore, let us do some physical consideration.

First of all the diffusivity imbalance r_d is ineffective in the ground state property, in fact it is present only in the gradient terms and being the ground state homogeneous, these are zero. Secondly, we focus on repulsive interband coupling $\lambda_{ij} < 0$, these indeed are quite generic in iron-pnictide superconductors. Therefore the clean ground state ($\Gamma = 0$) will always have a $s_\pm$ gaps structure, with a critical temperature of T_{c0}. As we said $s_\pm$ states are not favoured by the impurity scattering, which tends to average out the order parameter over the whole Fermi surface, suppressing the critical temperature. However, provide that interband pairing is weak, it can be transformed in a s_{++} state, and survive even in the extreme dirty limit where $\Gamma \gg T_{c0}$ (i.e. $\Gamma \gg 1$, being Γ always measured in unit of T_{c0}). In this case the critical temperature is $T_{c\infty}$, which reads as [31]:

$$\ln(T_{c0}/T_{c\infty}) = N_1(w_{11} + w_{12}) + N_2(w_{22} + w_{21})\,, \tag{3.30}$$

where $\hat{w} = \hat{\Lambda}^{-1} - \lambda^{-1}\hat{I}$ and λ is the maximal eigenvalue of the coupling matrix $\hat{\Lambda}$. According to Eq. (3.30), one can see that the interband interaction should be sufficiently weak, in order to avoid a drastic suppression of the critical temperature in the s_{++} state. To derive a criterion, note that $N_1 w_{11} + N_2 w_{22} > 0$, so that the r.h.s. of the Eq. (3.30) is larger than $N_1 w_{12} + N_2 w_{21} = (N_1|\lambda_{12}| + N_2|\lambda_{21}|)/(\lambda_{11}\lambda_{22})$. Therefore in order to have a $T_{c\infty}$ which is not much smaller than T_{c0}, we require the following condition $(N_1|\lambda_{12}| + N_2|\lambda_{21}|)/(\lambda_{11}\lambda_{22}) < 1$ to be satisfied, as we can see from Fig. (3.5).

The most important degree of freedom for the physics under discussion is the relative phase θ_{12}, therefore we will explore the ground states as phase diagrams. Also, thanks to the previous consideration,we are now in the position to construct physical meaningful phase diagrams, in the plane of parameter Γ, T. For that purpose, we numerically minimize the free energy Eq. (3.28) using a nonlinear conjugate gradient algorithm (see Chapter 4 for details). The results in Fig. (3.6) demonstrate the role of impurities on the ground state properties, for various representative cases.

Those diagrams illustrate the well understood fact that disorder may induce a transition from $s_\pm$ to s_{++} in two-band superconductors [31–33], as sketched in Fig. (3.4). The transition can happen in two qualitative different ways. Either via a crossover when one of the superconducting gap

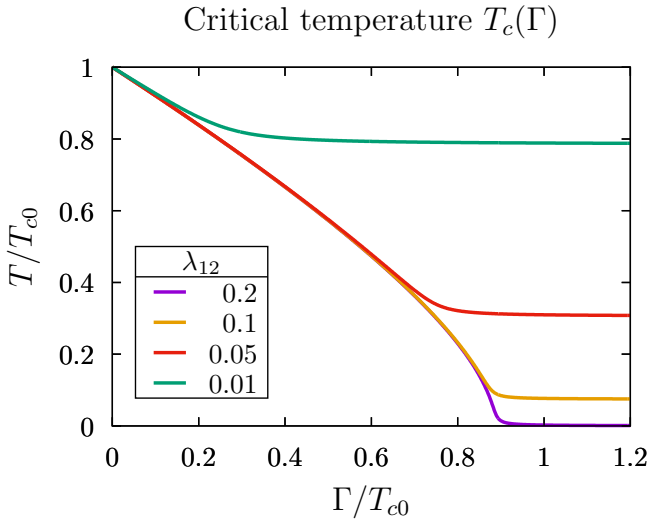

Figure 3.5: Critical temperature $T_c(\Gamma)$ as function of the impurity scattering strength, for nearly degenerate bands with $\lambda_{11} = 0.29$ and $\lambda_{22} = 0.3$. The different curves correspond to different repulsive interband coupling $\lambda_{12} = \lambda_{21}$. We can see how increasing this last term, the T_c is exponentially suppress with Γ. The critical temperature manages to reach a saturation value $T_{c\infty}$ in the extreme dirty limit for values of λ_{12} that respect the criteria stated above.

vanishes as a function of impurity concentration, or via an intermediate complex $s + is$ state that break time-reversal symmetry with $\theta_{12} \neq 0, \pi$.

As can be easily note, the BTRS dome is very narrow (sometimes infinitesimal as in panel (A)), thus is extremely unlikely to observe the impurity-induced $s + is$ states here. The BTRS region generally grows wider with increasing interband scattering (panels (A)-(C)), but T_c is simultaneously exponentially suppressed, according to eq. Eq. (3.30), so that basically it does not allow a significantly size increase. In addition, the transition lines go almost parallel to the T axis, and therefore can be observed practically only by changing impurity concentration, making it extremely challenging to detect. However, its presence can influence properties in a wider region, so it is still important as we will seen.

The crossover region generically occurs for temperature close to $T_c(\Gamma)$, where being close to criticality is not so energy expensive to suppress totally one gap to invert its sign, while at lower temperature the $s + is$ is more usual. In addition more the bands are degenerate and more the BTRS region starts close to T_c (when they are exactly degenerate $\lambda_{11} = \lambda_{22}$, the transition $s_\pm \to s_+$ happens always through a BTRS domain, it is never convenient to suppress one the gaps having equal weights).

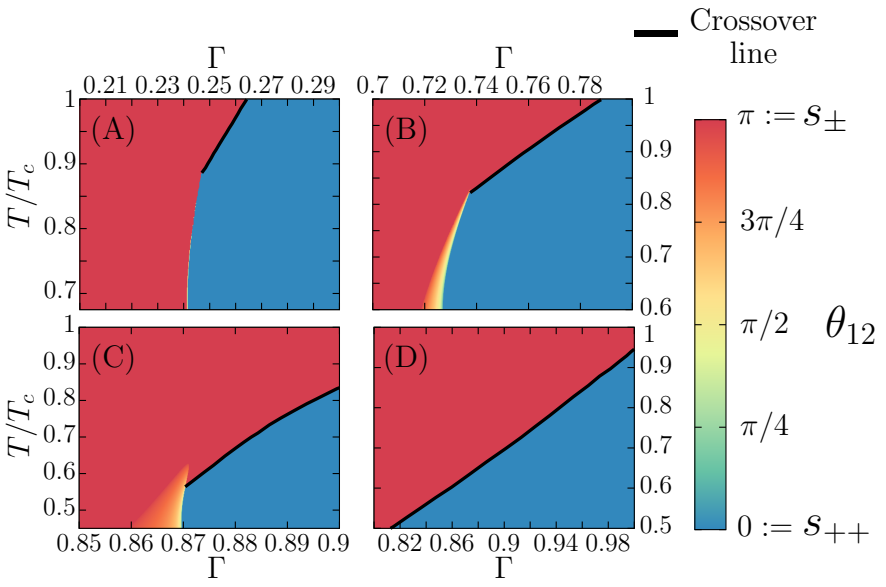

Figure 3.6: Phase diagrams of the Ginzburg-Landau free energy Eq. (3.28). These show the values of the lowest-energy-state relative phase θ_{12}, as function of the interband scattering strength Γ and the temperature T (note that now T is rescaled with respect to $T_c(\Gamma)$). The different pictures corresponds to different values of the coupling matrix $\hat{\Lambda}$. Panels (A), (B), and (C) respectivelly correspond to nearly degenerate bands with $\lambda_{11} = 0.29$ and $\lambda_{22} = 0.3$ with weak $\lambda_{12} = \lambda_{21} = -0.01$, intermediate $\lambda_{12} = \lambda_{21} = -0.05$ and strong $\lambda_{12} = \lambda_{21} = -0.1$ repulsive interband pairing interaction. The last panel (D) describes the case of intermediate band disparity $\lambda_{11} = 0.25$ and $\lambda_{22} = 0.3$ with intermediate $\lambda_{12} = \lambda_{21} = -0.05$ repulsive interband pairing interaction. The solid black line shows the zero of Δ_1, that is the crossover between $s_\pm$ and s_{++} states. In panels (A), (B) and (C), the crossover line is attached to a dome of time-reversal symmetry breaking $s + is$ state. In the panel (D), the crossover line does not connect to an $s + is$ state.

It can be shown analytically that $s + is$ dome can in general start from two different temperatures, $T^*_\pm \geq T^*_{++}$, depending if we are in the $s_\pm/s+is$ or $s_{++}/s+is$ transition [33]. Therefore there are three possible case: when $T^*_\pm = T^*_{++}$ the crossover line is attached to the summit of the BTRS dome as in panels (A) and (B); when $T^*_\pm > T^*_{++}$ the dome peak is detached as in panel (C); lastly there are cases, when there is important band disparity, where $T^*_{++} = 0$ so the dome is totally separated from the crossover line and is totally immerse in $s_\pm$ state [33].

The important difference between the crossover and the $s + is$ transition, is that the former occurs without additional symmetry breaking

(actually is not even a thermodynamical transition) while the latter spontaneously breaks the time-reversal symmetry, and both $s_{\pm}/s + is$ and $s_{++}/s + is$ transitions lines are of the second order, at the mean-field level [33]. The existence of the second order phase transition on the phase diagram dictates that there is softening of one of the normal modes near that transition. This softening has a number of possible physical consequences. In the next section we consider normal modes and fluctuations in this system.

3.5 Coherence lengths

A perturbative analysis around classical solutions like the ground state, or the normal state provides important informations such as the length scales of the theory, massless modes or second critical field. In this section we limit ourselves to the analysis of coherence lengths and normal modes. The perturbative analysis in this model was performed by Julien Garaud, Mihail Silaev and Egor Babaev in the upcoming article.

As we said in Chapter 2, the length-scales that characterize matter fields are called coherence lengths and they are associated to the exponent with which these fields recover asymptotically from a small perturbation (see e.g. [2, 66, 67]). Note that for the simplest single-component s-wave model the coherence length is often indirectly defined, for example through overall vortex core size or slope of the order parameter near the center of the vortex core. While in this case the results are somehow consistent, in general they are not, especially in multi-component systems, due to the intercomponent interactions.

Another consequence of intercomponent interactions, that was not present in the $\mathrm{U}(1) \times \mathrm{U}(1)$ case, is that one cannot a priori expect that independent coherence lengths are associated with single fields Δ_i. Instead one can expect to find linear combinations of the complex fields that recover from a perturbation with different exponential laws, and therefore one Δ_i can be characterized by different coherence lengths, with different weights. In general, in multi-component GL models different from $\mathrm{U}(1) \times \mathrm{U}(1)$, determination of the various coherence lengths cannot be done analytically but has to be carried out numerically.

To determine the coherence lengths one thus consider small perturbations in all relevant field degrees of freedom around the ground state solution and linearize the theory around it. The eigenvalue spectrum of the infinitesimal perturbation operator are the (squared) masses of the normal modes, and the coherence lengths are the inverse masses. The model we consider here has four degrees of freedom associated with the matter fields: two moduli and two phases of the complex fields. If one neglect coupling to vector potential (this is possible because in linear the-

ory the vector potential decouples from the matter fields) then the sum of the phases forms a mode with zero mass (Goldstone mode), since it is associated with U(1) gauge symmetry. When coupling to the vector potential is included this mode becomes massive via London-Anderson-Higgs mechanism. The inverse of that mass is the London's magnetic field penetration length, as already discussed in Chapter 2.

For the clean two-band s_{++} material, i.e. when the only intercomponent term is the bilinear Josephson one, the phase difference constitute a massive mode that is called Leggett's mode [17]. The length-scale associated with this mode (i.e. length scale at which the phase difference recovers from a perturbation) is also called Josephson length. Being this mode a pure phase mode, a phase perturbation does not affect the densities directly, but it is very important in the interaction between vortices, with the possibility of phase string connecting fractional vortices and bounding them together asymptotically linearly instead of logarithmically as in $\mathrm{U}(1) \times \mathrm{U}(1)$.

However it was discussed in clean three-band superconductors, that when time reversal symmetry is broken there is no Leggett-type (phase-only) mode, and instead the phase difference mode is hybridized with the density (Higgs) modes [36, 37, 40, 41]. In our case we find the same for the BTRS region, but in addition also outside this region there is some mixing for the softest mode, as we will see.

The perturbation theory is constructed as follows. The fields are expanded in series of a small parameter ϵ: $\Delta_i = \sum_a \epsilon^a \Delta_i^{(a)}$ and collected order by order in the functional. The zero-th order is the original functional, while the first order is identically zero provided the leading order in the series expansion satisfies the equations of motion. Therefore the physically relevant correction appear at the order ϵ^2 of the expanded Ginzburg-Landau functional. Choosing the following expansion in small perturbations around the ground state

$$|\Delta_i| = U_i + \epsilon\delta|\Delta_i|\,, \quad \theta_{12} = \bar{\theta} + \epsilon\delta\theta_{12}\,. \tag{3.31}$$

where U_i and $\bar{\theta}$ denote the ground state while $\delta|\Delta_i|$ and $\delta\theta_{12}$, stand for the perturbations. ϵ is the arbitrarily small parameter of the series expansion. Collecting the perturbations in a single vector $\Upsilon = (\delta|\Delta_1|, \delta|\Delta_2|, \delta\theta_{12})^T$, the term which is second order in ϵ reads as:

$$\frac{1}{2}\Upsilon^T \left(\mathcal{K}\boldsymbol{\nabla}^2 + \mathcal{M}^2\right)\Upsilon\,, \tag{3.32}$$

where $\mathcal{K}$ is the matrix containing k_{ij} elements, and $\mathcal{M}$ is the so called mass matrix. Now deriving with respect to vector Υ and setting to zero, the GL equations read as:

$$\boldsymbol{\nabla}^2\Upsilon = \mathcal{K}^{-1}\mathcal{M}^2\Upsilon = \tilde{\mathcal{M}}^2\Upsilon\,, \tag{3.33}$$

where $\tilde{\mathcal{M}}$ is the mass matrix in a new basis, called *rotated basis*. In this basis the free energy Eq. (3.28) is without the mixed gradient and easier to deal with for coherence lengths computation, even if the potential is more complicated (actually to benefit from this transformation you have to perform it before the application of the perturbation operator). The advantage in this basis is that now the perturbation operator Eq. (3.32) has off-diagonal terms coupling various excitations only in the mass matrix.

Finally, the length scales are given by finding the eigenvalues m_a^2 of the (symmetric) mass matrix $\tilde{\mathcal{M}}^2$, that are the (squared) masses of the elementary excitations. The corresponding coherence lengths are the inverse (eigen)masses: $\xi_a = 1/\sqrt{m_a^2}$ (and $a = I, II, III$). Similarly, the London's penetration depth of the magnetic field is the inverse mass of the gauge field: $\lambda = 1/m_{\boldsymbol{A}}$. The mass of the gauge field is similar to the U(1) × U(1) case due to decoupling in linear theory, i.e. $m_{\boldsymbol{A}}^2 = (q\varrho)^2$ where $\varrho = \sum_{ij} k_{ij}\Delta_i\Delta_j^*$ (here we account for mixed gradient terms), which implies that London's penetration depth reads as $\lambda = 1/q\varrho$.

The theory thus comprises four elementary length scales associated with different elementary perturbations of the ground state. The length scale associated with the gauge field excitations is the penetration depth λ, and the three remaining quantities are the coherence lengths ξ_a (with $a = I, II, III$). The eigenstates associate with the coherence lengths are different linear combinations of the complex fields moduli and phase differences. Being mixed modes, if one perturbs just one gap's modulus, several modes will be excited since it enters several linear combinations corresponding to different normal modes. Therefore there will, in general be several length scales in the recover of gap modules from perturbation.

The general behaviour of these characteristic length is the following. Both the largest coherence length ξ_I and the penetration depth λ naturally diverge at T_c, thus signaling the restoration of the U(1) symmetry via a second order phase transition. Additionally the model features additional phase transition associated with the time-reversal symmetry breaking: from $s_{++}/s_{\pm}$ to the $s + is$ state there is a breaking of $\mathbb{Z}_2$ symmetry. Being this a phase transition of second order, as demonstrated in Ref. [65], then the largest coherence length ξ_I will be divergent at that line as well, while here λ stays finite.

The second largest coherence length ξ_{II} is always finite (except at a single point of the phase diagram that corresponds to the summit of the $s + is$ dome). The shortest length scale ξ_{III} is always finite. In addition, all length scales are finite at the crossover lines where there is no phase transition but just one of the gap vanishing.

In order to analyze better the different normal modes, it is convenient to introduce the perturbations associated to the total ($\delta|\Delta_+|$) and relative

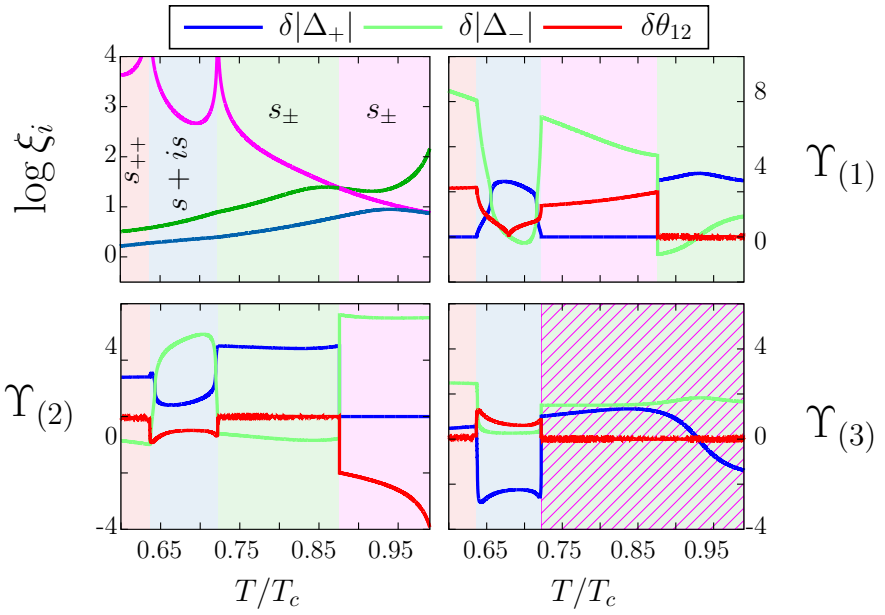

Figure 3.7: Behavior of the coherence lengths and corresponding eigenmodes of a dirty two-band superconductor with nearly degenerate bands and intermediate repulsive interband pairing interaction (corresponding to panel (B) of diagram Fig. (3.6)). This shows the length scales and the corresponding eigenmodes $\Upsilon_{(i)}$ as functions of the temperature for a given interband scattering $\Gamma = 0.7275$, thus corresponding to a vertical scan in Fig. 3.6(B). There are clearly four different regimes corresponding to different phases. [68]

$(\delta|\Delta_-|)$ density variations, defined as $\delta|\Delta_\pm| = \delta|\Delta_1| \pm \delta|\Delta_2|$. Fig. (3.7) shows the length scales and the corresponding eigenmodes as functions of the temperature for a given interband scattering $\Gamma = 0.7275$. This corresponds to a vertical scan in the panel (B) of diagram Fig. (3.6), going across $s_\pm$, $s+is$ and s_{++} phase.

That vertical scan, covers four qualitatively different regimes. At low temperature, the system is in the s_{++} state. There, the mode characterized by the largest coherence length mixes relative phase and relative densities and is decoupled from the total density variations. This phenomena is produced by impurity-scattering and is in contrast to clean two-band case where phase difference is decoupled from densities at linear level, producing a Leggett mode [17].

At a higher temperature, the system goes to the time-reversal symmetry breaking $s+is$ state. This is a second order phase transition that is signaled by the divergence of the largest coherence scale. In the $s+is$ state, all modes mix density and relative phase. Further increasing the

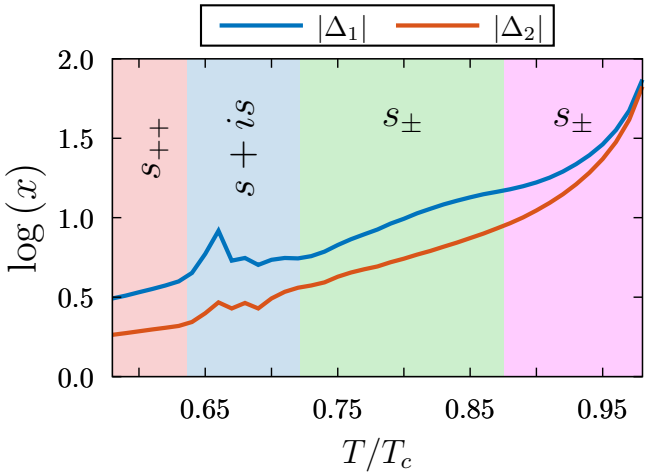

Figure 3.8: Behavior of the core size for the two different components of a dirty two-band superconductor with same coupling parameters as Fig. (3.7). Interband scattering is $\Gamma = 0.7275$, gauge coupling constant is $q = 0.8$ and equal diffusivities ($r_d = 1$). The core size is computed as full width at half maximum (FWHM) of the densities profiles.

temperature drives the system through another second order phase transition to the $s_\pm$ phase where the mode with the lightest mass again mixes relative phase and relative densities but is decoupled from the total density variations. Interestingly, upon further increase of the temperature within the $s_\pm$ phase, there is a sharp crossover at which the character of lightest mode changes. It becomes a pure density mode from which the relative phase mode decouples. This mode is associated with the coherence length that diverges at the superconducting phase transitions. So to summarize we can see how outside the BTRS region, there are always two pure density modes, and one hybridized with phase difference, while inside BTRS all the three modes have mixed contributions.

We can hope somehow to see the effect of the coherence lengths behavior analyzing the vortex cores in the two different components, as in Fig. (3.8). This plot shows the overall vortex core size evolution as the system is cooled down from T_c. In general the size of a vortex solution in a nonlinear theory should not be expected to be determined by coherence lengths, which are coming from a linear approximation valid only asymptotically. Nonetheless, in this particular model the general behavior of the two cores sizes as a function of temperature resembles the coherence lengths related to the pure density modes. In particular it has an overall smooth increasing trend from s_{++} to $s_\pm$ region, and then a divergence close to T_c when a pure density mode becomes the lightest one and the coherence length associated with it diverges. In addition it can be noted

how in $s+is$ there are maxima, related to the changing in modes mixing that happens in this region. Finally, the densities of the two components have different relative contributions from the pure density modes and that explains their quantitative difference.

Complicated variations of the coherence lengths in dirty case, as well as the existence of diverging coherence lengths, is a consequence of competing $s_{\pm}$ and s_{++} and the $s+is$ state. They should have physical manifestations in various responses that involve spatial or dynamical variations of the fields. The mixed modes dictate nontrivial thermoelectric properties [42, 43] and their softening manifests itself in anomalies of flux flow viscosity [44]. Likewise by the same mechanism the mode mixing produces nontrivial magnetic signatures of impurities [45, 46]. Existence of mixed soft modes also alter the magnetic response. In the Chapter 5 some manifestations of this exotic physics will be presented, but before that, the numerical methods will be introduced.

Chapter 4

Numerical methods

The numerical simulations in this thesis are based on Finite Element Method (FEM) and NonLinear Conjugate Gradient method (NLCG). This chapter will introduce shortly these two methods, without going in depth, since they are all well-known methods used in all branches of physics and engineering. In the last section all the particular implementation choices will be described.

The actual numerical computations were performed using the library *FreeFem++* [69, 70], which is a partial differential equation solver, implementing FEM in C++ language. In order to have a performing code and to exploit external computer clusters, the code has been parallelized with the Message Passing Interface (MPI) standard, through the Open MPI library [71]. Regarding the final plots, they are all produced with gnuplot [72], a command-line program that can generate two- and three-dimensional plots.

4.1 Finite Element Method

The finite element method (FEM) is a numerical method for solving boundary value problems for partial differential equations on general domains [73, 74]. It allows to pass from analytical to algebraic system of equations. To do that the domain has to be subdivided into discrete parts through a tessellation, obtaining a mesh. On each of these discrete parts, piece-wise functions are defined (the finite elements), the number of which depending on the order of the function. Together they will approximate the analytical function on the total domain, yielding a coefficient for each finite element, that can be stored in a vector transforming the system into an algebraic one.

To better see how this works let us take as toy problem the solution of the Poisson equation on a general domain Ω. The problem is than to

find u belonging to a general Hilbert space V, satisfying

$$\begin{cases} -\boldsymbol{\nabla}^2 u = f & \Omega \\ \partial_n u = 0 & \partial\Omega\,, \end{cases} \tag{4.1}$$

where f is a source term, $\partial\Omega$ the boundary of our domain and $\partial_n u = 0$ the boundary condition, in particular we choose an homogeneous Neumann boundary condition, indeed this kind of condition will be relevant for GL implementation. To implement finite element, two steps are needed: rephrasing the original problem in the weak formulation, and then applying the Galerkin projection.

The weak formulation is an alternative formulation of Eq. (4.1) but with respect to weaker solutions, therefore solutions with less "regularity". So the space of the solutions in the weak formulation will be larger with respect to the strong formulation Eq. (4.1), in particular in this case while the strong form requires that the solution u is at least continuous in the second order derivative, in the weaker form we just need the solution to be $L^2(\Omega)$ integrable with respect its first derivative, i.e. belonging to the first Sobolev space.

Practically the transformation is done by multiplying Eq. (4.1) by a test function v, belonging to the same solutions space of u, and then integrating as

$$-\int_\Omega d\boldsymbol{r}\, v\boldsymbol{\nabla}^2 u = -\oint_{\partial\Omega} dS\, v\,\partial_n u + \int_\Omega d\boldsymbol{r}\,\boldsymbol{\nabla}u\boldsymbol{\nabla}v = \int_\Omega d\boldsymbol{r}\, fv\,, \tag{4.2}$$

where we have used the first Green identity in the first equality. Now it is the moment to use the Neumann boundary condition, so the boundary integral on $\partial\Omega$ will be zero. So we are left with the weak formulation

$$\int_\Omega d\boldsymbol{r}\,\boldsymbol{\nabla}u\boldsymbol{\nabla}v = \int_\Omega d\boldsymbol{r}\, fv \quad \rightarrow \quad a(u,v) = F(v)\,, \tag{4.3}$$

where we have introduced the bilinear form $a(u,v)$ and the linear functional $F(v)$ to represent the integral operations. We can see how now we only need the solution to have integrable gradient. A fundamental property of weak formulation is that the existence and uniqueness of a solution can be formally demonstrated by the Lax-Milgram theorem. This theorem requires the bilinear form $a(u,v)$ to be continuous (i.e. bounded) and coercive (i.e. positive constrained), and the functional $F(v)$ to be continuous, all conditions that are easily met in physics.

Once we know that the solution exists, the main obstacle to solve the equation is that u, being defined on an Hilbert space V, has infinite dimensions. Here the second step toward finite element comes into play, the so called Galerkin method. The idea is to project the infinite Hilbert

space V onto a subspace V_k with dimension k, so that increasing the finite dimensions we should get a better approximation. Choosing a base $\phi_1, \phi_2, ..., \phi_k$ for V_k we can then express the solution as

$$u = \sum_i^k u_i \, \phi_i \, . \tag{4.4}$$

Now we are in position to pass from the analytical equation Eq. (4.3) to an algebraic one:

$$a \left(\sum_i^k u_i \phi_i \, , \, \phi_j \right) = F(\phi_j) \quad \forall j = 1, ..., k \, , \tag{4.5}$$

where Eq. (4.5) is the so called Galerkin problem, and being $a(u, v)$ bilinear can be transformed in the matrix form,

$$A \, \boldsymbol{u} = \boldsymbol{f} \, , \tag{4.6}$$

where $A_{ij} = a \left(\phi_i, \phi_j \right)$ is the stiffness matrix, $f_j = F(\phi_j)$ is the source vector, u_i the solution vector. Now that the problem is in algebraic form can be easily solve with standard numerical procedure.

In GL case the difference is that we have to deal with nonlinear equations, so we cannot reduce the system to an easy matrix form. However in the case $a(u, v)$ is also symmetric, we can exploit another result of the Lax-Milgram theorem, which states that the solution of Eq. (4.3) corresponds to the function v that minimizes the "energy" functional

$$E(u, v) = \frac{1}{2} \, a(u, v) - F(v) \, , \tag{4.7}$$

which in GL equations corresponds to the free energy functional. Therefore now discretizing Eq. (4.7) with Garlekin method, the problem reduces to find the minimum of $E(u, v)$ in a k dimensional space.

Specifically in GL case, taking the simple $\mathrm{U}(1) \times \mathrm{U}(1)$, to find the minimum of its free energy Eq. (2.1), we need to set the functional differential (or variational form) to zero

$$D\mathcal{F}[\psi_1, \psi_2, \boldsymbol{A}] = \int_\Omega d\boldsymbol{r} \left(\sum_j \left(\frac{\delta \mathcal{F}}{\delta \psi_j} \cdot \delta \psi_j \right) + \frac{\delta \mathcal{F}}{\delta \boldsymbol{A}} \cdot \delta \boldsymbol{A} \right) = 0 \, , \tag{4.8}$$

where the functional derivatives are the terms of the GL equations Eq. (2.3) and the small variations can be considered as the test function v in Eq. (4.2), in each degree of freedom. Now to decrease the regularity

we apply similar identities as before, obtaining the possibility to set the boundary condition with the terms

$$\oint_{\partial\Omega} dS\, \delta\psi_j \left(\mathbf{\Pi}\psi_j\right) \cdot \boldsymbol{n} = 0 \tag{4.9a}$$

$$\oint_{\partial\Omega} dS \left(\delta\boldsymbol{A} \times \boldsymbol{\nabla} \times \boldsymbol{A}\right) \cdot \boldsymbol{n} = \oint_{\partial\Omega} dS \left(\delta\boldsymbol{A} \times \boldsymbol{B}_{ext}\right) \cdot \boldsymbol{n}\,, \tag{4.9b}$$

where both are conditions on the derivatives, so generalized Neumann conditions. The first condition Eq. (4.9a) physically implies that no currents are flowing through the boundary (to understand that check the last current formulation in Eq. (2.4)), and with the second Eq. (4.9b) we can impose an external magnetic field when needed.

As previously said the weak form cannot be reduced to a matrix formulation since the equations are not linear, therefore is impossible to solve exactly the equation. However treating the test functions as small variations, so having defined Eq. (4.8) as a differential, allows us to move in the free energy space, looking for the minima in an iterative way. To do that we will use the nonlinear conjugate gradient method.

4.2 Nonlinear Conjugate Gradient method

Nonlinear conjugate gradient (NLCG) is an iterative unconstrained optimization method for nonlinear problem, exploiting only the gradient information. A complete reference for this method can be find in Ref. [75] while a faster and more intuitive understanding can be gained by reading Ref. [76].

NLCG derives from the simpler steepest descent method, or simply gradient method, which similarly exploits the knowledge of the gradient of a function to find its minima. The foundation of the steepest descent method can be analyzed from the simplest example, when the energy to minimize takes a quadratic form as

$$E(\boldsymbol{u}) = \frac{1}{2}\boldsymbol{u}^T A\boldsymbol{u} - \boldsymbol{u}^T\boldsymbol{f}\,, \tag{4.10}$$

which is the matrix parallel of Eq. (4.7). If now we suppose that the matrix A is symmetric positive definite, than Eq. (4.10) has a paraboloid shape in the space of solutions, so the presence of a single minimum is assured. The gradient of this quadratic form is

$$\boldsymbol{\nabla} E(\boldsymbol{u}) = A\boldsymbol{u} - \boldsymbol{f}\,. \tag{4.11}$$

Obviously if we move oppositely to the gradient we are decreasing the free energy the most quickly. We start then from an initial guess $\boldsymbol{u}^{(0)}$ and we

move with a step $\boldsymbol{u}^{(1)} = \boldsymbol{u}^{(0)} - \alpha^{(0)}\boldsymbol{\nabla}E(\boldsymbol{u}^{(0)})$. We could choose a static α but then the convergence will be very slow in case α is too small or we are not assured that the energy will decrease if α is too big. The better thing is therefore to choose dynamically $\alpha^{(n)}$ every step. The procedure of choosing the best $\alpha^{(n)}$ is called *line search*, and corresponds to minimize $E(\boldsymbol{u})$ along the search line $\boldsymbol{d}_n$, where in this case $\boldsymbol{d}_n = -\boldsymbol{\nabla}E(\boldsymbol{u})$. With a quadratic form this choice is simple:

$$\alpha^{(n)} = \frac{||\boldsymbol{\nabla}E(\boldsymbol{u}^{(n)})||^2}{\boldsymbol{\nabla}E(\boldsymbol{u}^{(n)})^T\, A\, \boldsymbol{\nabla}E(\boldsymbol{u}^{(n)})}\,, \tag{4.12}$$

where the numerator is the norm squared. It is easy to see how this constant will always assure that we are decreasing our energy, at least at the second order, in fact expanding with Taylor with respect to the step $-\alpha^{(n)}\boldsymbol{\nabla}E(\boldsymbol{u}^{(n)})$ reads as

$$\begin{aligned} E(\boldsymbol{u}^{(n+1)}) &= E(\boldsymbol{u}^{(n)}) - \alpha^{(n)}||\boldsymbol{\nabla}E(\boldsymbol{u}^{(n)})||^2 + \frac{1}{2}(\alpha^{(n)})^2\boldsymbol{\nabla}E(\boldsymbol{u}^{(n)})^T\, A\, \boldsymbol{\nabla}E(\boldsymbol{u}^{(n)}) \\ &= E(\boldsymbol{u}^{(n)}) - \frac{1}{2}\frac{||\boldsymbol{\nabla}E(\boldsymbol{u}^{(n)})||^2}{\boldsymbol{\nabla}E(\boldsymbol{u}^{(n)})^T\, A\, \boldsymbol{\nabla}E(\boldsymbol{u}^{(n)})} < E(\boldsymbol{u}^{(n)})\,, \end{aligned} \tag{4.13}$$

where the Hessian matrix of $E(\boldsymbol{u})$ coincide with A, in the last passage we substitute $\alpha^{(n)}$ and finally we used the positive definite hypothesis. This choice geometrically coincides with the fact that the new gradient will be orthogonal to the previous search direction (but not with respect to all the directions searched before) Now we can build the algorithm (after initial guess $\boldsymbol{u}^{(0)}$):

1. Compute the search direction $\boldsymbol{d}_n = -\boldsymbol{\nabla}E(\boldsymbol{u}^{(n)})$
2. Compute the step size constant $\alpha^{(n)}$
3. Move to the new point $\boldsymbol{u}^{(n+1)} = \boldsymbol{u}^{(n)} - \alpha^{(n)}\boldsymbol{\nabla}E(\boldsymbol{u}^{(n)})$
4. Check the stopping criterion, if not satisfied iterate

If the stopping criterion is met the algorithm stops and the last point is the closest to the minimum. Usually as stopping criterion one uses the ratio between the magnitude of the new gradient and the initial one, comparing it with a tolerance.

The problem of the steepest descent method is that, in more complicate systems, it has a really slow convergence due to the fact that it often found itself taking steps in the same direction as the previous ones. The idea is therefore to improve the algorithm by assuring that every search direction $\boldsymbol{d}_n$ is "conjugated" with all the previous ones, i.e. A-orthogonal satisfying the relation

$$\boldsymbol{d}_n^T A \boldsymbol{d}_i = 0 \quad \forall i = 0, 1..., n-1\,. \tag{4.14}$$

In this way in a linear system we are sure that we need at maximum as many steps as the dimensions of the space of solutions to reach the minimum. To satisfy Eq. (4.14) the conjugate Gram-Schmidt process is exploited, so we construct every steps as

$$\begin{aligned} \boldsymbol{d}_n &= \beta_n \boldsymbol{d}_{n-1} - \boldsymbol{\nabla} E(\boldsymbol{u}^{(n)}) \\ \text{where } \beta_n &= \frac{\boldsymbol{\nabla} E(\boldsymbol{u}^{(n)})^T \boldsymbol{\nabla} E(\boldsymbol{u}^{(n)})}{\boldsymbol{\nabla} E(\boldsymbol{u}^{(n-1)})^T \boldsymbol{\nabla} E(\boldsymbol{u}^{(n-1)})} \,. \end{aligned} \tag{4.15}$$

Being the new search direction different from the pure gradient the new optimal step size constant will be

$$\alpha^{(n)} = \frac{||\boldsymbol{\nabla} E(\boldsymbol{u}^{(n)})||^2}{\boldsymbol{d}_n^T \, A \, \boldsymbol{d}_n} \,, \tag{4.16}$$

The final algorithm will be therefore (after initial guess $\boldsymbol{u}^{(0)}$ and the first pure steepest descent step):

1. Compute the search direction $\boldsymbol{d}_n = \beta_n \boldsymbol{d}_{n-1} - \boldsymbol{\nabla} E(\boldsymbol{u}^{(n)})$
2. Compute the step size constant $\alpha^{(n)}$
3. Move to the new point $\boldsymbol{u}^{(n+1)} = \boldsymbol{u}^{(n)} + \alpha^{(n)} \boldsymbol{d}_n$
4. Check the stopping criterion, if not satisfied iterate

In case we have *nonlinear* system obviously the matrix A cannot be defined globally, but it can be defined locally as a linear approximation, therefore the concept of conjugacy Eq. (4.14) is not completely lost. The main changes in the algorithm are two. First there is not an optimal Gram-Schmidt constant β_n, but there are several possibilities, each one with different properties and complexity, and find new performing constants is still an ongoing research [77, 78]. Two of the classical and most used choices, when high performances are not mandatory (defining the gradient of the nonlinear energy in $\boldsymbol{u}_n$ as $\boldsymbol{g}_n$):

$$\beta_n^{FR} = \frac{\boldsymbol{g}_n^T \boldsymbol{g}_n}{\boldsymbol{g}_{n-1}^T \boldsymbol{g}_{n-1}} \qquad \beta_n^{PR} = \frac{\boldsymbol{g}_n^T (\boldsymbol{g}_n - \boldsymbol{g}_{n-1})}{\boldsymbol{g}_{n-1}^T \boldsymbol{g}_{n-1}} \,, \tag{4.17}$$

where the first one is the Fletcher-Reeves formula (equal to Eq. (4.15)), while the second one the Polak-Ribière formula.

The second difference is about the computation of $\alpha^{(n)}$, in fact now A is not defined. Two possible solutions are based on minimization of the nonlinear function on the search line. The Newton-Raphson method consists in calculating the Hessian matrix in $\boldsymbol{u}_n$ and uses that as A matrix (in fact we have seen that they coincide if we have a quadratic form), while

the Secant method is similar but avoids the computation of the Hessian by approximating it with gradients in different positions.

Two important considerations are in order to utilize the nonlinear conjugate gradient at the best. The first one is the importance of the initial guess in nonlinear system. In fact having these problems more local minima, the solution will tend to the closer one with this method. Second we have seen how in linear systems the solution is found after at maximum the number of steps equal to the space dimensions, when the conjugacy is complete. In case of a nonlinear system this obviously will not happen, but it is still true that after that number of conjugated steps, the conjugacy will be "complete" and so there is no reason to keep going, and it is better to restart with a clean steepest descent step. Additionally we have seen how actually the concept of conjugacy is only locally defined (the Hessian changes in every point of the system), therefore if the Hessian changes a lot the conjugacy will be lost even faster, and this imply a clean restart well before the number of dimensions.

4.3 Numerical implementation

In this thesis we mostly used the dimensionless Ginzburg-Landau theory in Eq. (3.28), simulating it in two-dimensions, in the xy-plane, while neglecting the contribution coming from the z direction. The solutions therefore describe a purely two dimensional problem or a bulk configuration assuming translational invariance. The actual numerical investigation was performed on a bounded domain $\Omega \subset \mathbb{R}^2$, which can assume different shapes, in general rectangular or circular.

In this thesis two usual configuration are studied: the one with *intrinsic* topological defects and the other with topological defects driven naturally by *external field*. The first configuration is useful to study defects without any other contribution. Having topological defects an energy higher than the ground state, the initial guess is fundamental to create them, without external field. In general, vortices are generated by enforcing a winding in the starting condition, and due to the topology protection the components will not be able to unwind toward the ground state. Therefore the minimization procedure will bring the system to the local minimum, related to that exact given number of vortex charges.

The only possibility to decrease the charge numbers is by moving the vortex across the boundary. Indeed, as we said in Eq. (4.9a), the boundary condition where always chosen such that $\boldsymbol{n} \cdot \boldsymbol{\Pi}\Delta_j = 0$, where $\boldsymbol{n}$ is the normal vector to the boundary $\partial\Omega$. Physically this implies that no currents is flowing through the boundary. This boundary condition allows a topological defect to escape from the domain, since without external field, there is no Meissner current to prevent that. To avoid

this situation the grid had to be chosen large enough with respect to the size of the topological defects, such that the attractive interaction with the boundaries is negligible. The problem of this choice is that, needing large numerical grids, leads the computation to be demanding. The advantage, however, is the certainty that the obtained solutions are not influenced at all by the boundaries. Most of the plots are indeed close-up views of the real domain Ω.

Regarding the second type of configuration, the one with external field, we have two usual kind of experiments. In both the external field is imposed through the boundary condition Eq. (4.9b). One experiment is the magnetization process, where the external magnetic field is increased slowly, such that the superconductor from the initial Meissner state goes through all the different states up to the normal state when $\boldsymbol{H}_{ext} > \boldsymbol{H}_{c2}$. The other experiment is the field-cooling, where the temperature of the system is lowered while keeping the external magnetic field constant.

For the actual numerical implementation, as we said, the variational problem of minimizing the free energy is defined using finite element formulation provided by the FreeFem++ library. The tessellation of the domain Ω is done via a homogeneous triangulation, based on Delaunay-Voronoi algorithm. Functions are then decomposed over a continuous piecewise quadratic basis on each triangle. This means that on a given triangle, each of the six physical degrees of freedom of the problem $(\mathrm{Re}\,\Delta_1, \mathrm{Im}\,\Delta_1, \mathrm{Re}\,\Delta_2, \mathrm{Im}\,\Delta_2, A_x, A_y)$ is parametrized by the six coefficients of the second-order interpolating polynomials (there are six independent coefficients for a second-order polynomial in two dimension). The second-order Lagrange interpolation defines the six coefficients at vertices and midedges, for a total of $6 \times 6 = 36$ numerical degrees of freedom per triangle.

The overall accuracy is determined by the number of triangles that constitute the mesh, as well as the order of the interpolation method and the order of the quadrature formula for computing the integrals in each triangle. Generally the number of triangles used is around $3 \sim 6 \times 10^4$.

A nonlinear conjugate gradient algorithm is used to solve the variational nonlinear problem (i.e. to find the minima of $\mathcal{F}$). The algorithm is iterated until the relative variation of the norm of the functional $\mathcal{F}$ "gradient" with respect to all degrees of freedom in Eq. (4.8) is less than 10^{-6} - 10^{-8}, and anyway one verifies always that the final configuration is not changing. Due to loss of conjugacy, the nonlinear conjugate gradient algorithm is restarted every 100 iterations, to better perform.

For studying the intrinsic properties of the topological defects the initial guess is very important, and was generally constructed as follows:

$$\begin{aligned}
\Delta_j &= |\Delta_j| \mathrm{e}^{i\theta_j} \\
|\Delta_j|(x,y) &= U_j \prod_{k=1}^{N_j} \sqrt{\frac{1}{2}\left(1 + \tanh\left(\frac{4}{\xi_j}(R_{j,k}(x,y) - \xi_j)\right)\right)} \\
\theta_j(x,y) &= \frac{1}{2}\phi_{jj'} + \sum_{k=1}^{N_j} \arctan\left(\frac{y - y_{j,k}}{x - x_{j,k}}\right) \\
R_{j,k}(x,y) &= \sqrt{(x - x_{j,k})^2 + (y - y_{j,k})^2}\,,
\end{aligned} \tag{4.18}$$

where (N_1, N_2) is the total topological charge, i.e. the number of fractional vortices in each condensates, and $(x_{j,k}, y_{j,k})$ the position of the k's vortex in the condensate Δ_j. The ground state module in each condensate is U_j, and is calculated by minimizing the potential for the specific GL parameters. The initial phase difference $\phi_{jj'}$ between the two condensates can be used to initialized a domain walls when we have a BTRS state. Also ξ_j parametrizes the core sizes, and they can be derived from the coherence lengths, even if not necessary, in fact the core size will adjust immediately after the first minimization iteration.

Finally, the starting configuration for the vector potential $\boldsymbol{A}$ is determined by solving the Ampère's law equation $\boldsymbol{\nabla} \times \boldsymbol{B} = \boldsymbol{J}$, where $\boldsymbol{J}$ is the supercurrent given by the initial guess winding. Being the equation linear in $\boldsymbol{A}$, this operation is directly solved with a matrix system similar to the one obtained in Eq. (4.6) starting from the Poisson equation. In this way we have a perfect initial guess for $\boldsymbol{A}$ given the condensates guess, so a faster convergence will be reached in the NLCG. Once the starting configuration is constructed, we can proceed by relaxing all degrees of freedom simultaneously.

Chapter 5

Results

Two-band superconductors with interband scattering have a complicated coherence lengths behaviour, arising from terms in the Ginzburg-Landau free energy (3.28) that compete with each other. In Chapter 3 it has been also stressed how the coherence lengths can diverge in the presence of $s + is$, due to a second order phase transition connected to the breaking of the discrete $\mathbb{Z}_2$ symmetry. Therefore the multiband nature of this model plus the presence of time-reversal broken symmetry (BTRS) can lead to characteristic phenomena, that can signal the presence of this particular physics in real materials. In this chapter we present some of these peculiar responses, starting with the presence of type-1.5 superconductivity and a possible way to observe it experimentally. The appearance of Skyrmionic charges will be also discussed, in connection with the clustering effect of type-1.5 and domain wall defects. Next we address BTRS states signatures, like the presence of spontaneous magnetic fields as response of domain walls or impurity fluctuations. Finally we will see how the competition between $s_{\pm}$ and s_{++} at the crossover can be signaled by the presence of new moat-core vortex solutions, characterized by the coexistence of the two s-wave phases.

5.1 Type-1.5 superconductivity

5.1.1 Clustering effect

The first phenomena that we will address is the clustering effect due to the divergence of the softest coherence length ξ_I during the $s + is$ transition. Indeed, from Fig. (3.7) it immediately follows that near the $s+is$ phase transition the system necessarily falls into a regime where one of the coherence lengths is the largest length scale of the system. Since the other length scales, including the magnetic field penetration length, are finite at this transition, there are only two possible hierarchies of the

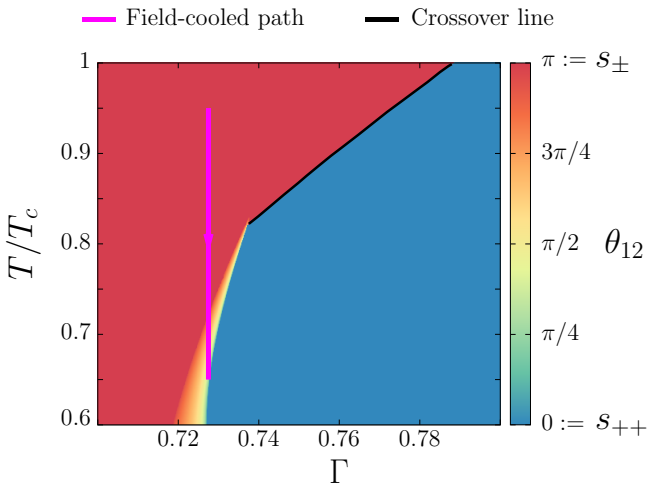

Figure 5.1: Phase diagram corresponding to a coupling matrix $\hat{\Lambda}$ with nearly degenerate bands ($\lambda_{11} = 0.29$ and $\lambda_{22} = 0.3$) and intermediate pairing interaction ($\lambda_{12} = \lambda_{21} = -0.05$), like panel (B) in Fig. (3.6). It shows the ground state value of the relative phases θ_{12} for different temperatures and impurity scattering Γ. The yellow region correspond to the BTRS region and the pink arrow corresponds to the cooling experiment.

length scales near that transition: (i) all coherence lengths are larger than λ (which is a type-1 behavior), (ii) ξ_I is larger than λ but λ is larger than some of the other coherence lengths.

As said in Chapter 2, a regime where some coherence lengths are smaller and some are larger than the magnetic field penetration length $... < \xi_i < \lambda < \xi_j < ...$ was earlier termed "type-1.5". When this hierarchy of the length scales holds one expects vortex solutions with long-range attractive, short-range repulsive interaction forces [15, 36, 79]. The range and strength of attractive intervortex interactions depends on the largest coherence length, therefore vortex clusters size should also be temperature dependent, following ξ_I behaviour.

To analyze this effect, we construct isolated vortex solutions, by imposing the same windings to both components Δ_1 and Δ_2, and minimizing the energy. The minimization procedure leads, after the convergence of the algorithm, to a vortex configuration that carries the number of flux quanta that is specified by the initial phase winding. The evolution of these bound states of vortices is then studied, while decreasing the temperature. This is equivalent of scanning the phase diagram like in Fig. (5.1).

In Fig. (5.2) we can see a cluster of 20 vortices at four different temperatures, corresponding to different regions in the phase diagram in Fig. (5.1). We start at temperature close to T_C completely in $s_\pm$ re-

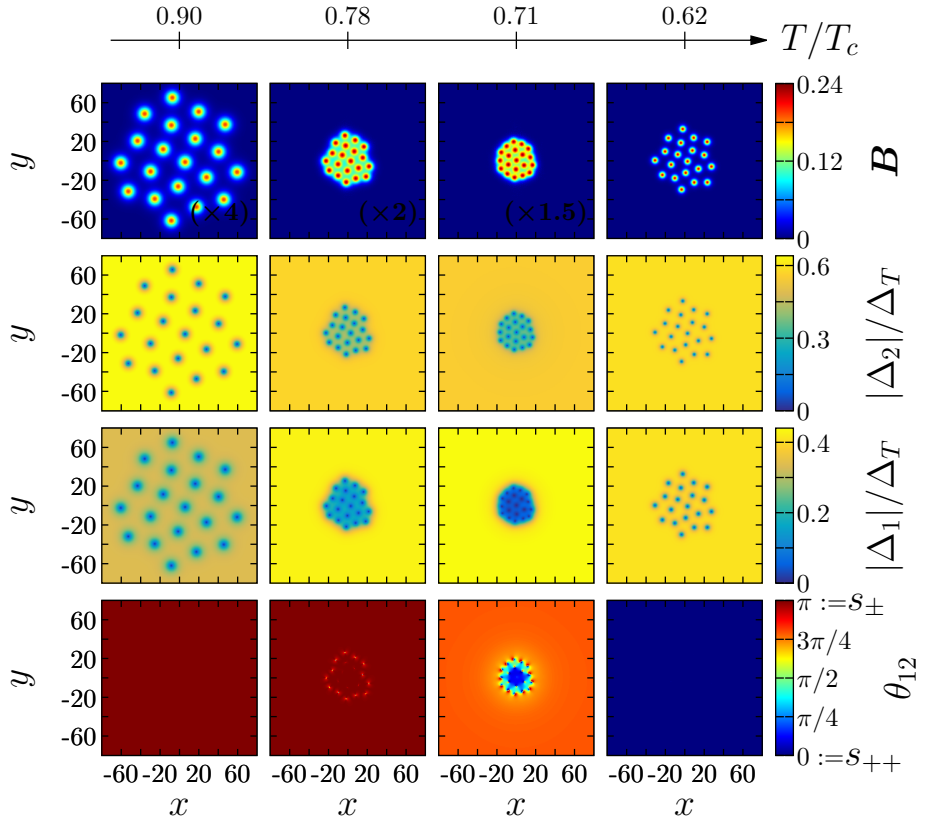

Figure 5.2: Evolution of bound state of 20 vortices during a cooling experiment like in Fig. (5.1). The interband scattering is $\Gamma = 0.7275$, the gauge coupling constant is $q = 0.8$ and diffusivities are equal ($r_d = 1$). The different lines respectively display the magnetic field $\boldsymbol{B}$, majority (Δ_2) and minority (Δ_1) gap components, and lastly the relative phase θ_{12}, that also signals the different ground state s-wave regions.

gion. Here both the components are clearly in type II region, and the vortices repel each other, theoretically up to infinite separation. Practically the numerical approximation limits this behaviour, in fact vortices do not feel each other after a critical separation. In real world pinning centers and general lattice potentials inside the material influence the intervortex distance in type II superconductors.

Decreasing the temperature the weaker component Δ_1 begins to form a cluster while Δ_2 is still in type II. In fact, being Δ_1 the weaker component, is more related to the softest coherence length ξ_I, and as we can see from Fig. (3.7), ξ_I increases rapidly cooling down after the transition between the two different $s_\pm$ regions.

After that point the type-1.5 character is always more evident, with the Δ_1 component being the one that shrinks the cluster more. Inside the

BTRS region we find the smallest cluster size, that is sensibly reduced with respect the starting point. The Δ_1 forms almost a macrovortex, signaling to be very close to type I region, while the second component retains visibly the short repulsive inter-vortex forces character.

Finally decreasing the temperature again we enter in s_{++} state, where even if the vortex sizes are smaller, there is repulsive interaction between vortices. Also the transition type-1.5 - type II is sharper here. From the behaviour of the bound states of vortices through this scanning is clear how the $s + is$ transition drives the clustering effect.

Additionally another important effect can be noted in Fig. (5.2). In the $s + is$ region, the cluster form a s_{++} state inside the vortex. This phenomenon can be explained with renormalization of Josephson coupling parameters, similarly as was noted in Ref. [36]. In fact in a cluster the densities tend to be depleted more with respect to isolated vortices (especially for the weakest component), and that affects the effective Josephson coupling. Qualitative the renormalization can be understood as follows. Let us consider the bilinear Josephson density energy term in Eq. (3.28c) in the form:

$$2a_{12}U_1U_2f_1(\boldsymbol{r})f_2(\boldsymbol{r})\cos(\theta_{12}(\boldsymbol{r}))\,, \tag{5.1}$$

where U_i are the ground states amplitudes and $f_i(\boldsymbol{r})$ is an ansatz representing the modulation of the densities due to vortices in the system. Hence the free energy in a domain Ω with N uniform distributed vortices can be written as:

$$\begin{aligned} V_J &= 2a_{12}U_1U_2\int d\boldsymbol{r}\, f_1(\boldsymbol{r})f_2(\boldsymbol{r})\cos(\theta_{12}(\boldsymbol{r})) \\ &\approx 2a_{12}U_1U_2\cos(\theta_{12}(\boldsymbol{r}))\int d\boldsymbol{r}\, f_1(\boldsymbol{r})f_2(\boldsymbol{r}) \\ &= 2\tilde{a}_{12}U_1U_2\cos(\theta_{12}(\boldsymbol{r}))\,, \end{aligned} \tag{5.2}$$

where $\tilde{a}_{12}$ is the renormalized bilinear Josephson parameter defined as

$$\tilde{a}_{12} = a_{12}\int d\boldsymbol{r}\, f_1(\boldsymbol{r})f_2(\boldsymbol{r})\,. \tag{5.3}$$

In Eq. (5.2) we have made the assumption that θ_{12} varies slowly in comparison with inter vortex distance, therefore considered constant as first approximation with uniform distribution of vortices (if this does not hold we cannot define a $\tilde{a}_{12}$ without spatial dependence).

We can see from Eq. (5.3) how the new parameter is depending on the modulation of the densities caused by vortices. The same can be done for the biquadratic Josephson coupling in Eq. (3.28d) obtaining (and similarly for the other Josephson terms depending quadratically on the densities):

$$\tilde{c}_{12} = c_{12}\int d\boldsymbol{r}\, f_1^2(\boldsymbol{r})f_2^2(\boldsymbol{r})\,. \tag{5.4}$$

Now inside a cluster the components are very depleted so $f_i \ll 1$. Therefore the quadratic renormalized parameter $\tilde{c}_{12}$ will be more suppressed with respect to $\tilde{a}_{12}$.

Inside the $s + is$ region $a_{12} < 0$ in the ground state, so the bilinear Josephson prefers an s_{++} state, but normally its contribution would be really small being a_{12} the one that changes sign close to $s+is$ (driving the transition from $s_\pm$ to s_{++}) and therefore close to zero. Nonetheless when big depletion is present it acquires strength and can drive a transition to s_{++} even if the ground state would be $s + is$ (note also that here the mixed gradient terms like in Section 5.4.1 do not have much effect being away from crossover, and therefore being Josephson terms much greater than it).

This mechanism could be very important in situation of high external field. In fact being the vortex density very high, it could prevent the formation of $s + is$ state driven by quadratic Josephson term, like in this model (this however does not apply in BTRS states produced by frustrated bilinear Josephson couplings like in three-component superconductors [36]).

5.1.2 Muon-spin rotation signatures

Here we focus on the unconventional magnetic response that the clustering effect explained above could produce in the vicinity of the $s + is$ transition. Indeed the temperature dependence of vortex cluster sizes can be deduced from μSR data in a similar way as it was done in Ref. [80] for Sr_2RuO_4.

Muon-spin rotation experiments are able to quantify the fraction of sample containing magnetic flux and subsequently the local internal flux density inside this area. This technique exploit spin polarized muons, that are brought at rest inside the sample, where they can precess if an internal $\boldsymbol{B}$ is present, at angular frequency $\boldsymbol{\omega} = \gamma_\mu \boldsymbol{B}$ where the gyromagnetic ratio of the muon is known. They then decay with a known lifetime, emitting positrons preferentially along the spin direction. The difference between the signal of two positron detectors placed at opposite edges of the sample can be used to evaluate the time evolution of the decay asymmetry $A(t) = (N_R(t) - N_L(t))/(N_R(t) + N_L(t))$ where $N_R(t)$ is the right detector signal and $N_L(t)$ the left one. This signal will oscillates with weights coming from different angular precessions $\boldsymbol{\omega}$. These weights can be separated by Fourier transforming, in order to obtain the probability of internal flux density $p(\boldsymbol{B})$, so we can know how much of the sample has a certain internal field $\boldsymbol{B}$ (equivalent to the local flux density). Now imposing a low threshold we can divide the sample in two part, one containing magnetic field and the other in Meissner state.

Now lowering the temperature across T_c we can see how the area

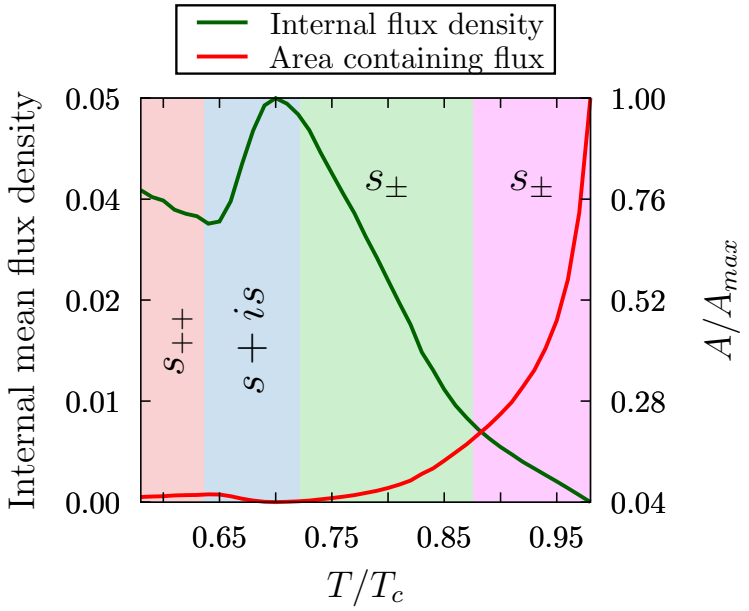

Figure 5.3: Evolution of a bound state of 7 vortices during a cooling procedure as in Fig. (5.1). The interband scattering is $\Gamma = 0.7275$, the gauge coupling constant is $q = 0.8$ and equal diffusivities ($r_d = 1$). The displayed quantities are the area of the region where the magnetic field $\boldsymbol{B}$ is above the threshold $\delta = 0.01 B_{max}$ (normalized with respect its maximum), and the internal mean magnetic flux density (corresponding to the magnetic field average) computed inside this area. A strong peak is produced in correspondence of the $s+is$ transition due to the divergence of the largest coherence length.

containing flux behaves. What happens usually for a type II material in external field, is that in normal state obviously the area containing flux is the total area, while at T_c there is a strong decreasing, in fact only in the vortices of the Abrikosov lattice the flux will be present. In a conventional type II this area would decrease really slowly lowering the temperature, in fact the vortices cores slowly decrease, due to the presence of a stronger condensate at lower temperature.

On the contrary if the superconductor allows the onset of type-1.5 at $T^* < T_c$, then exactly at this temperature we would see a fast fall in the area containing flux, as result from clustering. In addition being the number of vortices the same, and being the flux quantized in each vortex, the total flux will be the same, but on a smaller area. Therefore the flux density, i.e. the average magnetic field inside the flux area, will have a jump exactly at T^*.

The divergence of a coherence length is general in $s+is$ phase transi-

tion, so our model even if very simple, can helps to understand what would happen in material having this kind of time-reversal broken symmetry. Also very important is the fact that the substantial variation of the coherence lengths as a function of the temperature, dictates that in general vortex cluster size will also be temperature dependent. This opens up a possibility to discriminate the effect from pinning in muon-spin rotation measurements, in fact if the clustering was produced by inhomogeneous pinning center, the cluster would be independent of temperature, being the impurities not mobile.

In order to show the effect that this strong clusterization could have on the local mean magnetic flux density measured by this kind of experiments, we simulate a group of 7 vortices in Fig. (5.3) going through a cooling procedure as in Fig. (5.1). The strong peak in the magnetic flux density in correspondence of the $s + is$ transition is due to a type-1.5 state. Note that being the $s + is$ really small in this model, the effects of the two divergences of ξ_I in $s_{++}/s + is$ and $s + is/s_{\pm}$ transitions are merged, producing a single peak in the long-range attractive intervortex force in the full non-linear theory.

5.2 Skyrmionic states

Skyrmion were introduced in Chapter 2 as a different kind of topological excitation. In two components, they can be represented as a bound states of two spatially separated fractional vortices [81]. Skyrmions have usually a dipolar nature, that can strongly influence long-range proprieties of the model in which they develop. For example they can alter dramatically the collective behaviour of vortex matter, like during a magnetization process [19]. They can also form a Skyrmion lattice that could be easily observable [20]. In this model Skyrmions are produced in two different ways, one through the effect of type-1.5 superconductivity and the other as domain wall stabilized states [48].

5.2.1 Skyrmions driven by type-1.5

The clustering effect seen in the previous section can bring about the formation of Skyrmion on the border of the cluster. Indeed, in Section 5.1.1 it has been noted that it is the weaker component that tends to shrink the cluster, being more correlated with the softest coherence length. The fractional vortices of this component have therefore the tendency to shrink more toward the center with respect to the fractional vortices of the other component. This produces a radial splitting on the border of the cluster, which is more accentuated the bigger the cluster is.

The relevant signatures of Skyrmions can be noticed observing the

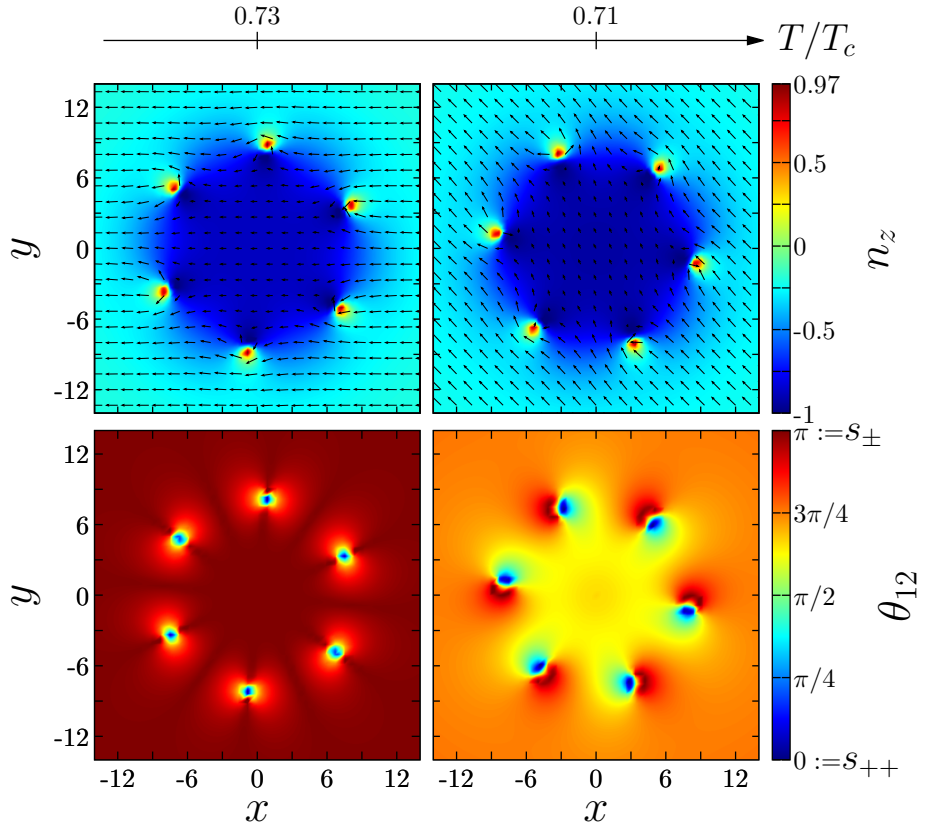

Figure 5.4: Cluster of 7 vortices showing 6 Skyrmion charges. Parameters corresponding to Fig. (5.2). The plots correspond to $s+is$ ($T/T_c = 0.71$) and $s_{\pm}$ ($T/T_c = 0.73$) states. The first line shows the pseudo-spin, with n_z in color while other components as vectors, while second line shows the phase difference. Numerical Skyrmion charges have been also computed, resulting in $Q(\boldsymbol{n}) = 5.98$ for $s + is$ while $Q(\boldsymbol{n}) = 5.95$ for $s_{\pm}$.

phase difference and the pseudo-spin $\boldsymbol{n}$ quantities. As explained in Chapter 2, the phase difference shows the dipolar and long-range nature of these defects, associated with the normal phase modes. In this model away from T_c we have always mixed phase-density modes, therefore the long-range nature is even more complicated. The pseudo-spin $\boldsymbol{n}$, shows the topological defects itself, as a wrapping of all the possible relative configurations of the two complex fields Δ_i around a sphere derived from the compactification of the 2D region, as explained in Chapter 2. In particular the n_z component regards the densities, so to have a complete Skyrmion charge it has to go from $n_z = 1$, i.e. the presence of only the first component, to $n_z = -1$ meaning the presence of only the second one, passing through all the possible relative densities.

In figure 5.4 a small cluster of 7 vortices is analyzed, in type-1.5 region. As seen in previous section the type-1.5 region can be present both in $s{+}is$ and in $s_\pm$ close to $s+is$. Therefore this confirms that Skyrmions are produced by the clustering and are not correlated to the s-wave structure of the gaps. In both regions the phase difference signature is present. The pseudo-spin $\boldsymbol{n}$ also shows clearly 6 Skyrmions on the border, while the central fractional vortices are concentric. We can notice that n_z does not reach +1, but it has been checked that it is just a problem of convergence of the numerical procedure.

5.2.2 Skyrmions and domain walls

Skyrmion can be obtained also in an alternative way. In fact in BTRS states, having broken the $\mathbb{Z}_2$ symmetry it is possible to have new topological defects called domain walls (DWs). To pass spatially from a state to its complex conjugate, the gaps have to change their relative phase. In this region the superconducting state will be weaker and the density of the gaps will be generally lowered. The presence of vortices or general impurity defects, can stabilize domain walls, being parts of the material were the SC state is weaker as well [50, 82].

Additionally was noted in Ref. [48, 49] that domain wall can stabilized Skyrmionic charges. In fact at the domain wall one has unfavorable values of the phase difference, and that could generate energetic terms that prefer to split integer flux vortices into fractional ones, to attain more favourable phase differences in between the split fractional vortices.

To see if this stabilization happens also in this model, we proceed with a field-cooling experiment in type II range of parameters, therefore with a lower gauge coupling q (to avoid type-1.5 effects). In this simulation a ground state outside $s+is$ is exposed to an external magnetic field, and its energy minimized. After that, it is cooled down, entering in $s+is$ region with constant external magnetic field, and with vortices inside.

It is well known that going through a phase transition allows uncorrelated regions to fall into different ground states [83, 84]. This is the Kibble-Zurek (KZ) mechanism for the formation of topological defects [85, 86]. As different regions fall into either of the $\mathbb{Z}_2$ states, domain walls are created. Since their energy increases linearly with their length, closed domain walls contract and collapse or are absorbed by boundaries. However in the presence of defects, like vortices produced by the external magnetic field, they can stabilize.

In Fig. (5.5) we can see the field cooling simulation, where big temperature steps have been chosen to facilitate KZ mechanism. At the beginning the system is in $s_\pm$ state with $T/T_c = 0.6$. Lowering to $T/T_c = 0.55$ the system enter in $s+is$ region and the vortices manage to pin two domain walls. These domain walls will last up to $T/T_c = 0.45$ where they

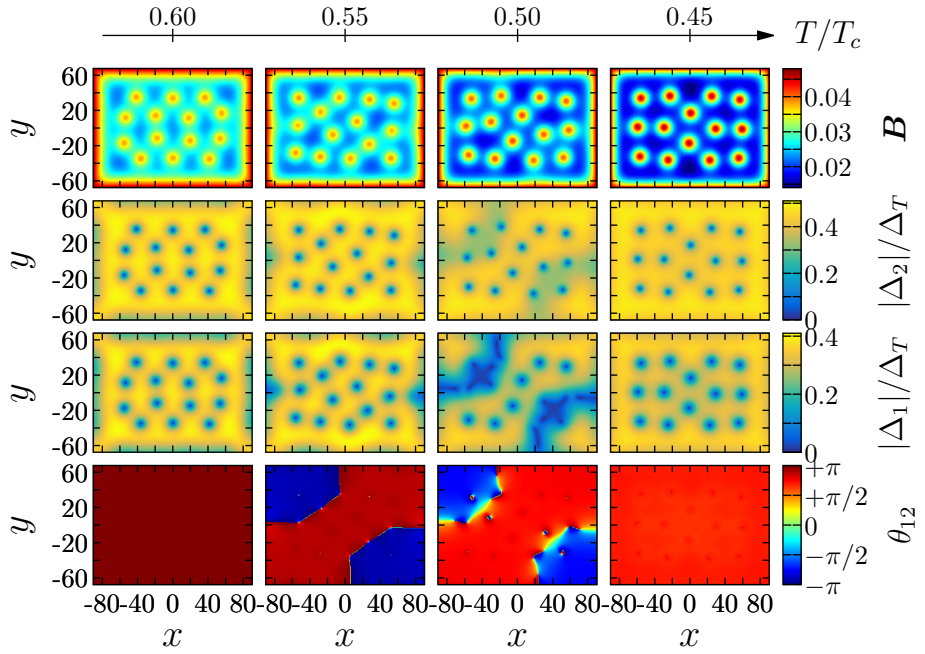

Figure 5.5: Field cooled experiment for nearly degenerate bands ($\lambda_{11} = 0.29$ and $\lambda_{22} = 0.3$) and strong pairing interaction ($\lambda_{12} = \lambda_{21} = -0.1$). The interband scattering is $\Gamma = 0.867$, the gauge coupling constant is $q = 0.25$ and equal diffusivities are assumed ($r_d = 1$). The external field is $B_{ext} = 0.0475$. The different lines respectively display the magnetic field $\boldsymbol{B}$, majority (Δ_2) and minority (Δ_1) gap components, and the relative phase θ_{12}.

are absorbed.

Analyzing the phase difference we can notice dipolar signatures on the domain walls. This is even easier to see in Fig. (5.6), where the close-up of one domain wall is plotted. The absolute phase difference and the pseudo-spin $\boldsymbol{n}$ signal the presence of 3 Skyrmions at $T/T_c = 0.55$ and 4 at $T/T_c = 0.50$.

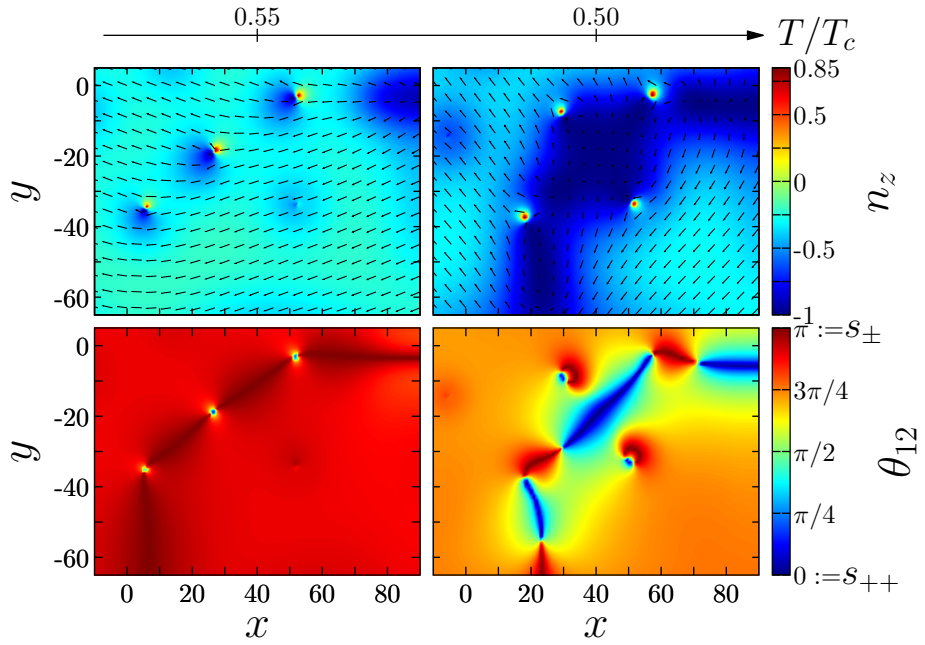

Figure 5.6: Zoom of the bottom-right domain wall in Fig. (5.5), presenting Skyrmions. The first line represents the pseudo-spin $\boldsymbol{n}$ vector and the second the absolute relative phase. Planar components of $\boldsymbol{n}$ as arrows, while n_z in color.

5.3 Spontaneus magnetic field

Spontaneous magnetic field can be produced in multicomponent superconductor that break time-reversal symmetry. This peculiar phenomena can be exploit to discern indirectly that a material is in BTRS state. In fact the direct measuring of the relative phase of the gaps is an hard job, while measuring indirect effects like spontaneous field can be easily done, with multiple techniques.

As we analyzed in Chapter 2, the spontaneous field is generated by an interband counterflow in the presence of the relative density gradients. The counterflow does transport current, even if the components flows are opposed, because the presence of gradients in the relative densities assures that the two flows are not balanced if these gradients have components perpendicular to the flows. This counterflow currents will generate the magnetic field, that will be then partially screened by the Meissner current.

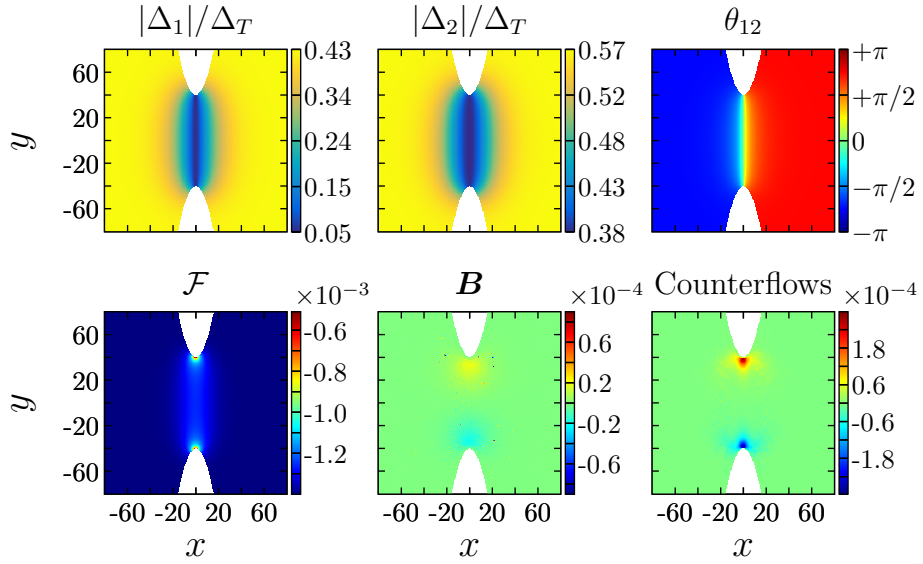

Figure 5.7: Geometrically pinned domain wall in non-convex domain. The superconductors is with nearly degenerate bands $\lambda_{11} = 0.29$ and $\lambda_{22} = 0.3$ and strong pairing interaction $\lambda_{12} = \lambda_{12} = -0.1$. The temperature is $T/T_c = 0.5$ and the strength of the interband scattering is $\Gamma = 0.867$. Gauge coupling constant is chosen as $q = 0.25$ and equal diffusivities are assumed ($r_d = 1$). The different plots display from the top left, the density of gap Δ_1, Δ_2, the phase difference θ_{12}, the energy density $\mathcal{F}$, the magnetic field $\boldsymbol{B}$, and finally the field produced by the counterflow.

From Chapter 2 we generalize the formula Eq. (2.8) for the total magnetic field, in the mixed gradients case:

$$\begin{aligned}\boldsymbol{B} = &-\boldsymbol{\nabla}\times\left(\frac{\boldsymbol{J}}{q^2\sum_{i,j}k_{ij}\Delta_i\Delta_j^*}\right)\\ &+\boldsymbol{\nabla}\times\left[\frac{i}{2q\sum_{i,j}k_{ij}\Delta_i\Delta_j^*}\left(\sum_{i,j}k_{ij}\left(\Delta_i^*\boldsymbol{\nabla}\Delta_j-\Delta_i\boldsymbol{\nabla}\Delta_j^*\right)\right)\right], \quad (5.5)\end{aligned}$$

where the first contribution is the one coming from the Meissner current while the second one from the counterflow. In the simulations the counterflow will be generated in two different ways, through domain wall solutions and through impurity fluctuations.

5.3.1 Counterflows induced by domain walls

Domain walls by definition ensure an interpolation between different phase differences, and in addition can produce a variation of both fields

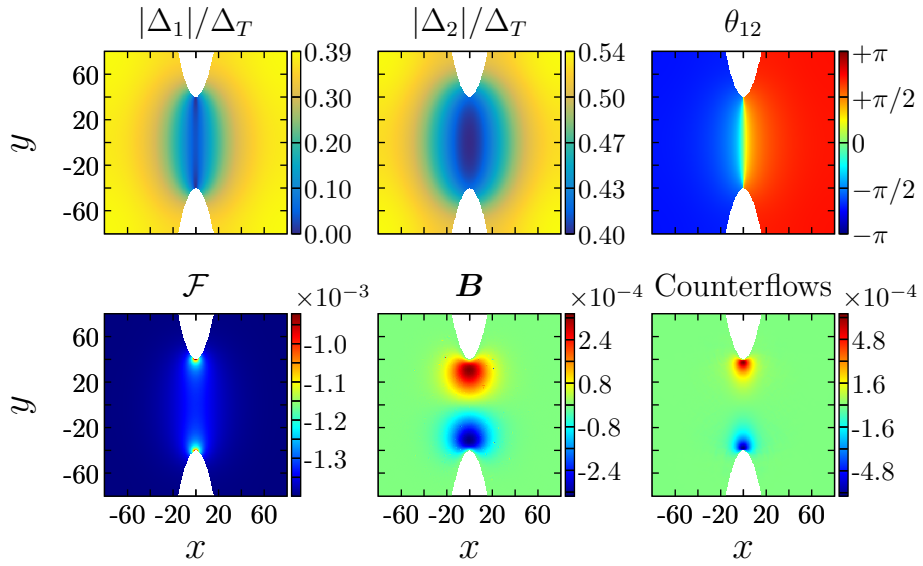

Figure 5.8: Geometrically pinned domain wall in non-convex domain with same parameters as Fig. (5.7). Here however the mixed gradient terms are switched off manually, imposing $k_{12} = k_{21} = 0$. The more pronounced magnetic field and counterflows are easily noted.

densities. Therefore they can in principle support counterflows, as was noted in Ref. [50].

To stabilize domain walls a geometrical barrier is produced. The DW is pinned by a non-convex geometry of the domain, in fact the wall to be absorbed would need to join its ends and collapse, but that means increasing its length first, so increasing the total energy. It is thus in stable equilibrium while trapped by the bumps of the domain. Another characteristic of the non-convex domain is that produces gradient in relative density and phase that are not collinear, so ensuring a counterflow.

In Fig. (5.7) it can be noted how the domain wall carries opposite, nonzero magnetic fields at its ends, therefore the total net flux in the material is still zero. The magnetic field produced is however very weak, with respect to the one in three-band clean model[50]. Nonetheless could be observable, being approximately 1‰ of the magnetic field in a vortex. Different gauge coupling q and different diffusivity imbalance r_d have been tried without obtain notably different results.

The mild spontaneous magnetic field could be caused by compensatory effects in the interband counterflow due to mixed gradient terms, not present in the clean model. To check this hypothesis, the simulation was repeated with same parameters as Fig. (5.7), but manually switching off the mixed gradients terms ($k_{12} = k_{21} = 0$). The results are shown in Fig. (5.8).

In this case the magnetic field generated is more pronounced, and around 10 times greater than the previous one. This fact seems to confirm that the mixed gradient terms has a compensatory phenomena.

In both Fig. (5.7) and Fig. (5.8) the magnetic field is lower with respect to the field produced by the counterflows, and also in general more distributed in space. That is due to the Meissner currents circulating around the bumps and screening the counterflows contribution.

5.3.2 Counterflows induced by impurity fluctuations

An alternative mechanism that could produce spontaneous magnetic field inside the sample, when it is in BTRS state, is a modulation of impurities. In fact the local ground state of the system changes with the impurity scattering strength Γ, being the Ginzburg-Landau parameters of Eq. (3.28) all dependent on Γ. So a fluctuation in space of $\Gamma(x, y)$ can yield gradients in the phase difference and densities, and therefore counterflows in principle.

Moreover the recent paper Ref. [23] reported experimental evidence for broken time-reversal-symmetry breaking state in multiband superconductor $Ba_{0.27}K_{0.73}Fe_2As_2$, one of the material thought to have an $s + is$ state in some window of doping [34–38, 62]. The conclusion was obtained through a zero field muon spin rotation measurements that signaled appearance of spontaneous magnetic fields at a certain characteristic temperature well below superconducting phase transition, after the sample was ion-irradiated to produce controlled defects inside.

It was demonstrated that the $s+is$ states can host spontaneous magnetic fields and currents in different ways. They could originate from domain walls interacting with defects and boundaries similarly as the previous discussion [50], or they can be generated from non-axially symmetric impurities states [45, 46]. Another possible mechanism is the counterflows produced by impurity fluctuations, as said above.

In Fig. (5.9) a sinusoidal modulation of the impurity scattering strength $\Gamma(x, y)$ is imposed in a dirty two-band superconductors, without any other constrain. The modulation effect is clearly visible in the pattern formed by densities and phase difference. The spontaneous magnetic field is produced where the sinusoidal modulation has its maximum gradient, so in between the maximum and minimum of $\Gamma(x, y)$.

As the domain wall case, the sample is crossed by a zero total magnetic flux. Furthermore in this case the magnetic field $\boldsymbol{B}$ is even weaker than in domain wall case, being around 10^{-5} of the usual magnetic field inside a vortex. This mild effect is due to the very narrow $s + is$ dome with respect to Γ variation. Therefore it is not possible to have big Γ fluctuations (otherwise we go outside the BTRS region), and consequently is not possible have big relative density gradients.

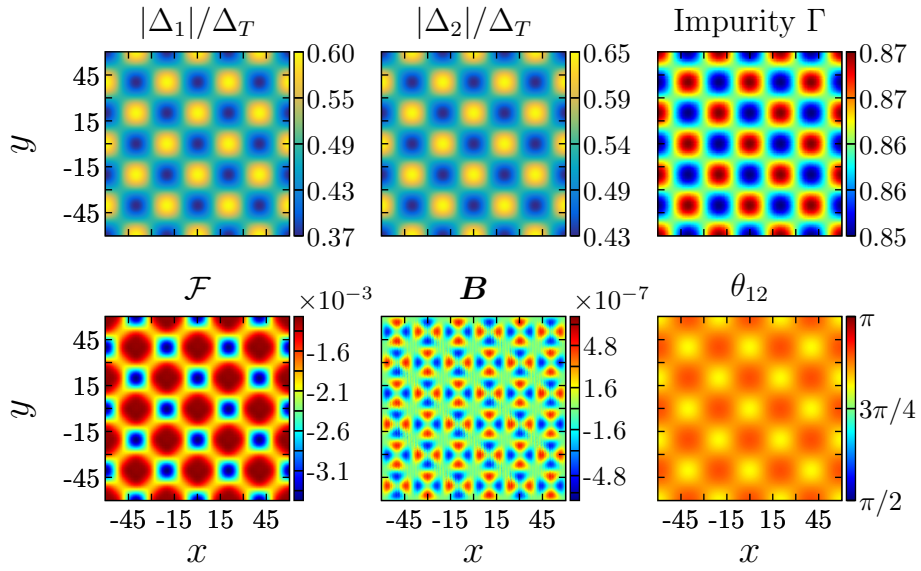

Figure 5.9: Spontaneous magnetic field obtained with impurities fluctuations on a dirty two-band superconductor with same coupling parameters as Fig. (5.7). The quantities displayed are from the top left: the density of gaps Δ_1, Δ_2, the fluctuation of the impurity scattering strength Γ, the energy density $\mathcal{F}$, the magnetic field $\boldsymbol{B}$, and the phase difference θ_{12}.

5.4 Impurity-driven $s_{\pm}/s_{++}$ crossover

In Chapter 3 it has been seen how the presence of disorder can lead to a crossover between $s_{\pm}$ and s_{++} in dirty two-band superconductors with repulsive interband pairing. The crossover always happen closer to T_c with respect to the $s+is$ state, being in this region the subdominant gap weak enough to be suppressed. In addition in the s_{++} region close to the crossover, there is a strong competition between terms in the free energy associated with mixed contributions. These energy terms competition can produce exotic phenomena in vortex structure, like the appearance of $s_{\pm}$ inside the vortex, while outside the ground state prefers a s_{++} state. Moreover the weakness of the subdominant gap can drive changes in its vortex structure, forming the so called "moat-like" cores [87]. The coexistence of $s_{\pm}$ and s_{++} can be accentuated in the presence of external field, up to drive a field-induced $s_{\pm}$ phase transition for elevated fields.

5.4.1 Moat-core vortex structure

It was recently demonstrated that the crossover line is accompanied by a non-trivial transition in the core structure of vortices [87]. Indeed typically singularities that occur in quantum vortices are point-like: i.e. in

two dimensions, the modulus of the complex order parameter (the density of superconducting electrons) vanishes at some point in the vortex core [12, 88, 89].

In this model however the vortices can acquire a circular nodal line around the singular point in one of the superconducting components $\Delta_i(r_0) = 0$, in the vicinity of the crossover line. This singular nodal line, which in three dimensions extends to a cylindrical nodal surface surrounding the vortex line, results in the formation of a peculiar "moat"-like profile in the subdominant superconducting gap.

As a result, the inner region of the vortex core shows a π relative phase between the gaps while it is zero in the outer region. This means that these moat-core vortices consist of an $s_\pm$ phase inclusion in the vortex core, which is separated from the bulk s_{++} phase by the nodal line.

Figure (5.10) shows the numerically calculated single vortex solutions in the vicinity of the impurity-induced crossover, in the case of a two-band superconductor with nearly degenerate bands and weak repulsive interband pairing interaction. The vortex profiles features a non-monotonic distribution of the subdominant component Δ_1 when approaching the $s_\pm/s_{++}$ crossover line.

It can be observed that $\Delta_1(r)$ exhibits a strong increase near the core, strongly overshooting its ground-state value, which is then retained asymptotically at $r \to \infty$. Small density overshoot effects were also obtained in a two-band model in the context of ballistic and diffusive bands [90]. However here the near-core overshoot can be very large, reaching about 100% of the subdominant ground-state amplitude.

Once the s_{++} ground state is reached, we can see the formation of the circular nodal lines of the subdominant component $\Delta_1 = 0$. Due to the competition between energetic terms, it is more favorable to achieve a $\theta_{12} = \pi$ ($s_\pm$ state) in the vicinity of the core singularity, while the ground state recovers far from the vortex center $\theta_{12} \to 0$. The transition between the localized "core" states with $\theta_{12} = \pi$ and the asymptotic states $\theta_{12} = 0$ is realized by nullifying the subdominant gap $\Delta_1(r_0) = 0$ at a given distance r_0 from the center.

The effect should be present rather generically in the presence of the interband impurity scattering since it originates from the mixed-gradient term in Eq. (3.28b) that tend to become negative. In addition a similar effect, not driven by mixed gradient terms, was found in clean three component case, due to the renormalization of Josephson couplings close to the vortex core [36].

To qualitative understanding the phenomenon we can analyze the free energy functional in Eq. (3.28) as in [87], assuming a axially symmetric vortex ansatz for the order parameter components, i.e. $\Delta_j(\boldsymbol{r}) = \tilde{\Delta}_j(r)e^{i\theta}$, where $\tilde{\Delta}_j(r)$ are the real-valued profiles of the order parameter compo-

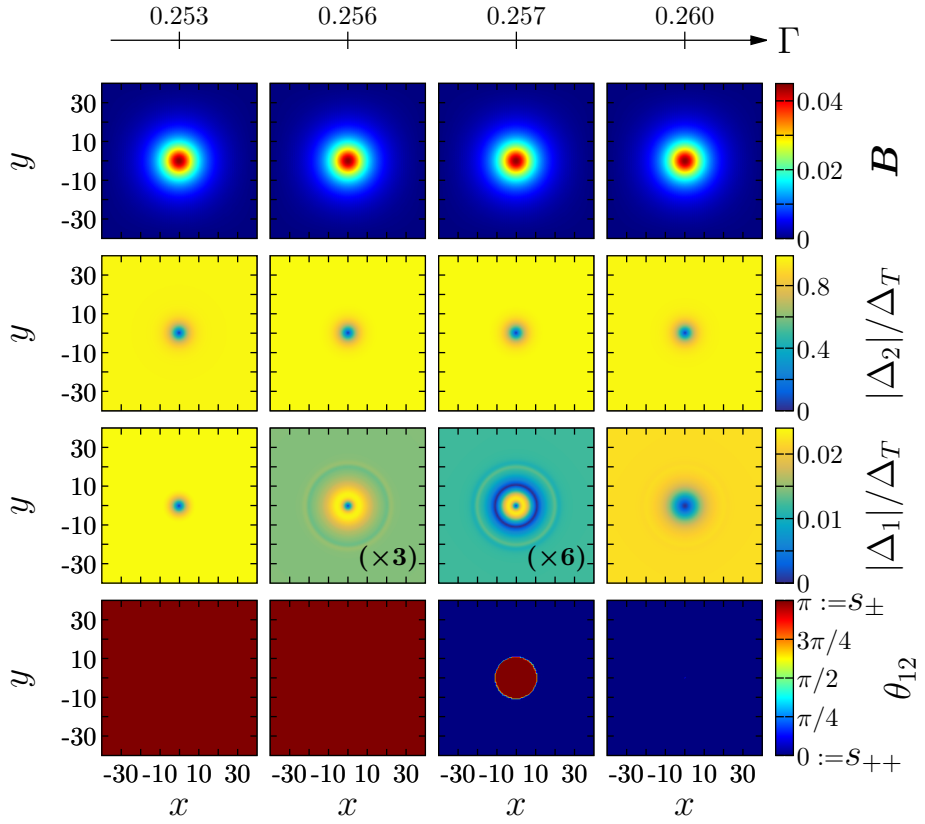

Figure 5.10: Transition in vortex solutions in the vicinity of the impurity induced crossover line of a two-band superconductor with nearly degenerate bands and weak repulsive interband pairing interaction ($\lambda_{11} = 0.29$, $\lambda_{22} = 0.3$, and $\lambda_{12} = \lambda_{21} = -0.01$), and with equal electron diffusivities ($D_2/D_1 = 1$). The temperature is $T/T_c = 0.95$, $q = 0.25$, and tuning the strength of the effective interband impurity scattering drives the system from bulk $s_\pm$ to bulk s_{++}. The quantities displayed are the same as in Fig. (5.2). The third column shows a vortex solution that has a point like and a "moat"-like zero in Δ_1. The figure is a reproduction of the one in [87].

nents and the polar coordinates r, θ are determined relative to the vortex center. Therefore the GL contribution from the mixed-gradient can be written as

$$\begin{aligned} F_G &\equiv \frac{k_{12}}{2}\Big((\mathbf{\Pi}\Delta_1)^*\mathbf{\Pi}\Delta_2 + c.c\Big) \\ &= k_{12}\left(\nabla_r\tilde{\Delta}_1\nabla_r\tilde{\Delta}_2 + r^{-2}\tilde{\Delta}_1\tilde{\Delta}_2\right), \end{aligned} \tag{5.6}$$

where the vector potential contribution is neglected since it is small inside the vortex core. This term has a spatially-modulated contribution that

is in a way similar to the interband Josephson energy in Eq. (3.28):

$$F_J \equiv 2\left(a_{12} + c_{11}|\tilde{\Delta}_1|^2 + c_{22}|\tilde{\Delta}_2|^2\right)\tilde{\Delta}_1\tilde{\Delta}_2\,. \tag{5.7}$$

In the homogeneous bulk phase the gradient energy is zero $F_G = 0$ and the phase locking corresponds to the $s_{++}/s_{\pm}$ state depending on the sign of the effective Josephson coupling $J = a_{12} + c_{11}|\tilde{\Delta}_1|^2 + c_{22}|\tilde{\Delta}_2|^2$, therefore the crossover line can be defined parametrically in the Γ, T plane as $J(\Gamma, T) = 0$.

In spatially non-homogeneous states, e.g., in the presence of vortices, the relative sign of the gap functions $\tilde{\Delta}_{1,2}$ is determined by the local interplay of two phase-locking energies F_G and F_J. Let us consider what happens within the vortex core, where the order parameter profiles can be approximated by linear dependencies $\tilde{\Delta}_j(r) \approx r d\tilde{\Delta}_j/dr$, thus yielding $F_G \approx k_{12}(d\tilde{\Delta}_1/dr)(d\tilde{\Delta}_2/dr)$. In this case since the mixed-gradient coefficient is always positive $k_{12} > 0$ (see appendix A), the energy F_G favors the opposite signs of the order parameter slopes, e.g. $d\tilde{\Delta}_2/dr > 0$ and $d\tilde{\Delta}_1/dr < 0$, leading to the opposite signs of the gap function near the vortex center $\tilde{\Delta}_2 > 0$ and $\tilde{\Delta}_1 < 0$.

This tendency competes with that favored by the Josephson energy if $J < 0$, corresponding to the bulk s_{++} phase when the gaps have the same signs far from the core. Therefore, provided that the gradient energy dominates close to the vortex center ($|F_G| > |F_J|$), one can expect the non-monotonic distribution for the component $\Delta_1(r)$, crossing zero at some finite distance $r = r_0$ determined by the competition of F_G and F_J The scenario discussed above is therefore generic for any two-band s_{++} superconductor with interband impurity scattering, having that mixed gradient terms.

Additionally it should be noted that this effect is stronger away from the SC phase transition. Indeed being the system breaking only a single symmetry, at mean-field level only one (critical) mode survives in the limit $\tau \equiv (1 - T/T_c) \to +0$. Therefore close to T_c the other subdominant modes are much smaller in amplitude, and the slopes of the gap functions near the core can be estimated through $|d\tilde{\Delta}_i/dr| \propto |\Delta_i^{(0)}|/\xi_c(T)$, where $\xi_c(T) \propto 1/\sqrt{\tau}$ is the critical coherence length and $\Delta_i^{(0)}$ the ground state value of the gap parameter. Hence the magnitude of the mixed gradient term is $|F_G| \propto k_{12}|\Delta_1^{(0)}\Delta_2^{(0)}|/\xi_c^2(T)$ which should be compared to the Josephson energy $F_J \propto J\Delta_1^{(0)}\Delta_2^{(0)}$. The condition of the vortex transition $|F_G| > F_J$ is satisfied only provided that the coupling is small enough, $|J| \ll k_{12}/\xi_c^2(T)$, which certainly does not hold near the critical temperature in the limit $\tau \to 0$ when $\xi_c(T) \to \infty$. However, one can expect that inside the vortex core the gradient energy always dominates in the vicinity of the impurity-driven $s_{\pm}/s_{++}$ crossover where the effective Josephson coupling disappears, $J(\Gamma, T) = 0$.

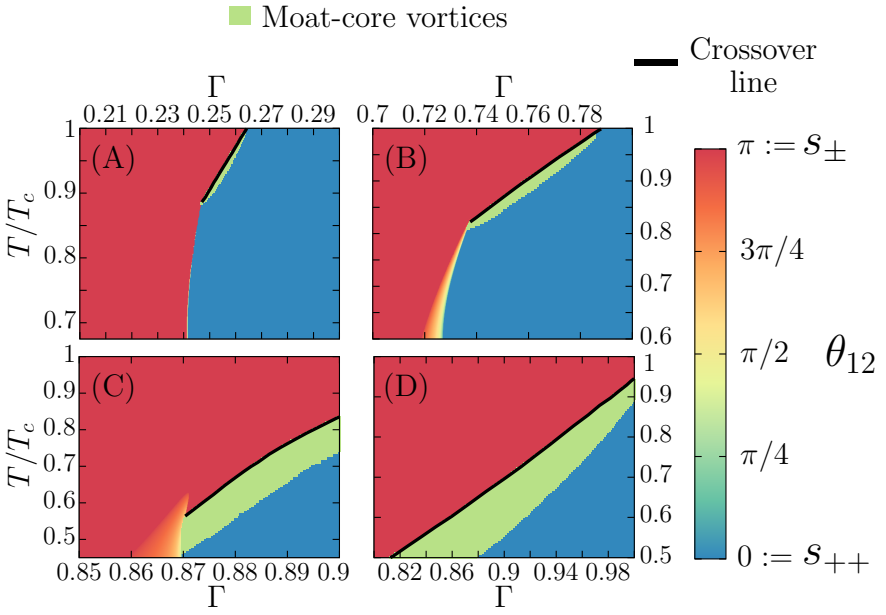

Figure 5.11: Phase diagrams of the Ginzburg-Landau free energy Eq. (3.28) with same panels as Fig. (3.6). This shows the values of the lowest-energy state relative phase θ_{12} and the regions of existence of moat-core vortices, as functions of the temperature and interband scattering Γ. The solid black line shows the zero of Δ_1, that is the crossover between $s_\pm$ and s_{++} states. It is clear here that vortices with nodal zero-line are quite generic solutions in the vicinity of the crossover line.

Accordingly to the qualitative analysis, we find that existence of this kind of "moat-core" vortices does not depend on the specific values of the pairing coefficients. Rather, the investigation of the vortex solutions for various parameter sets, shows that the moat-cores are common feature in the proximity to the crossover line. The region of the existence of moat-core vortices is shown in Fig. (5.11). It is is clearly visible that the region with moat-core vortex solutions shrinks close to Tc and eventually suppress (panel A,B). For the investigated regimes the moat-core-vortices "region" increases in width ($\delta\Gamma$) increasing bands disparity λ_{ii}, i.e. compare panel B and D. Furthermore in these regimes the moat "region" increases in width increasing interband coupling λ_{12}, compare panel A-B-C. Moreover, we find that typically, the region of moat-core vortices in the Γ, T phase diagram tends to become larger with the increased ratio of diffusion coefficients D_2/D_1. This effect can be explained by the softening of the order parameter in the subdominant band which facilitates the formation of additional zeros in the $\Delta_1(r)$ gap distribution.

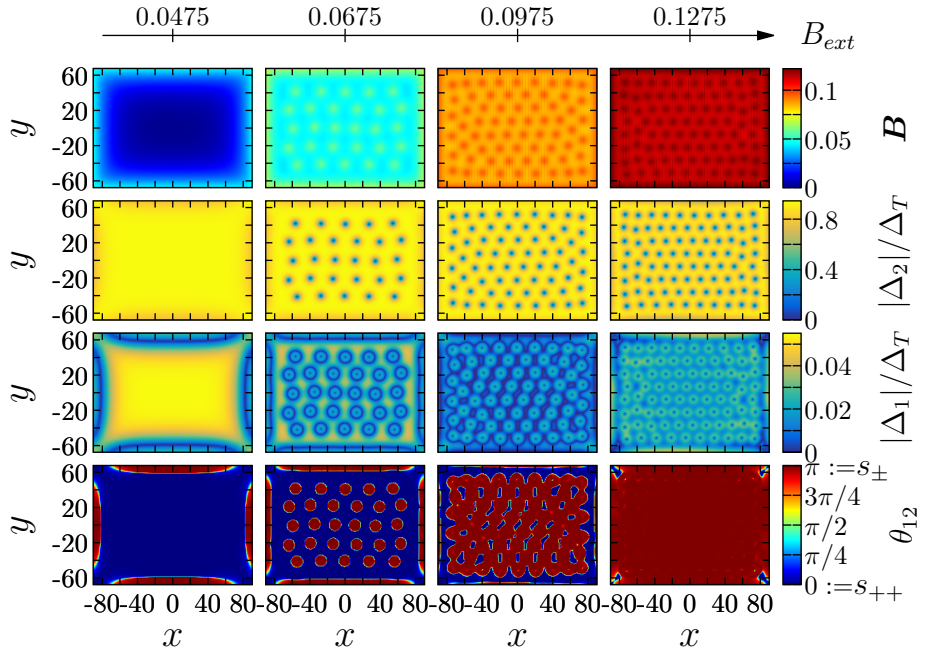

Figure 5.12: Magnetization process of a dirty two-band superconductor. The coupling parameters are those of Fig. (5.10), the temperature is $T/T_c = 0.9$, $q = 0.25$, and the strength of the interband impurity scattering $\Gamma = 0.7625$ places the system in bulk s_{++} state, in the vicinity of the crossover line. The different lines respectively display the magnetic field $\boldsymbol{B}$, the majority (Δ_2) and minority (Δ_1) gap components. The last line shows the relative phase θ_{12} that specifies whether the superconducting ground state is s_{++} or $s_\pm$. The preferred phase-locking in the bulk is $\theta_{12} = 0$ (the s_{++} state).

5.4.2 Field-induced coexistence of s_{++} and $s_\pm$ states

The inner $s_\pm$ phase in the vortex structure close to the crossover in s_{++} ground state, can obviously have consequences on the phase diagram of the system in an external field. Here, following the upcoming article by Garaud et al. , we study the properties of this system, under different magnitudes of external field. In a low applied external field the lattices and liquids of such moat-core vortices represent a macroscopic phase separation or a microemulsion of such $s_\pm$ inclusions inside the bulk s_{++} state. At elevated fields the system has a field-induced phase transitions between the $s_\pm$ and s_{++} states.

In Fig. (5.12) is shown the external-magnetic-field-driven crossover between the $s_\pm$ and s_{++} states, where the sample is place in s_{++} state really close to the crossover. At low external field the preferred phase-locking in the bulk is $\theta_{12} = 0$. Upon increasing the external field, vortices

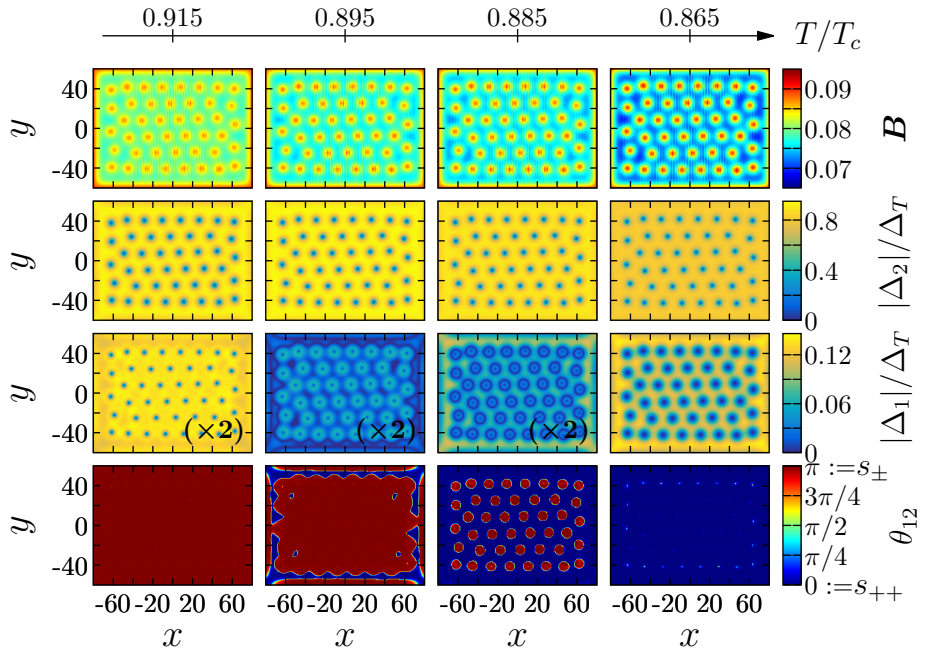

Figure 5.13: A field cooled simulation for a dirty two-band superconductors, in the vicinity of the impurity induced crossover line. The displayed quantities are the same as in Fig. (5.12). The constant external magnetic field is $\boldsymbol{B} = 0.09$. The preferred phase-locking at high temperatures is $\theta_{12} = \pi$ ($s_\pm$ state), while it is $\theta_{12} = 0$ (s_{++} state) at low temperatures.

start to enter the system, introducing small inclusions of $\theta_{12} = \pi$ state in their core. When the density of vortices becomes important, the cores of the subdominant component start to overlap until the whole system shows a $\theta_{12} = \pi$ phase-locking everywhere. Thus the crossover here is driven by the external magnetic field.

Interestingly even in low applied field, below the first critical field, the Meissner state also exhibits particular properties. As can be seen from the first column of Fig. (5.12), the system can be in $s_\pm$ near the boundaries, while s_{++} in the bulk. Close to the boundaries the region is carrying Meissner currents, and what happens is really similar to what occurs in vortex cores. The phase separation is indeed achieved through the formation of a line of zero subdominant component.

Also a field-cooled simulation show unusual properties. Figure (5.13) displays this kind of experiment, where the system is at high temperature in $s_\pm$ phase and cooling down the sample at constant field, it reaches the s_{++} phase. We can see how the sharp crossover found in ground state is rather washed-out to a finite temperature range. Indeed it can be seen in the second column how after the ground state crossover, the

regions is still mostly with $s_{\pm}$ phase, due to the overlap between the subdominant gaps vortices. When lowering the temperature, they do not overlap anymore, the $s_{\pm}$ phase remains only as inclusions in the bulk. Therefore the lattice (or liquid) of moat-core vortices represents a macroscopic phase separation or a microemulsion of $s_{\pm}$ inclusions inside the s_{++} state. Such configurations can in principle be resolved in local phase-sensitive probes [91].

Chapter 6

Conclusions

6.1 Summary

Recent discovery of iron-based superconductors motivated research on two-band superconductors where the pairing between electrons is produced by interband electron-electron repulsion [24, 26, 27]. This two-band model is the simplest one that can shed some light on these materials, having the tendency to be in $s_{\pm}$ state, i.e. possessing a relative phase between the complex gaps of π, in contrast to the more usual s_{++} that has a zero relative phase.

Additionally the presence of disorder is known to potentially lead in such a systems a transition from $s_{\pm}$ to s_{++}. The transition can be either direct [32] or via an intermediate state called $s + is$ which breaks time-reversal symmetry [30, 31, 33], and characterized by a relative phase between the gaps that is neither 0 or π. Therefore this model it is also the simplest one endowed with $s + is$ state, and all its properties.

The Ginzburg-Landau dirty two-band model for superconductors in this thesis is consistently derived from the Usadel equations, microscopic equations based on Green functions in their dirty limit. This GL model has generally more complicated free energy terms with respect to the clean case, these new terms describe the physics arising from impurity interband scattering.

The objective of the thesis was generally to study numerically topological defects and their possible experimental magnetic signatures in this kind of model. The focus was mostly on the BTRS region, and all its peculiarity. The existence of BTRS states in ground states was assessed through phase diagrams in the two dimensional temperature-impurity parameter space (T, Γ), for different values of coupling coefficients λ_{ij} between gaps (always with repulsive interband pairing, i.e. $\lambda_{12} = \lambda_{21} < 0$). An $s + is$ dome was found frequently away from T_c, even if the width in Γ results always very small, and probably impossible to evaluate directly

by experiments.

Furthermore the coherence lengths effects on vortex structures were studied. The coherence lengths have a really complicate behaviour in this model, thanks to the presence of impurities which tend to produce mixed normal modes. Additionally the presence of BTRS phase causes the divergence of the softest coherence lengths during second order phase transitions $s_{\pm}/s+is$ or $s_{++}/s+is$. These divergences can yield stunning changes in the behaviour of vortex matter, due to the connection between the coherence lengths and the attractive intervortex forces. In particular it has been seen how the vicinity of $s+is$ region can drive the system from a type II behaviour to a type-1.5 one, where vortices are stable in cluster configurations, where intervortex forces are short-range repulsive and long-range attractive. Additionally it has been simulated how this effect could be detected through characteristic signatures in muon-spin rotation experiments like the one in Ref. [80].

The above cited clustering effects can bring about new topological defects, called Skyrmions. These defects are basically bound states of separated fractional vortices. Type 1.5 superconductivity is involved helping the radial splitting of fractional vortices on a cluster boundary. In fact one component is more in the attractive region, and tries to shrink more the cluster, while the other component has still strong short-range repulsive forces, therefore a radial splitting between the two is obtained. Skyrmions were also found in concomitance with domain walls, during field cooling experiments. The domain walls pinned by vortices and boundaries, help the stabilization of Skyrmion formed in proximity of the walls, with a similar mechanism noted in Ref. [49].

Subsequently the project focuses on one of the experimental ways to detect BTRS states, i.e. spontaneous magnetic field inside superconductors. Thanks to their multicomponent nature this materials can have counterflow of the two components. When this counterflow is associated with gradients of relative density, it becomes unbalanced and supports currents, which generates internal fields. In this thesis two ways of generating counterflow in BTRS phase were explored, firstly through a domain wall pinned by non-convex geometry of the domain and secondly through impurity fluctuations in the sample. Both ways generate spontaneous field, even if very weak with respect to other models like in Ref. [50]. The milder effect has been hypothesized to originate in compensatory contributions of the mixed-gradient terms coming from impurity interband scattering. Greater spontaneous field when these terms are switched off manually seems to confirm it.

Finally the impurity-driven $s_{\pm}/s_{++}$ crossover has been analyzed in light of the previous article [87]. This crossover produces new vortex-core structure on the s_{++} side, named "moat"-core vortices, characterized by

a nodal density line around the usual singular point of the vortex. The nodal line is formed as consequence of different relative phase states inside and outside the vortex. In the inner part of the core we have a $s_{\pm}$ state, while outside a zero phase difference ground state is preferred. These unconventional vortex solutions have also consequences on the behaviour of the crossover in an applied field. Indeed, in contrast to the zero-field picture of sharp crossover, the lattice or liquids of moat-core vortices represent a macroscopic phase separation, a sort of "microemulsion" of $s_{\pm}$ inclusions inside the s_{++} state. Moreover raising the external field, a field-induced phase transition to $s_{\pm}$ state can be obtained.

6.2 Discussion

The dirty two-band model reveals itself as a very useful model for studying exotic properties in iron-based superconductors. Indeed in its simplicity manages anyway to show important phenomena like type 1.5 superconductivity or broken time-reversal symmetry, that could happen in real world iron-based materials.

The first significant aspect to notice is that in this model the BTRS region is very narrow and for all practical purposes directly unobservable. Nonetheless is fundamental to study what happens theoretically in the vicinity of it, in fact there are a lot of different cases where the $s + is$ region is very broad. For example in clean three bands superconductors BTRS regions are easily obtained by a different mechanism of frustration between interband interactions [34–38]. Therefore adding a new band, making it a dirty three-band model, most likely increases the size of the $s + is$ regions. Furthermore the $s + is$ domes in this model are usually somehow parallel to the temperature, and this is another problem for possible experimental signatures. The only way to detect it would be with impurity variation, definitely harder and less controllable with respect to temperature. However even if very small, the BTRS can influence properties in a broader region, through softening of the normal modes, that have direct impact on intervortex behaviour, opening the possibility for type 1.5 superconductivity.

Secondly, the demonstration that $s + is$ phases are able to produce a spontaneous field, is also considerable. Indeed nowadays there is a lot of attention in the SC community to detect BTRS states in material. This model has the great characteristic of being directly linked with microscopic parameter, such as impurity variations, hence it can be easier to interface experimental results and theory with respect to other models.

Lastly the moat-core phenomenon represents a new kind of vortex physics inside superconductors. This physics could be utilized to detect a crossover between $s_{\pm}$ and s_{++}. In fact in the ground state this

crossover is really sharp and hard to detect, while under external field condition, where vortices are present, the crossover is washed out and the "microemulsion" of $s_{\pm}$ in s_{++} could be resolved with local phase-sensitive probes.

Appendix A

Ginzburg-Landau coefficients

The coefficients of the Ginzburg-Landau functional a_{ij}, b_{ij}, c_{ij} and k_{ij} can be calculated from the inputs λ_{ij}, T and Γ of the microscopic self-consistency equation. N_i are the densities of states and D_i the electron diffusivities. We always assume $N_i = 1$ during the simulations, since densities imbalance does not influence much the calculations. First, the coefficients of gradient terms are given by

$$k_{ii} = 2\pi T N_i \sum_{n=0}^{N_d} \frac{D_i(\omega_n + \gamma_{ji})^2 + \gamma_{ij}\gamma_{ji}D_j}{\omega_n^2(\omega_n + \gamma_{ij} + \gamma_{ji})^2} \tag{A1a}$$

$$k_{ij} = 2\pi T N_i \gamma_{ij} \sum_{n=0}^{N_d} \frac{D_i(\omega_n + \gamma_{ji}) + D_j(\omega_n + \gamma_{ij})}{\omega_n^2(\omega_n + \gamma_{ij} + \gamma_{ji})^2}\,, \tag{A1b}$$

with $j \neq i$. The coefficients of the potential terms can be found for example from Ref. [31] and they read as

$$a_{ii} = \frac{N_i\lambda_{jj}}{\det(\hat{\lambda})} - 2\pi T \sum_{n=0}^{N_d} \frac{(\omega_n + \gamma_{ji})N_i}{\omega_n(\omega_n + \gamma_{ij} + \gamma_{ji})}\,, \tag{A2a}$$

$$a_{ij} = -\frac{N_i\lambda_{ij}}{\det(\hat{\lambda})} - 2\pi T \sum_{n=0}^{N_d} \frac{\gamma_{ij}N_i}{\omega_n(\omega_n + \gamma_{ij} + \gamma_{ji})}\,. \tag{A2b}$$

The other parameters read as

$$b_{ii} = \pi T N_i \sum_{n=0}^{N_d} \frac{(\omega_n + \gamma_{ji})^4}{\omega_n^3(\omega_n + \gamma_{ij} + \gamma_{ji})^4} \tag{A3a}$$
$$+ \pi T N_i \sum_{n=0}^{N_d} \frac{\gamma_{ij}(\omega_n + \gamma_{ji})(\omega_n^2 + 3\omega_n\gamma_{ji} + \gamma_{ji}^2)}{\omega_n^3(\omega_n + \gamma_{ij} + \gamma_{ji})^4}\,,$$
$$b_{ij} = -\pi T N_i \sum_{n=0}^{N_d} \frac{\gamma_{ij}}{(\omega_n + \gamma_{ij} + \gamma_{ji})^4} \tag{A3b}$$
$$+\pi T N_i \sum_{n=0}^{N_d} \frac{\gamma_{ij}(\gamma_{ij} + \gamma_{ji})(\omega_n(\gamma_{ij} + \gamma_{ji}) + 2\gamma_{ij}\gamma_{ji})}{\omega_n^3(\omega_n + \gamma_{ij} + \gamma_{ji})^4}\,,$$

and

$$c_{ii} = \pi T N_i \tag{A4a}$$
$$\sum_{n=0}^{N_d} \frac{\gamma_{ij}(\omega_n + \gamma_{ji})(\omega_n^2 + (\omega_n + \gamma_{ji})(\gamma_{ij} + \gamma_{ji}))}{\omega_n^3(\omega_n + \gamma_{ij} + \gamma_{ji})^4}\,,$$
$$c_{ij} = \pi T N_i \sum_{n=0}^{N_d} \frac{\gamma_{ij}(\omega_n + \gamma_{ji})(\omega_n + \gamma_{ij})(\gamma_{ij} + \gamma_{ji})}{\omega_n^3(\omega_n + \gamma_{ij} + \gamma_{ji})^4}\,. \tag{A4b}$$

Thus for a given set of input microscopic parameters, λ_{ij}, Γ and T close to T_c, we can reconstruct the coefficients Eq. (A1)–Eq. (A4) and investigate the ground-state properties of the GL theory by minimizing the free energy Eq. (3.28) with respect to $|\Delta_j|$ and θ_{12}.

Bibliography

[1] M. Tinkham. *Introduction to Superconductivity: Second Edition*. Dover Books on Physics. Dover Publications, 2004. ISBN: 9780486435039. URL: https://books.google.se/books?id=k6AO9nRYbioC.

[2] B.V. Svistunov, E.S. Babaev, and N.V. Prokof'ev. *Superfluid States of Matter*. Taylor & Francis, 2015. ISBN: 9781439802755. URL: https://books.google.se/books?id=IU-QQAAACAAJ.

[3] H. Kamerlingh Onnes. "Further experiments with liquid helium. C. On the change of electric resistance of pure metals at very low temperatures etc. IV. The resistance of pure mercury at helium temperatures". In: *KNAW, Proceedings* 13.II (1991), pp. 261–263. DOI: 10.1007/978-94-009-2079-8_15. URL: http://www.springerlink.com/index/10.1007/978-94-009-2079-8{_}15.

[4] W. Meissner and R. Ochsenfeld. "Ein neuer Effekt bei Eintritt der Supraleitfähigkeit". In: *Naturwissenschaften* 21 (Nov. 1933), pp. 787–788. DOI: 10.1007/BF01504252.

[5] F. London London and H. "The electromagnetic equations of the supracon- ductor". In: *Proc. Roy. Soc. (Lond.)* A149 (1935), p. 71.

[6] F. London. "On the Problem of the Molecular Theory of Superconductivity". In: *Physical Review* 74.5 (1948), pp. 562–573. ISSN: 0031-899X. DOI: 10.1103/PhysRev.74.562. arXiv: arXiv:1305.1498v1. URL: https://link.aps.org/doi/10.1103/PhysRev.74.562.

[7] V. L. Ginzburg and L. D. Landau. "On the Theory of superconductivity". In: *Zh. Eksp. Teor. Fiz.* 20 (1950), pp. 1064–1082.

[8] L. D. Landau. "On the theory of phase transitions". In: *Zh. Eks. Teor. Fiz.* 7.1937 (1937), pp. 19–32. ISSN: 0028-0836. DOI: 10.1038/138840a0.

[9] J. Bardeen, L. N. Cooper, and J. R. Schrieffer. "Microscopic Theory of Superconductivity". In: *Phys. Rev.* 106 (1 1957), pp. 162–164. DOI: 10.1103/PhysRev.106.162. URL: https://link.aps.org/doi/10.1103/PhysRev.106.162.

[10] L. P. Gor'kov. "Microscopic Derivation of the Ginzburg-Landau Equations in the Theory of Superconductivity". In: *Soviet Phys. JETP* 9.6 (1959), p. 1364.

[11] P. W. Anderson. "Plasmons, Gauge Invariance, and Mass". In: *Physical Review* 130.1 (1963), pp. 439–442. ISSN: 0031-899X. DOI: 10.1103/PhysRev.130.439. URL: https://link.aps.org/doi/10.1103/PhysRev.130.439.

[12] Alexei Alexeyevich Abrikosov. "On the Magnetic Properties of Superconductors of the Second Group". In: *Soviet Physics Jetp* 5.6 (1957), pp. 1174–1182. ISSN: 00385646.

[13] Victor Moshchalkov et al. "Type-1.5 superconductivity". In: *Physical Review Letters* 102.11 (2009), pp. 1–4. ISSN: 00319007. DOI: 10.1103/PhysRevLett.102.117001. arXiv: 0902.0997.

[14] D R Tilley. "The Ginzburg-Landau equations for pure two band superconductors". In: *Proceedings of the Physical Society* 84.4 (1964), p. 573. URL: http://stacks.iop.org/0370-1328/84/i=4/a=313.

[15] Egor Babaev and Martin Speight. "Semi-Meissner state and neither type-I nor type-II superconductivity in multicomponent superconductors". In: *Physical Review B - Condensed Matter and Materials Physics* 72.18 (2005), pp. 1–5. ISSN: 10980121. DOI: 10.1103/PhysRevB.72.180502. arXiv: 0411681 [cond-mat].

[16] Yoichi Kamihara et al. "Iron-based layered superconductor La[O1-xFx]FeAs (x= 0.05-0.12) with Tc = 26 K". In: *Journal of the American Chemical Society* 130.11 (2008), pp. 3296–3297. ISSN: 00027863. DOI: 10.1021/ja800073m. arXiv: ja063355c [10.1021].

[17] A. J. Leggett. "Number-Phase Fluctuations in Two-Band Superconductors". In: 36.5 (1966), pp. 901–930.

[18] A. A. Zyuzin, Julien Garaud, and Egor Babaev. "Nematic Skyrmions in Odd-Parity Superconductors". In: *Physical Review Letters* 119.16 (2017), pp. 1–6. ISSN: 10797114. DOI: 10.1103/PhysRevLett.119.167001. arXiv: 1705.01718.

[19] Julien Garaud et al. "Skyrmions induced by dissipationless drag in U(1) × U(1) superconductors". In: *Physical Review B - Condensed Matter and Materials Physics* 89.10 (2014), pp. 1–13. ISSN: 10980121. DOI: 10.1103/PhysRevB.89.104508. arXiv: 1307.3211.

[20] Daniel F. Agterberg, Egor Babaev, and Julien Garaud. "Microscopic prediction of skyrmion lattice state in clean interface superconductors". In: *Physical Review B - Condensed Matter and Materials Physics* 90.6 (2014), pp. 1–10. ISSN: 1550235X. DOI: 10.1103/PhysRevB.90.064509. arXiv: 1403.6655.

[21] Julien Garaud and Egor Babaev. "Properties of skyrmions and multi-quanta vortices in chiral p-wave superconductors". In: *Scientific Reports* 5 (2015), pp. 1–9. ISSN: 20452322. DOI: 10.1038/srep17540. arXiv: 1201.2946. URL: http://dx.doi.org/10.1038/srep17540.

[22] Nicholas Manton and Paul Sutcliffe. *Topological Solitons*. Cambridge Monographs on Mathematical Physics. Cambridge University Press, 2004. DOI: 10.1017/CBO9780511617034.

[23] V. Grinenko et al. "Superconductivity with broken time-reversal symmetry in ion-irradiated Ba 0. 27 K 0. 73 Fe 2 As 2 single crystals". In: *Physical Review B* 95.21 (2017), pp. 1–5. ISSN: 24699969. DOI: 10.1103/PhysRevB.95.214511.

[24] P. J. Hirschfeld, M. M. Korshunov, and I. I. Mazin. "Gap symmetry and structure of Fe-based superconductors". In: (2011). ISSN: 0034-4885. DOI: 10.1088/0034-4885/74/12/124508. arXiv: 1106.3712. URL: http://arxiv.org/abs/1106.3712{\%}0Ahttp://dx.doi.org/10.1088/0034-4885/74/12/124508.

[25] Fa Wang and Dung-Hai Lee. "The Electron-Pairing Mechanism of Iron-Based Superconductors". In: *Science* 332.6026 (2011), pp. 200–204. ISSN: 0036-8075. DOI: 10.1126/science.1200182. eprint: http://science.sciencemag.org/content/332/6026/200.full.pdf. URL: http://science.sciencemag.org/content/332/6026/200.

[26] A. V. Chubukov. "Pairing mechanism in Fe-based superconductors". In: (2011). ISSN: 1947-5454. DOI: 10.1146/annurev-conmatphys-020911-125055. arXiv: 1110.0052. URL: http://arxiv.org/abs/1110.0052.

[27] I. I. Mazin et al. "Unconventional superconductivity with a sign reversal in the order parameter of LaFeAsO1-xFx". In: *Physical Review Letters* 101.5 (2008), pp. 1–4. ISSN: 00319007. DOI: 10.1103/PhysRevLett.101.057003. arXiv: 0912.2752.

[28] P. W. Anderson. "Knight Shift in Superconductors". In: *Phys. Rev. Lett.* 3 (7 1959), pp. 325–326. DOI: 10.1103/PhysRevLett.3.325. URL: https://link.aps.org/doi/10.1103/PhysRevLett.3.325.

[29] K. H. Bennemann and John B. Ketterson. *Superconductivity: Conventional and Unconventional Superconductors*. Springer-Verlag Berlin Heidelberg, 2008.

[30] A. M. Bobkov and I. V. Bobkova. "Time-reversal symmetry breaking state near the surface of an s+- superconductor". In: *Physical Review B - Condensed Matter and Materials Physics* 84.13 (2011), pp. 1–8. ISSN: 10980121. DOI: 10.1103/PhysRevB.84.134527.

[31] Valentin Stanev and Alexei E. Koshelev. "Complex state induced by impurities in multiband superconductors". In: *Physical Review B - Condensed Matter and Materials Physics* 89.10 (2014), pp. 1–7. ISSN: 10980121. DOI: 10.1103/PhysRevB.89.100505. arXiv: 1306.4268.

[32] D. V. Efremov et al. "Disorder-induced transition between s± and s++ states in two-band superconductors". In: *Physical Review B - Condensed Matter and Materials Physics* 84.18 (2011), pp. 3–6. ISSN: 10980121. DOI: 10.1103/PhysRevB.84.180512. arXiv: 1104.3840.

[33] Mihail Silaev, Julien Garaud, and Egor Babaev. "Phase diagram of dirty two-band superconductors and observability of impurity-induced s+is state". In: *Physical Review B* 95.2 (2017), pp. 1–9. ISSN: 24699969. DOI: 10.1103/PhysRevB.95.024517. arXiv: 1610.05846.

[34] TK Ng and N Nagaosa. "Broken time-reversal symmetry in Josephson junction involving two-band superconductors". In: *EPL (Europhysics Letters)* (2009), p. 9. ISSN: 0295-5075. DOI: 10.1209/0295-5075/87/17003. arXiv: 0809.3343. URL: http://arxiv.org/abs/0809.3343{\%}5Cnhttp://iopscience.iop.org/0295-5075/87/1/17003.

[35] Valentin Stanev and Zlatko Tešanović. "Three-band superconductivity and the order parameter that breaks time-reversal symmetry". In: *Physical Review B - Condensed Matter and Materials Physics* 81.13 (2010), pp. 1–9. ISSN: 10980121. DOI: 10.1103/PhysRevB.81.134522. arXiv: 0912.5214.

[36] Johan Carlström, Julien Garaud, and Egor Babaev. "Length scales, collective modes, and type-1.5 regimes in three-band superconductors". In: *Physical Review B - Condensed Matter and Materials Physics* 84.13 (2011), pp. 1–14. ISSN: 10980121. DOI: 10.1103/PhysRevB.84.134518. arXiv: 1107.4279.

[37] Saurabh Maiti and Andrey V. Chubukov. "S+is state with broken time-reversal symmetry in Fe-based superconductors". In: *Physical Review B - Condensed Matter and Materials Physics* 87.14 (2013), pp. 1–14. ISSN: 10980121. DOI: 10.1103/PhysRevB.87.144511. arXiv: 1302.2964.

[38] Jakob Böker et al. "S+is superconductivity with incipient bands: Doping dependence and STM signatures". In: *Physical Review B* 96.1 (2017), pp. 45–47. ISSN: 24699969. DOI: 10.1103/PhysRevB.96.014517.

[39] Shi Zeng Lin and Xiao Hu. "Massless leggett mode in three-band superconductors with time-reversal-symmetry breaking". In: *Physical Review Letters* 108.17 (2012), pp. 1–5. ISSN: 00319007. DOI: 10.1103/PhysRevLett.108.177005. arXiv: 1107.0814.

[40] Valentin Stanev. "Model of collective modes in three-band superconductors with repulsive interband interactions". In: *Physical Review B - Condensed Matter and Materials Physics* 85.17 (2012), pp. 1–5. ISSN: 10980121. DOI: 10.1103/PhysRevB.85.174520.

[41] M. Marciani et al. "Leggett modes in iron-based superconductors as a probe of time-reversal symmetry breaking". In: *Physical Review B - Condensed Matter and Materials Physics* 88.21 (2013), pp. 1–20. ISSN: 10980121. DOI: 10.1103/PhysRevB.88.214508. arXiv: 1306.5545.

[42] Mihail Silaev, Julien Garaud, and Egor Babaev. "Unconventional thermoelectric effect in superconductors that break time-reversal symmetry". In: *Physical Review B - Condensed Matter and Materials Physics* 92.17 (2015), pp. 1–7. ISSN: 1550235X. DOI: 10.1103/PhysRevB.92.174510. arXiv: 1503.02024.

[43] Julien Garaud, Mihail Silaev, and Egor Babaev. "Thermoelectric Signatures of Time-Reversal Symmetry Breaking States in Multiband Superconductors". In: *Physical Review Letters* 116.9 (2016), pp. 1–13. ISSN: 10797114. DOI: 10.1103/PhysRevLett.116.097002. arXiv: 1507.04712.

[44] Mihail Silaev and Egor Babaev. "Unusual mechanism of vortex viscosity generated by mixed normal modes in superconductors with broken time reversal symmetry". In: *Physical Review B - Condensed Matter and Materials Physics* 88.22 (2013), pp. 1–5. ISSN: 10980121. DOI: 10.1103/PhysRevB.88.220504. arXiv: 1306.6159.

[45] Saurabh Maiti, Manfred Sigrist, and Andrey Chubukov. "Spontaneous currents in a superconductor with s+is symmetry". In: *Physical Review B - Condensed Matter and Materials Physics* 91.16 (2015), pp. 1–5. ISSN: 1550235X. DOI: 10.1103/PhysRevB.91.161102. arXiv: 1412.7439.

[46] Shi Zeng Lin, Saurabh Maiti, and Andrey Chubukov. "Distinguishing between s+id and s+is pairing symmetries in multiband superconductors through spontaneous magnetization pattern induced by a defect". In: *Physical Review B* 94.6 (2016), pp. 1–8. ISSN: 24699969. DOI: 10.1103/PhysRevB.94.064519. arXiv: 1607.00109.

[47] E. Babaev et al. “Type-1.5 superconductivity in multicomponent systems”. In: *Physica C: Superconductivity and its Applications* 533 (2017), pp. 20–35. ISSN: 09214534. DOI: 10.1016/j.physc.2016.08.003. arXiv: 1608.02211. URL: http://dx.doi.org/10.1016/j.physc.2016.08.003.

[48] Julien Garaud, Johan Carlstrom, and Egor Babaev. “Topological solitons in three-band superconductors with broken time reversal symmetry”. In: *Physical Review Letters* 107.19 (2011), pp. 1–7. ISSN: 00319007. DOI: 10.1103/PhysRevLett.107.197001. arXiv: 1107.0995.

[49] Julien Garaud et al. “Chiral CP^2 skyrmions in three-band superconductors”. In: i (2012), pp. 1–30. DOI: 10.1103/PhysRevB.87.014507. arXiv: 1211.4342. URL: http://arxiv.org/abs/1211.4342{\%}0Ahttp://dx.doi.org/10.1103/PhysRevB.87.014507.

[50] Julien Garaud and Egor Babaev. “Domain walls and their experimental signatures in s + i s superconductors”. In: *Physical Review Letters* 112.1 (2014), pp. 1–5. ISSN: 00319007. DOI: 10.1103/PhysRevLett.112.017003. arXiv: arXiv:1308.3220v1.

[51] Troels Arnfred Bojesen, Egor Babaev, and Asle Sudbø. “Time reversal symmetry breakdown in normal and superconducting states in frustrated three-band systems”. In: *Physical Review B - Condensed Matter and Materials Physics* 88.22 (2013), pp. 1–4. ISSN: 10980121. DOI: 10.1103/PhysRevB.88.220511. arXiv: 1306.2313.

[52] Troels Arnfred Bojesen, Egor Babaev, and Asle Sudbø. “Phase transitions and anomalous normal state in superconductors with broken time-reversal symmetry”. In: *Physical Review B - Condensed Matter and Materials Physics* 89.10 (2014), pp. 1–11. ISSN: 10980121. DOI: 10.1103/PhysRevB.89.104509. arXiv: 1401.5802.

[53] Johan Carlström and Egor Babaev. “Spontaneous breakdown of time-reversal symmetry induced by thermal fluctuations”. In: *Physical Review B - Condensed Matter and Materials Physics* 91.14 (2015), pp. 1–5. ISSN: 1550235X. DOI: 10.1103/PhysRevB.91.140504. arXiv: arXiv:1411.3202v2.

[54] Takafumi Kita. *Statistical Mechanics of Superconductivity*. Graduate Texts in Physics. Tokyo: Springer Japan, 2015. ISBN: 978-4-431-55404-2. DOI: 10.1007/978-4-431-55405-9. URL: http://link.springer.com/10.1007/978-4-431-55405-9.

[55] N. B. Kopnin. *Theory of nonequilibrium superconductivity*. Oxford University Press, 2009.

[56] Leon N. Cooper. "Bound Electron Pairs in a Degenerate Fermi Gas". In: *Phys. Rev.* 104 (4 1956), pp. 1189–1190. DOI: 10.1103/PhysRev.104.1189. URL: https://link.aps.org/doi/10.1103/PhysRev.104.1189.

[57] J. Bardeen, L. N. Cooper, and J. R. Schrieffer. "Theory of Superconductivity". In: *Phys. Rev.* 108 (5 1957), pp. 1175–1204. DOI: 10.1103/PhysRev.108.1175. URL: https://link.aps.org/doi/10.1103/PhysRev.108.1175.

[58] N N Bogoliubov. "A New Method in the Theory of Superconductivity. I*". In: *J. Exptl. Theoret. Phys. (U.S.S.R.)* 34.34 (1958), pp. 58–65. URL: http://www.jetp.ac.ru/cgi-bin/dn/e{_}007{_}01{_}0041.pdf.

[59] L. P. Gor'kov. "On the energy spectrum of superconductors". In: *Soviet Phys. JETP* 7.3 (1958), p. 505.

[60] Gert Eilenberger. "Transformation of Gorkov's equation for type II superconductors into transport-like equations". In: *Zeitschrift für Physik A Hadrons and nuclei* 214.2 (1968), pp. 195–213. ISSN: 0939-7922. DOI: 10.1007/BF01379803. URL: https://doi.org/10.1007/BF01379803.

[61] Mihail Silaev and Egor Babaev. "Microscopic derivation of two-component Ginzburg-Landau model and conditions of its applicability in two-band systems". In: *Physical Review B - Condensed Matter and Materials Physics* 85.13 (2012), pp. 1–10. ISSN: 10980121. DOI: 10.1103/PhysRevB.85.134514. arXiv: 1110.1593.

[62] Julien Garaud, Mihail Silaev, and Egor Babaev. "Microscopically derived multi-component Ginzburg–Landau theories for s+is superconducting state". In: *Physica C: Superconductivity and its Applications* 533 (2017), pp. 63–73. ISSN: 09214534. DOI: 10.1016/j.physc.2016.07.010. arXiv: 1601.02227. URL: http://dx.doi.org/10.1016/j.physc.2016.07.010.

[63] Klaus D. Usadel. "Generalized Diffusion Equation for Superconducting Alloys". In: *Phys. Rev. Lett.* 25 (8 1970), pp. 507–509. DOI: 10.1103/PhysRevLett.25.507. URL: https://link.aps.org/doi/10.1103/PhysRevLett.25.507.

[64] A. Gurevich. "Enhancement of the upper critical field by nonmagnetic impurities in dirty two-gap superconductors". In: *Physica C: Superconductivity and its Applications* 456.1-2 (2007), pp. 160–169. ISSN: 09214534. DOI: 10.1016/j.physc.2007.01.008. arXiv: 0701281 [cond-mat].

[65] Mihail Silaev, Julien Garaud, and Egor Babaev. "Phase diagram of dirty two-band superconductors and observability of impurity-induced s+is state". In: *Physical Review B* 95.2 (2017), pp. 1–9. ISSN: 24699969. DOI: 10.1103/PhysRevB.95.024517. arXiv: 1610.05846.

[66] M. Tinkham. *Introduction to Superconductivity*. International series in pure and applied physics. McGraw Hill, 1996. ISBN: 9780070648784. URL: https://books.google.se/books?id=XP_uAAAAMAAJ.

[67] M. Plischke and B. Bergersen. *Equilibrium Statistical Physics*. World Scientific, 2006. ISBN: 9789812560483. URL: https://books.google.se/books?id=KYu7igYEkhwC.

[68] J.Garaud, A.Corticelli, M.Silaev, E.Babaev to be published.

[69] F. Hecht. "New development in freefem+". In: *Journal of Numerical Mathematics* 20.3-4 (2012), pp. 251–265. ISSN: 15702820. DOI: 10.1515/jnum-2012-0013.

[70] *freefem++ manual*. URL: http://www.freefem.org/ff++.

[71] *Open MPI website*. URL: https://www.open-mpi.org.

[72] *gnuplot website*. URL: http://www.gnuplot.info.

[73] David V. Hutton. *Fundamentals of finite element analysis*. McGraw-Hill Higher Education, 2004.

[74] Junuthula Narasimha. Reddy. *An introduction to the finite element method*. McGraw-Hill, 2006.

[75] Jorge Nocedal and Stephen J. Wright. *Numerical optimization*. Springer, 2006.

[76] Jonathan Richard Shewchuk. "An Introduction to the Conjugate Gradient Method Without the Agonizing Pain". In: *Science* 49.CS-94-125 (1994), p. 64. ISSN: 14708728. DOI: 10.1.1.110.418. arXiv: 1102.0183. URL: http://www.cs.cmu.edu/{~}quake-papers/painless-conjugate-gradient.pdf.

[77] W.W. William W Hager and Hongchao Zhang. "A Survey of Nonlinear Conjugate Gradient Methods". In: *Pacific journal of Optimization* 2.1 (2006), pp. 35–58. URL: http://www.math.lsu.edu/{~}hozhang/papers/cgsurvey.pdf.

[78] Yu-hong Dai. "Nonlinear Conjugate Gradient Methods". In: *Wiley Encyclopedia of Operations Research and Management Science* (2011), pp. 1–36. ISSN: 1055-6788. DOI: 10.1002/9780470400531.eorms0183. URL: http://lsec.cc.ac.cn/{~}dyh/worklist.html.

[79] Mihail Silaev and Egor Babaev. "Microscopic theory of type-1.5 superconductivity in multiband systems". In: *Physical Review B - Condensed Matter and Materials Physics* 84.9 (2011), pp. 1–9. ISSN: 10980121. DOI: 10.1103/PhysRevB.84.094515. arXiv: arXiv:1102.5734v1.

[80] S. J. Ray et al. "Muon-spin rotation measurements of the vortex state in Sr2 RuO4: Type-1.5 superconductivity, vortex clustering, and a crossover from a triangular to a square vortex lattice". In: *Physical Review B - Condensed Matter and Materials Physics* 89.9 (2014), pp. 6–11. ISSN: 10980121. DOI: 10.1103/PhysRevB.89.094504. arXiv: arXiv:1403.1767v1.

[81] Egor Babaev. "Non-Meissner electrodynamics and knotted solitons in two-component superconductors". In: *Physical Review B - Condensed Matter and Materials Physics* 79.10 (2009), pp. 1–6. ISSN: 10980121. DOI: 10.1103/PhysRevB.79.104506. arXiv: arXiv:0809.4468v3.

[82] Yasushi Matsunaga, Masanori Ichioka, and Kazushige Machida. "Flux flow and pinning of the vortex sheet structure in a two-component superconductor". In: *Physical Review B - Condensed Matter and Materials Physics* 70.10 (2004), pp. 1–4. ISSN: 01631829. DOI: 10.1103/PhysRevB.70.100502. arXiv: 0409376 [arXiv:cond-mat].

[83] T W B Kibble. "Topology of cosmic domains and strings". In: *Journal of Physics A: Mathematical and General* 9.8 (1976), p. 1387. URL: http://stacks.iop.org/0305-4470/9/i=8/a=029.

[84] W. H. Zurek. *Cosmological experiments in superfluid helium?* 1985. URL: http://adsabs.harvard.edu/abs/1985Natur.317..505Z.

[85] R. J. Rivers. "Zurek-Kibble Causality Bounds in Time-Dependent Ginzburg-Landau Theory and Quantum Field Theory". In: *Journal of Low Temperature Physics* 124.1 (2001), pp. 41–83. ISSN: 1573-7357. DOI: 10.1023/A:1017513531901. URL: https://doi.org/10.1023/A:1017513531901.

[86] Vasily Vadimov and Mihail Silaev. "Predicted nucleation of domain walls in px+ipy superconductors by a Z2 symmetry-breaking transition in external magnetic fields". In: *Physical Review Letters* 111.17 (2013), pp. 1–5. ISSN: 00319007. DOI: 10.1103/PhysRevLett.111.177001.

[87] Julien Garaud, Mihail Silaev, and Egor Babaev. "Change of the vortex core structure in two-band superconductors at impurity-scatering-driven s+-/s++ crossover". In: 1 (2017), pp. 1–5. arXiv: 1707.06412. URL: http://arxiv.org/abs/1707.06412.

[88] L. Onsager. “Statistical hydrodynamics”. In: *Il Nuovo Cimento Series 9* 6.2 Supplement (1949), pp. 279–287. ISSN: 00296341. DOI: 10.1007/BF02780991.

[89] R. P. Feynman. “Chapter II Application of Quantum to Liquid Helium”. In: *Progress in Low Temperature Physics* (1955), pp. 17–53.

[90] K. Tanaka, M. Eschrig, and D. F. Agterberg. “Theory of vortices in hybridized ballistic/diffusive-band superconductors”. In: *Physical Review B - Condensed Matter and Materials Physics* 75.21 (2007), pp. 1–18. ISSN: 10980121. DOI: 10.1103/PhysRevB.75.214512. arXiv: 0702270 [cond-mat].

[91] P. J. Hirschfeld et al. “Robust determination of the superconducting gap sign structure via quasiparticle interference”. In: *Physical Review B - Condensed Matter and Materials Physics* 92.18 (2015), pp. 1–13. ISSN: 1550235X. DOI: 10.1103/PhysRevB.92.184513. arXiv: 1507.08317.